การวัดสัดส่วนปริมาตรของวัฏภาคของแข็งและก๊าซภายในฟลูอิไดซ์เบดสามวัฏภาคสองมิติโดยใช้
เทคนิคคลื่นเหนือเสียงและภาพถ่าย

นายพรเทพ สิทธิศักดิ์

MEASUREMENT OF SOLID AND GAS HOLDUPS IN TWO-DIMENSIONAL THREE-
PHASE FLUIDIZED BED USING ULTRASOUND AND IMAGING TECHNIQUES

Mr. Pornthep Sittisak

A Thesis Submitted in Partial Fulfillment of the Requirements

For the Degree of Master of Engineering in Chemical Engineering

Department of Chemical Engineering

Chulalongkorn University

Academic Year 2001

ISBN 974-03-1313-2

Thesis Title   MEASUREMENT OF SOLID AND GAS HOLDUPS IN TWO-DIMENSIONAL THREE-PHASE FLUIDIZED BED USING ULTRASOUND AND IMAGING TECHNIQUE

By   Mr. Pornthep Sittisak

Field of Study   Chemical Engineering

Thesis Advisor   Associate Professor Tawatchai Charinpanitkul, D. Eng.

Thesis Co-advisor Assistant Professor Hathaichanok Vanisri, Ph. D.

Accepted by the Faculty of Engineering, Chulalongkorn University in Partial Fulfillment of the Requirements for the Master's Degree

…………………………………………..……Dean of Faculty of Engineering

(Professor Somsak Panyakeaw, D. Eng.)

THESIS COMMITEE

…………………………………………….…..Chairman

(Associate Professor Chirakarn Muangnapoh, D. Ing.)

……………………………………………....Thesis Advisor

(Associate Professor Tawatchai Charinpanitkul, D. Eng.)

…………………………………….…………Thesis Co-advisor

(Assistant Professor Hathaichanok Vanisri, Ph.D.)

……………………………………………….Member

(Professor Dr. Wiwut Tanthapanichakoon, Ph.D.)

……………………………………………….Member

(Assistant Professor Prasert Pavasant, Ph.D.)

พรเทพ สิทธิศักดิ์ : การวัดสัดส่วนปริมาตรของวัฏภาคของแข็งและก๊าซภายในฟลูอิไดซ์เบดสามวัฏภาค สองมิติโดยใช้เทคนิคคลื่นเหนือเสียงและภาพถ่าย (MEASUREMENT OF SOLID AND GAS HOLDUPS IN TWO-DIMENSIONAL THREE-PHASE FLUIDIZED BED USING ULTRASOUND AND IMAGING TECHNIQUE) อ. ที่ปรึกษา : รศ.ดร. ธวัชชัย ชรินพาณิชกุล, อ. ที่ปรึกษาร่วม : ผศ. ดร. หทัยชนก ดุริยะบรรเลง : จำนวนหน้า 123 หน้า. ISBN 974-03-1313-2

งานวิจัยนี้ใช้คอลัมน์ 2 มิติ ที่มีความกว้าง 30 เซนติเมตร หนา 1.5 เซนติเมตร และสูง 113 เซนติเมตร เพื่อศึกษาอุทกพลศาสตร์ของระบบฟลูอิไดซ์เบดสามวัฏภาค จากการทดลองพบว่าความเร็วของทั้งก๊าซและของ เหลวมีอิทธิพลต่อพฤติกรรมของฟองก๊าซ และอนุภาคของแข็งภายในระบบ โดยที่อิทธิพลเนื่องจากอัตราการไหล ของของเหลวมีผลมากกว่าของอัตราการไหลของก๊าซ ซึ่งจากการวิเคราะห์ภาพถ่ายพบว่าขนาดเฉลี่ยของฟองก๊าซ จะลดลงเมื่อความเร็วตามผิวของก๊าซ หรือ ของเหลวเพิ่มมากขึ้น สำหรับในกรณีที่ระบบมียีสต์แขวนลอยอยู่ พบ ว่าเมื่อเพิ่มความเข้มข้นของยีสต์จะทำให้ขนาดเฉลี่ยของฟองก๊าซเล็กลง

การใช้วิธีการส่งผ่านคลื่นเหนือเสียง พบว่าเมื่ออนุภาคของของแข็งมีขนาดใหญ่ขึ้นจะทำให้การส่งผ่าน ของสัญญาณจากตัวส่งผ่านเบดไปถึงตัวรับน้อยลง ความสัมพันธ์ระหว่างสัดส่วนปริมาตรของของแข็งและอัตรา ส่วนของแอมปลิจูดเป็นแบบเอ็กโปเนนเชียล การเพิ่มขึ้นของความเร็วตามผิวของก๊าซส่งผลต่อการลดลงของอัตรา ส่วนของแอมปลิจูด ซึ่งแสดงโดยการเพิ่มขึ้นของสัดส่วนปริมาตรของของแข็ง เทคนิคการส่งผ่านคลื่นเหนือเสียง สามารถประยุกต์ใช้เพื่อสังเกตการกระจายตัวของอนุภาคของแข็งในเบด ในขณะที่เทคนิคการสังเกตด้วยภาพ ถ่ายดิจิตอลได้นำมาใช้เพื่อวัดการกระจายขนาดของฟองก๊าซเพื่อนำมาใช้ในการหาสัดส่วนปริมาตรของของก๊าซ

ภาควิชา..........วิศวกรรมเคมี.............. ลายมือชื่อนิสิต..

สาขาวิชา..........วิศวกรรมเคมี.............. ลายมือชื่ออาจารย์ที่ปรึกษา............................

ปีการศึกษา.........2544.................... ลายมือชื่ออาจารย์ที่ปรึกษาร่วม.......................

4170430921 : MAJOR ENGINEERING

KEY WORD : THREE-PHASE FLUIDIZED BED / VISUALIZATION / ULTRASONIC

PONRTHEP SITTISAK: MEASUREMENT OF SOLID AND GAS HOLDUPS IN TWO-DIMENSION THREE-PHASE FLUIDIZED BED USING ULTRASOUND AND IMAGING TECHNIQUE. THESIS ADVISOR: ASSOC. PROF. TAWATCHAI CHARINPANITKUL, THESIS CO-ADVISOR: ASSIST. PROF. HATHAICHANOK VANISRI, 123 PP. ISBN 974-03-1313-2

In this present work, a two-dimensional column with width of 30 cm., thickness of 1.5 cm., and height of 113 cm was employed to investigate the hydrodynamics of Three-Phase Fluidized Bed (TPFB) system. From the experiments, it was found that both superficial liquid and gas velocities affect the behavior of gas bubbles and solid particles in the system. The effect of liquid flow rate was more significant than that of gas flow rate. From image processing analysis, the bubble size decreased when the superficial velocity of either liquid or gas phase was increased. Within yeast suspension system, an increase in yeast concentration gave rise to the smaller bubble size.

Using ultrasonic transmission, it was found that the larger particle could lead to the less signal transmitted through the bed to the receiver. The relationship between solid holdup and amplitude ratio was found to be exponential. An increase in superficial gas velocity resulted in a decrease in the amplitude ratio which represented the higher solid holdup. Ultrasonic transmission technique was mainly applied for investigating distribution of solid particle in the bed while visualization technique with digital image processing was employed to measure bubble size distribution which is used for determining the local gas holdup.

สถาบันวิทยบริการ
จุฬาลงกรณ์มหาวิทยาลัย

Department…….Chemical Engineering…..   Student's signature………………..……………….

Field of study……..Chemical Engineering….   Advisor's signature…………………..………….

Academic year…………2001……………..…   CO-advisor's signature……………………………

ACKNOWLEDGEMENTS

CONTENTS

CONTENTS (Continued)

CONTENTS (Continued)

LIST OF TABLES

LIST OF FIGURES

Page

LIST OF FIGURES(Continued)

LIST OF FIGURES (Continued)

Page

LIST OF FIGURES (Continued)

NOMENCLATURES

A	Amplitude of the transmitted signal (-)
A/A_0	Amplitude ratio (-)
A_0	Amplitude of the transmitted signal in absence of air/nitrogen or solid (-)
b	bubble breath (cm)
c	sound velocity through medium (m/s)
d_b	bubble feret diameter (cm)
d_e	equivalent bubble diameter: diameter of a sphere having the same volume as the bubble in three dimensions (3D) or diameter of a circle having the same area as the bubble in two dimension (2D) (cm)
E	bubble eccentricity = b/h (-)
Eo	Eötvös number (or Bond number) = $g\rho_l d_e^2/\sigma$ (-)
h	bubble height (cm)
H_c	column height (cm)
H_l	the static liquid surface height (cm)
Mo	Morton number (or property) = $\nabla p\mu_l^4/\rho_l^2\sigma^3 : g\mu_l^4/\rho_l^2\sigma^2$ in a gravitational field (-)
M_s	mass of dry particles (kg)
V_g	superficial gas velocity (m/s)
V_l	superficial liquid velocity (m/s)
Z	travel distance (m)

Greek Letters

ε	Bed voidage (-)
ε_g	the gas holdup (-)
ε_l	holdups of the the liquid (-)
ε_s	holdups of the solid particle (-)
λ	wavelength (μm)
ρ_s	solid density (g/cm^3)

CHAPTER I

INTRODUCTION

Many investigations in fluidization technology have been conducted for investigating influences of various operating condition on its performance in real process. Even though, fluidization technology have been recognized as a well established technology, there still exist many unclear understanding, especially hydrodynamics of some systems such as gas-liquid-solid three phase fluidized bed system.

1.1 Background

Type of the reactor in the real-world processes can be classified to many categories such as bubble column, packed column, gas-solid fluidized bed, gas-liquid-solid three-phase fluidized bed reactor and so on each type of the reactor has difference in advantages and disadvantages. At present, Gas-Liquid-Solid Three-Phase Fluidized Beds (TPFB) have gained increasing attention because of their broad applications as reactors in various commercial processes ranging from petrochemical to biochemical industries. In order to achieve effective design of such reactor bubble characteristics, namely, bubble size, its distribution, and bubble rise velocity as well as its local holdup are of fundamental importance. So far many researchers (Chen et al., 1998; Comte et al., 1997; Kikuchi et al., 1996; Soong et al., 1996; Lee et al., 1990; Fan et al., 1985) have carried out investigations of these bubble characteristics in numerous different aspects and systems using various measuring techniques, for instance, employing intrusive devices (electro-conductivity probes, optical fiber probes), and using pressure sensor or non-intrusive ultrasonic transducers.

Chen et al., (1998) have conducted experiments to study the local behavior of bubbles in three-phase fluidized beds. Employing dual electro-conductivity probes, they

have found that the bubble behavior changes with respect to their position in the column and operating conditions, giving rise to different flow regimes. Average bubble size and local gas holdup are found to be second-order and fourth-order polynomial functions of the column radius position, respectively. Comet et al., (1997) have carried out experiments in a distinct system of inverse turbulent bed, in which loaded solid particles have density lower than that of the liquid. The operation of such column was governed by the superficial gas velocity, Unfortunately no holdup data was reported. Ultrasonic measurement has successfully been employed to detect the flow of bubbles inside a slurry reactor by Soong et al., (1996). According to their experimental results, the local gas holdup in a bubble column without solid particles has a well-defined correlation with the amplitude ratio of the ultrasonic signals transmitted through the column. However, at the present moment it may be perceived that there is still insufficient understanding of the actual behavior of bubbles existing in such system, judging from in the inconsistency among the information gathered by numerous previous investigations.

1.2 Objectives of Present Study

Recently, visual observation has become more efficient and promising due to the remarkable development in digital technology as well as image processing technology. Higher resolution together with faster recording capability allows this technique to be applied for tracing dynamic behavior of fast moving objects like bubbles rising in liquids. However, the visualization technique is appropriate and applicable for transparent column and could not be of use for opaque column (stainless steel or iron column). So the ultrasonic transmission technique is another alternative for inferior of the visualization technique. Using the visualization technique and the ultrasonic transmission technique to investigate the solid and gas holdups in the Three-Phase Gas-Liquid-Solid Fluidized Bed, which is fabricated in two-dimensional fashion, is object of the research. The effects of various operating conditions on bubble behavior and hydrodynamics have been investigated experimentally.

1.3 Scope of Study

Hydrodynamics and bubble behavior inside a two-dimensional Three-Phase Fluidized Bed have been investigated under various conditions, which were mentioned below.

1.3.1 Superficial gas velocities at 0 up to 40 mm/sec and superficial liquid velocities at 0 up to 40 mm/sec.

1.3.2 The solid particle employed were glass beads (with D_p nominal size of 250 and 500 micrometer) and Baker's yeast suspension with concentration of 0.1-2.0 % by weight would also be employed for simulating a system of microbial cell disruption(approximately size distribution 4-6 micrometer).

1.3.3 Both ultrasonic and visualization techniques were employed for investigating and measuring bubble behavior, i.e. its average size and size distribution, as well as bed hydrodynamic, i.e. each phase holdup and flow pattern.

CHAPTER II

LITERATURE REVIEW

In order to capture the present situation of study involving with three-phase reactor and relevancy, literature survey had been conducted. Most of literature could be found in various technical journals as well as textbooks. Here, the previous study was mainly focused on Three-phase Fluidized Bed and measurement of its hydrodynamic characteristics.

2.1 Three-Phase Fluidized Bed review

Yasunishi, A. et al., (1986) investigated the fundamental properties of gas bubbles and gas holdup in a slurry bubble column using a dual electroresistrivity probe method. It was found that the shape of the radial distributions of local gas holdup and bubble frequency was parabolic in range of mean solid holdup less than 0.2, over 0.2 they were decrease considerably in the region of r/R_w. The cross-sectionally averaged gas holdup decreased with increasing mean solid holdup.

Tzeng et al., (1993) Investigated macroscopic flow structures of gas-liquid and gas-liquid-solid fluidization systems using visualization technique in two-dimensional column under various operation conditions. The gas distributor in the column comprised 9 injectors which were individually regulated to generate desired, bubble injection rate, frequencies and bubble size. The formation of gross circulation can be interpreted in part based on two simplified flow conditions involving single bubbles rising in a stationary liquid and chains of bubbles injected in a batch liquid. The effects of particle size, inlet liquid velocity and gas flow distribution on the macroscopic flow structure were also examined.

Miura, H., and Kawase, Y., (1996) investigated effect of solids loading on hydrodynamic in three-phase fluidized beds with Newtonian and non-Newtonian fluids and Low-density plastic particles and glass beads were used as solid. This experiment found that the minimum fluidization velocity with Newtonian and non-Newtonian fluids decreased as superficial gas velocity increased. The bed voidage was influenced by gas holdup, the ratio of the wake volume to the wake volume to the bubble volume and the concentration of solid particles in the wake.

Chen, Z. et al., (1998) studied local bubble behavior including bubble Sauter diameter, bubble rise velocity, bubble frequency and local gas holdup at various radial and axial positions using a dual electro-conductivity probe in air-water-glass bead fluidization systems. It was found that the bubble characteristics differed significantly in various flow regimes, depending on the operating conditions; the radial distribution of bubble parameters also changed from one flow regime to another. Thus, it was concluded that local bubble behavior was necessary the modeling of three-phase fluidized beds.

2.2 Bed Characteristics measurement

Okamura et al., (1989) investigated relation between solid holdup to time ratio $[(t_a-t_b)/t_d]$ in three-phase fluidized bed which the solid phase are glass bead (D_p 194 micrometer) and activated carbon (D_p 1,540 micrometer), solid concentration 1.0 to 7.0 %wt using ultrasonic transmission technique. The experiment result found that solid holdup increased affected time ratio increased and size diameter of solid increased , time ratio decreased.

Uchida, S. et al., (1989) studied measurement of longitudinal distribution of solids holdup in three-phase reactor, which without being affected the presence of gas bubbles, using analyzing the shape and the phase lag or lead of an ultrasonic wave. This experiment found that the value of time ratio increase with increasing solid holdup and the measurement has been limited to a solid concentration of 5 % and the experiment

value measured by the ultrasonic technique a reasonable agreement with an empirical correlation previous experimental data obtained by other methods.

Soong, Y. et al., (1996) studied the slurry reactor which consist of two phase, tab water and nitrogen gas and measurement attenuation. It was found that gas velocity increased with the attenuation decreased. Including comparison result of the attenuation with hydrodynamic properties using dual conductivity probe. Then **Soong, Y. et al., (1997)** measurement the amplitude ratio and time ratio compared with gas velocity or solid concentration. For three-phase system, tab water, air and glass bead, it was found that gas velocity increased, amplitude ratio decreased but no effect to transit time. As solid concentration increased affected time ratio increased and transit time decreased.

Warsito et al., (1997) investigated the axial and radial distribution of gas and solid concentration in slurry bubble column using ultrasonic penetration technique. The macroscopic flow structure of the slurry bubble column was analyzed based on the structures of the phase distributions. The flow structure became important in determining the particle distribution in the column. The relationships between the gas bubble distribution, the flow structure and the particle concentration distribution are discussed. It was found that in the solid particles were partly concentrated in the region near but not adjacent to the column wall and in the region between the central bubble stream and the region where the vortical-spiral liquid flow is established.

Stolojanu, V. and Prakash, A. (1997) studied effect of solid concentration and gas holdup on the attenuation of ultrasonic signal in various condition using ultrasonic technique, solid concentration in this work up to 90 %wt and gas holdup 0-40 %vol, glass bead 35 micrometer. Comparison with the attenuation of solid concentration and gas velocity. In both cases, it was found that attenuation decreased as exponential function when solid concentration increased or gas velocity increased. As gas velocity increased, for high solid concentration system will be measured low attenuation. In additional, determination bubble size and its distribution using image photography technique.

From above researches, the main obstacle of the research consisting of both equipment and various conditions that used in experiment. For the previous research which using visualization technique has limitation in photography technology which couldn't capture clear picture of fast flow bubbles. Additionally, fludization technology has few research related to biofluidization for application of the fluidization technique in biotechnology. In part of ultrasonic technique, limitation of solid concentration and performance of measurable equipment was performed in these researches.

CHAPTER III

FUNDAMENTAL AND THEORETICAL ASPECTS

3.1 Three-Phase Fluidized Bed

3.1.1 General Bed Behavior

The overall fluid mechanics of hydrodynamic behavior of three-phase fluidized bed reflects the complex interactions between the three individual phases. The most prominent interaction occurs between the rising gas bubbles and the surrounding liquid-solid medium. Three distinct regions above the gas-liquid distributor are identifiable based on the prevailing physical phenomena: the distributor region, the bulk fluidized bed region, and the freeboard region. A schematic diagram is show in Figure 3.1.1.
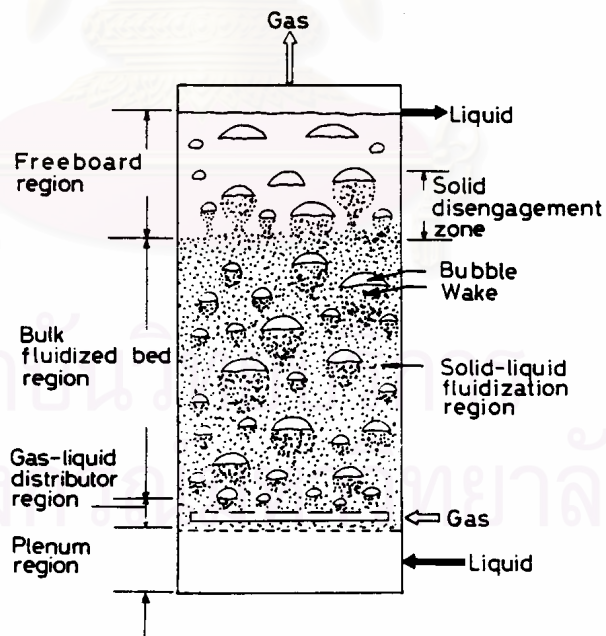
Figure 3.1.1 Schematic diagram illustrating each section in Three-Phase Fluidized Bed

(Redrawn from L.–S. Fan, Gas-liquid-solid fluidization engineering.1989, p.35.)

First, the distributor region refers to the region immediately above the gas-liquid distributor where gas spouts may occur. It includes the region from initial bubble formation to the establishment of the final bubble shape. The hydrodynamic behavior in the distributor region inherently depends on the gas-liquid distributor design and the physical properties of the liquid-solid medium.

Secondly, the bulk fluidized bed region includes the main portion of the fluidized bed. The hydrodynamic behavior in the bulk fluidized bed region varies drastically over large range of operating conditions based on the gas and liquid flow rate as well as the solid properties. The last section is the freeboard region which mainly contains liquid and gas bubbles with some solid particles entrained from the bulk fluidized bed region. Particle entrainment leads to a solids holdup profiles above the fluidized bed surface. The solid concentration decreases vertically in a manner similar to that in a gas-solid fluidized bed. The demarcation between the freeboard region and the bulk fluidized bed region is much more distinct for large/heavy particles than for small/light particles. Certainly understanding the hydrodynamic behavior in the freeboard region is essential for proper design, scale-up and operation of such apparata.

3.1.2   Phase Holdups

Among the various methods of determining the minimum liquid fluidization velocity, the method of direct observation of the bed was chosen for its simplicity and efficiency. The fluidization was considered to begin from the condition at which each visible particle continually changes its position.

Bed voidage ε and the holdups of the solid particle ε_s, of the liquid ε_l and of the gas ε_g are interrelated by the following relationships:

$$\varepsilon = \varepsilon_g + \varepsilon_l = 1 - \varepsilon_s \qquad (3\text{-}1)$$

The mean holdup of solid phase in the bed ε_s was calculated on the basis of the mass of dry particles M_s before their introduction into the column, the solid density (ρ_s),

the cross section of the column (*A*) and a measurement of the height (*H*) of the three-phase bed using the following equation:

$$\varepsilon_s = \frac{M_s}{\rho_s AH} \qquad (3\text{-}2)$$

Here, uncertainty in the estimation of ε_s is small and reaches 5% only when slugs caused by large gas velocities make the measurement of bed height difficult.

Determination of the gas holdup ε_g was carried out by visual measurement of the static liquid surface height H_l and column height H_c. The gas holdup was calculated from the following equation :

$$\varepsilon_g = \frac{(H_c - H_l)}{H_c} \qquad (3\text{-}3)$$

3.1.3   Macroscopic flow structures

In general, circulation structure in gas-liquid-solid system can be represented by four distinct flow regions based on the local liquid flow characteristics and bubble dynamics. These regions, namely descending flow, vortical flow, fast bubble flow, and central plume regions, have been investigated and could be described as shown in Figure 3.2.

Descending Flow Region. This region represents the area adjacent to the sidewalls where the liquid phase flows downward. At low gas velocities, this region is free of bubbles. At relatively high gas velocities, small bubbles are observed in this region and they can be either stationary or mobile depending on the bubble sizes and the descending liquid velocity. The descending velocity, however, is rather dynamic as most of the bubbles in this region are observed to move up and down. The dynamic nature of this region is related closely to the formation and movement of vortices nearby (that is, in the vortical flow region as discussed below).
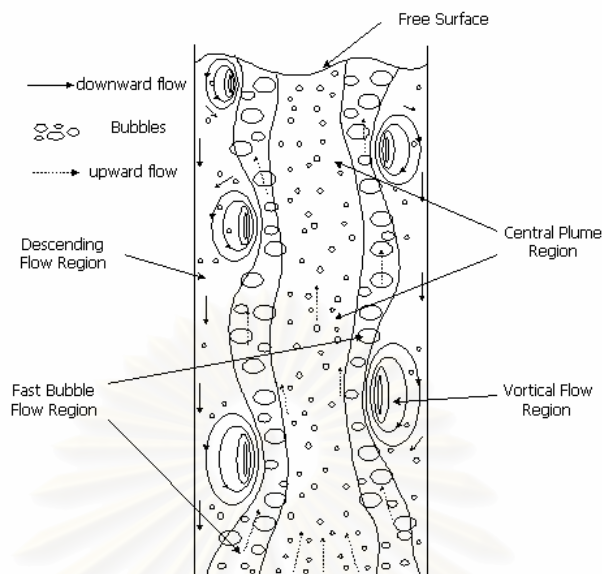
Figure 3.1.2 Classification of regions accounting for the macroscopic flow structure

(Redrawn from J.-W. Tzeng, AIChE., 1993, p.738)

Vortical Flow Region. Adjacent to the descending flow region is the vortical flow region characterized by the existence of moving (primarily descending) vortices. Vortices form steadily near the free bed surface. It is observed that vortices descend relatively steadily along the sidewalls at low gas velocities. As the gas velocity increases, vortices become rather unstable due to disturbances caused by small bubbles trapped in the cells and by large bubbles rising in the neighboring fast bubble flow region. The descending vortices will deform and eventually disappear after traveling over some distance; the deformation often yields new vortices in the nearly downward stream.

Fast Bubble Flow Region. This region is located between the vortical flow region and the central plume region, and is characterized by cluster bubbles at relatively low gas velocities or relatively high velocities by coalesced bubbles moving at high velocities. The coalesced bubble flow is typically noted for the churn-turbulent region. The bubble clustering or coalescence is caused by the migration of bubble chains near

the sidewalls promoted by the presence of the vortices near the gas distributor in the vortical flow region. The bubble coalescence occurs when the vortices are large and neighboring bubbles are sufficiently close. Note that the gas velocity required for transition from clustered bubbles to coalescence bubbles also depends on the extent of contamination of the liquid medium (Fan and Tsuchiya, 1990).

The existence of wakes of these large bubbles induces acceleration of the nearly trailing bubbles forming even larger bubbles at the upper part of the bed. These fast moving bubble-coalesced streams rise up in a wakelike manner. The wakelike bubble movement in this region intensifies the formation and the motion of vortices in the vortical flow region. This liquid vortical flow motion, however, also enhances the wavelike motion of the fast bubble stream. The vortices are confined between the sidewalls and the concavity of the fast-moving bubble-coalesced stream. In another way, the vortices are squeezed and then either decimated or pushed down along the descending flow region between sidewalls and convexity of coalesced bubble streams. Through the use of both visualization and full-field measurement techniques (Chen and Fan, 1992), this wavelike motion in the 2-D column is verified to translate into a spiral motion in the 3-D column as observed by Reese et al. (1992).

In the fast bubble flow region, bubbles are larger and rise faster than those in the central plume region (to be discussed later). In addition to coalescence, bubble break-up due to the local flow disturbance or turbulent stress takes place more significantly in this region than in the central plume region. Through observing the tracer particles and colored bed particles in the flow field, very little direct mass exchange is observed between the bubbly upward flow region and the vortical flow region except through the top and bottom of the fast bubble flow region, especially when the gas velocity is high. This observation implies that the fast bubble flow region serves as a baffle on the radial mass transfer for both the solid and liquid phases. This is because the axial liquid velocity in the fast bubble flow region is so large that the bed particles and liquid elements are essentially moving also axially. When the gross circulation is established, the fast bubble flow region dictates the macroscopic flow structure of the system.

Central Plume Region. The central plume region is in the column center and is surrounded by the fast bubble flow region. In this region, the distribution of bubble sizes is relatively uniform with less bubble-bubble interaction compared to those in the fast bubble flow region. At high gas velocities, the bubble chains in this region also move in a wavelike movement and swing laterally back and forth over almost the entire bed width. Such a swinging phenomenon is observed to synchronize with the wavelike bubble movement in the fast bubble flow region. The liquid is observed to flow downward in the region between each bubble chain at low gas flow rates. No such downward liquid flow pattern, however, has been observed for high gas flow rate conditions.

At a relatively low gas velocity (but larger than bubbly-churn turbulent transient velocity), the bubble-bubble interactions in the central plume region are not noticed despite the occurrence of significant bubble coalescence in the fast bubble flow region. Vortices form between two adjacent bubble streams, but their presence is only transient and their movement is rather random. On the other hand, at a high gas velocity, vertical bubble coalescence takes place which differs from lateral, coalescence-dominated bubble-bubble interaction in the fast bubble flow region.

3.1.4   Bubble behavior

3.1.4.1 Bubble shape and General behavior

Bubble in motion are generally classified by shape as sphere, oblate ellipsoidal and spherical/ellipsoidal cap, and so on. The actual shape of bubbles depends upon the relative magnitudes of relevant forces acting on the bubbles, such as surface tension and inertial force. Figure 3.1.3 shows sketches of bubble shapes thus classified in addition to other diversified shapes. The ellipsoidal shape, or more generally, spheroidal shape with a vertical axis of symmetry, represents generically all the bubble shape deformed from spheres in the intermediate size range. To be more specific, in liquids of low viscosity such as water, the shape of intermediate-size bubbles

is very irregular and unsteadily oscillates. In some liquids of high viscosity under quiescent conditions, the formation of skirts, thin annular films of gas trialing behind the rim of the large spherical-cap bubbles, has been observed.
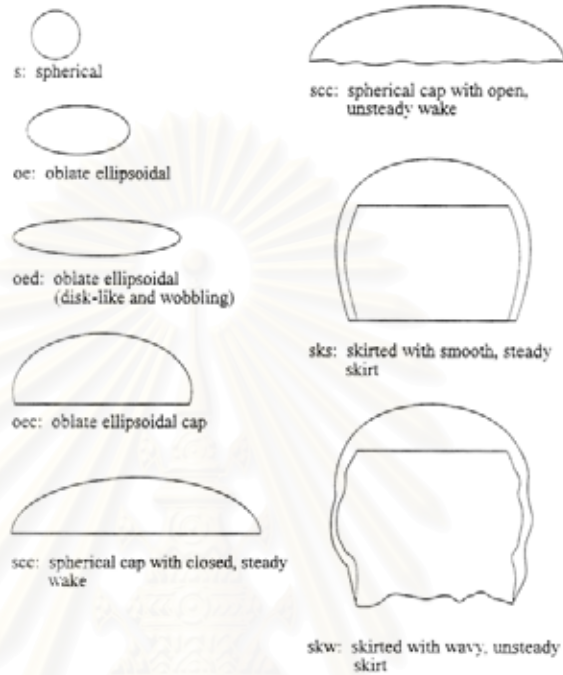
Figure 3.1.3 Sketches of various bubble shapes observed in infinite Newtonian liquids (after Bhaga and Weber, 1981)

In general, the bubble shape cannot be completely predicted unless one takes into account all the physical variables pertinent to the bubble rise phenomenon. Haberman and Morton (1953) suggested a dimensional analysis based on eight variables: the acceleration due to gravity (g), the terminal velocity of bubble rise (U_b), the diameter of volome-equivalent sphere (d_e), the density (ρ_l) and the viscosity (μ_l) of the surrounding medium, the interfacial tension (σ), and the density (ρ_g) and viscosity (μ_g) of the gas inside the bubble. From these variables five independent dimensionless groups can be derived. If the last two variables, ρ_g and μ_g, are considered negligible compared to ρ_l and μ_l, respectively, two groups can be eliminated. Under special circumstances, further simplification may be possible. For instance, for liquid of high viscosity or high Morton number, $Mo = g\mu^4/\rho_l\sigma^3$, the bubble shape is a function of the

bubble Reynold number, $Re_e = \rho_l d_e U_b / \mu_l$, alone; for low-$Mo$ liquids the shape also depends on Mo.

When the bubble is small (d_e less than 1 mm in water), surface tension forces predominate and the bubble shape is approximately spherical. For small spherical bubbles at very low Reynolds number, therefore, the flow does not separate from the bubble surface and the wake does not exist. For bubbles of intermediate size, the effects of both surface tension and the inertia of the medium flowing around the bubble are important. In addition, the bubble dynamics are profoundly influenced by liquid viscosity and the presence of surface-active contaminants.

Large bubbles, whose volumes are greater than 3 cm^3 (d_e larger than 18 mm) in general, are dominated by inertial or buoyancy forces with negligible effects of surface tension, viscosity and purity of liquid media. The bubble shape is approximately a spherical cap and generate a relatively large-volume wake.

In systems other than gas-liquid systems, such as gas-slurry bubble columns and gas-liquid-solid fluidized bed of small, light particles, bubble behavior has been often observed to resemble that in viscous liquids, e.g., large bubbles assume the spherical-cap shape mentioned above. This similarity is attributed to the premise that the liquid-solid mixture in such systems can be regarded as a pseudo-homogeneous medium of apparently higher viscosity compared to the suspending liquid.

3.1.4.2 Bubble Motion

As a bubble rises through a continuous medium, work is done on the medium by the bubble by the bubble at a rate equal to the bubble rise velocity times the net buoyancy force acting on the bubble (Fan, L.-S, and Tsuchiya, K., 1990). In a very viscous medium, energy generate through this work can be completely dissipated in the medium due to viscosity (laminar viscous dissipation), resulting in a purely rectilinear motion of the bubble. In a low viscosity medium, however, the energy generated by the rising bubble may not be consumed by the viscous dissipation alone; some energy is released through wake shedding (turbulent dissipation) which induces bubble oscillations known as secondary motion. This secondary motion is claimed to be closely

associated with the periodic shedding of vortices behind the bubble. Bubble oscillations are known to start with the one set of vortex shedding from the wake. (e.g., Edge and Grant, 1971; Tsuchiya and Fan, 1986)

Secondary motion of the bubble, which has been observed over a wide range of bubble Reynolds numbers, is very complicated. It can be any extent of superimposition of two types of motion:

(1) A "rigid body" type vibration characterized by zigzag or spiral trajectories and/or rocking and

(2) A "non-rigid body" deformation characterized by shape dilation or base oscillations (Clift et al., 1978; Bhaga and Weber, 1981). The following discusses the motion of freely rising bubble, when they are regarded as rigid bodies. This is followed by some discussion on fluctuations in bubble shape.

3.1.4.3 Type of Bubble Motion

The bubble rising path (defined as the trajectory of the bubble centroid) and change in its orientation (defined as the angle between the bubble major axis and the vertical axis of the system) of the bubble are known to be strongly related to the bubble shape. The motion of the spherical bubbles is usually rectilinear. Once the bubble becomes deformed into the oblate spheroid, instability sets in the results in a spiral or zigzag trajectory; at the same time the bubble orientation changes in such a way that the bubble major axis tends to be perpendicular to the direction of instantaneous motion (Miyagi, 1925; Haberman and Morton, 1953), although some phase shift in the orientation angle is observed for some bubble sizes. (Hibino, 1969; Tsuge and Hibino, 1971). As the bubble form a ellipsoidal to spherical-cap shape, the radius of the spiral or the amplitude of the zigzag gradually decreases and the motion becomes rectilinear, but with rocking. The spherical-cap bubble, as its size increases, eventually rises rectilinearly.

The above description is generally valid in systems of low Morton number, while in high-Mo systems, such as mineral oil ($Mo = 1.5 \times 10^{-2}$) and corn syrup

aqueous solutions ($Mo = 1.6 \times 10^{-4}$-2.1×10^{-3}) (Haberman and Morton, 1953), the bubble motion is always rectilinear regardless of bubble shape. The bubble Reynolds number must be sufficiently high (with d_e usually on the order of magnitude of 100) for the bubble to oscillate. Bubbles in high-Mo systems, however, usually go through a transition from a spherical to spherical-cap shape before Re_e reaches 100 (Haberman and Morton, 1953; Bhaga and Weber, 1981).

3.1.4.4 Spiral or Zigzag Motion

The spiral path of the bubbles assumes either a clockwise or counter-clockwise direction, depending upon conditions at generation (Haberman and Morton, 1953). The zigzag path results from a side-to-side movement in the vertical plane, the orientation of which has been observed both to remain constant (Garner and Hammerton, 1954; Saffman, 1956; Hartunian and Sears, 1957) and to change randomly (Hibino, 1969; Tsuge and Hibino, 1971) as the bubble rises. All investigators, however, reported that there is no apparent tendency for the bubble to prefer any particular plane.

There is no unanimous agreement on the conditions which decide whether the oscillating rise path of ellipsoidal bubbles is spiral or zigzag; however, it has been claimed that the mode of oscillation is controlled by mainly two factors:

(1) The physical properties of the surrounding medium, especially in the presence or absence of surfactants (Garner and Hammerton, 1954; Kubota et al., 1967; Tsuge and Hibino, 1971).

(2) The way the bubble is released and thus its initial motion (Miyagi, 1925; Saffman, 1956).

The dependence of the bubble rise mode on the first factor is generally accepted in the literature to be as follows. When a bubble rises through a liquid with impurities, its centroid follows zigzag path, while in pure system the bubble exhibits a spiral path when the bubble is small ($1.5 < d_e < 3$-5 mm in distilled water) or a zigzag path when the bubble size is large (3-$5 < d_e < 10$-15 mm in distilled water) (Garner and

Hammerton, 1954; Kubota et al., 1967; Hibino, 1969; Tsuge and Hibino, 1971; Tsuge, 1982).

The effect of any impurities, which act mainly as surface-active agents, is significant even at very low concentrations. Therefore, the majority of the existing experimental results are regarded as those in impure systems unless great care is exercised to eliminate contaminants from the system. Note that some organic solvents of reagent grade are known to behave as pure media (Tsuge and Hibino, 1971).

The contribution of the second factor has been less extensively studied. Some useful observations, however, were made by Saffman (1956) for air bubbles in filtered water over size range d_e = 1.0 – 4.6 mm to clarify the effect to disturbances introduced at the bubble injection and induced by the external flow. The following summarizes his observations:

(1)   For d_e<1.4 mm, the bubble rise rectilinearly with no oscillations.

(2)   For 1.4 < d_e < 2.0 mm , bubble always zigzagged.

(3)   For d_e > 2.0 mm, the bubble zigzagged if the injection was made with minimum disturbances.

The bubble, however, moved along the spiral path once it was hit by an obstacle placed above the injector or in the bubble path. The spiral motion was also observed when a large bubble broke up at the injector exit and a part of it (with d_e usually greater than 2.6 mm) rose. This spiral motion could be attributed to disturbances induced by the breakup at the injection moment.

(4)   If a second bubble with d_e>2.0 mm was injected immediately after the first bubble, the trailing bubble tended to follow the same motion as the leading one. However, a bubble of d_e < 2.0 mm always moves with zigzag trajectory, even if it was released in the wake of a spiraling bubble.

(5)   The zigzag motion could change into a spiral one, but the reverse never happened.

Based on these observation Saffman (1956) concluded that (1) the zigzag motion occurred with the first instability, (2) it was inherently unstable to external

disturbances, and (3) if such disturbances were sufficiently large, a spiral motion occurred.

In summary, it is speculated that the bubble oscillates in a zigzag path (1) when the gas-liquid interface is "rigid" under the presence of surface contaminants or (2) when the bubble is introduced with minimum disturbances. The spiral path, on the other hand, may prevail (1) for bubbles with small size and "clean" surface or (2) in the presence of external disturbances.

3.1.4.5 Bubble Orientation

When the bubble exhibits zigzag, spiral or rocking motion, it also changes its orientation, as indicated earlier. The bubble orientation is usually described in terms of the angle of attack (α) defined as the angle between the bubble major axis and direction of the undisturbed incident flow. The variation in the angle of attack is closely associated with the variations in wake properties due to wake shedding.

An effective measure of the orientation of each bubble is the maximum deviation in α from 90°. This deviation is to be called the bubble inclined angle (θ_b). Figure 3.4 (a) shows θ_b measured for bubbles rising in tab water and in a water-fluidized bed containing various solids (Miyahara et al., 1988). As can be seen in the figure, for Re_e up to about 4000, θ_b is almost independent of Re_e with an average value of 25°. θ_b sharply decreases with increasing Re_e in transition range of $4000 < Re_e < 5000$. Miyahara et al. (1988) claimed that this demarcation Reynolds number ($Re_e = 5000$) also marks the transition from an ellipsoidal to spherical-cap bubble shape.
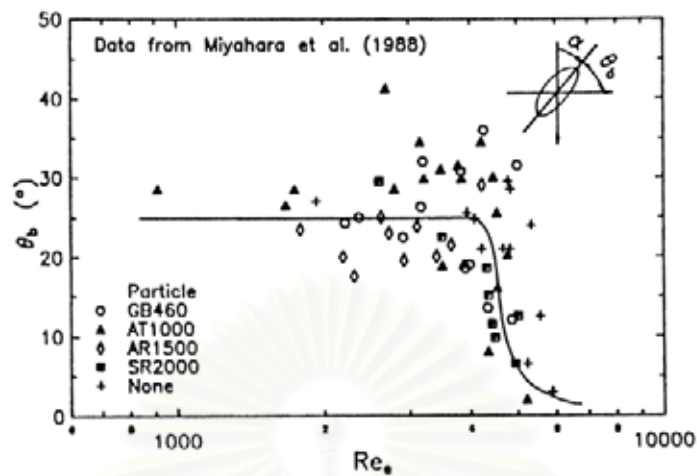
Figure 3.4 (a) Bubble inclined angle in a three-dimensional water-solid fluidized bed(after Miyahara et al., 1988)

Miyahara et al. (1988) noted that the mode of oscillation for smaller bubbles (Re_e < 5000) was a gyrational motion, which corresponded to rocking in two dimension; however, the bubble itself was not observed to revolve about its central axis. A vertically rising bubble thus followed helix-like path. As the bubble size increased (Re_e > 5000), bubble gyration became almost negligible (i.e., with very small θ_b) and the bubble rose almost rectilinearly.

Figure 3.4 (b) shows the corresponding plot for two-dimensional system (Tsuchiya, 1987). Although the data exhibit considerable scatter, the overall trends resemble those in a three-dimensional system. θ_b scatters around 25 for Re_e up to about 2000 and gradually (not abruptly as in the three-dimensional case) decreases with increasing Re_e in a range 2000-5000. At a Re_e around 2500 (or Re_b, based on bubble breadth, around 35000) the transition from an elliptic/circular-cap bubble with zigzag/rocking motion to a circular-cap bubble with base oscillations occurs (Tsuchiya and Fan, 1986).
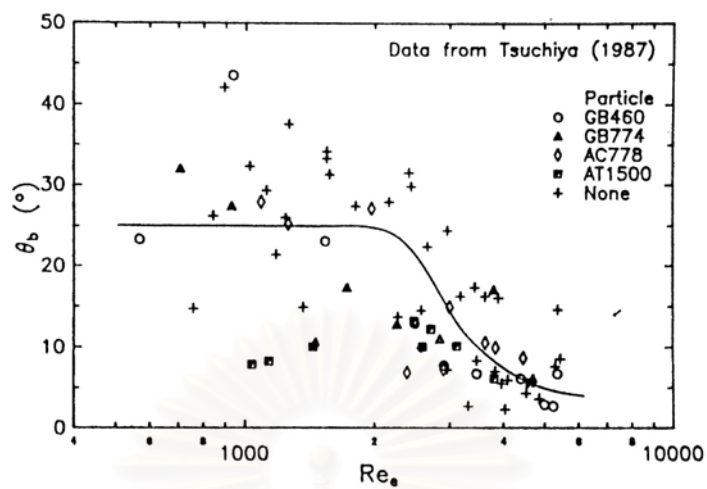
Figure 3.4 (b) Bubble inclined angle in a two-dimensional water-solid fluidized bed (from

Tsuchiya, 1987)

3.2 Fundamental of Ultrasound

3.2.1 Basic Principles

Sound generated above the human hearing range (typically 20 kHz) is called ultrasound. However, the frequency range normally employed in ultrasonic nondestructive testing and thickness gaging is 100 kHz to 50 MHz. Although ultrasound behaves in a similar manner to audible sound, it has a much shorter wavelength. This means it can be reflected off very small surfaces such as defects inside materials. It is this property that makes ultrasound useful for nondestructive testing of materials.

The Acoustic Spectrum in Figure 3.2.1 can be separated into 3 ranges of frequencies. The Ultrasonic Range is then broken down further into 3 sub sections.
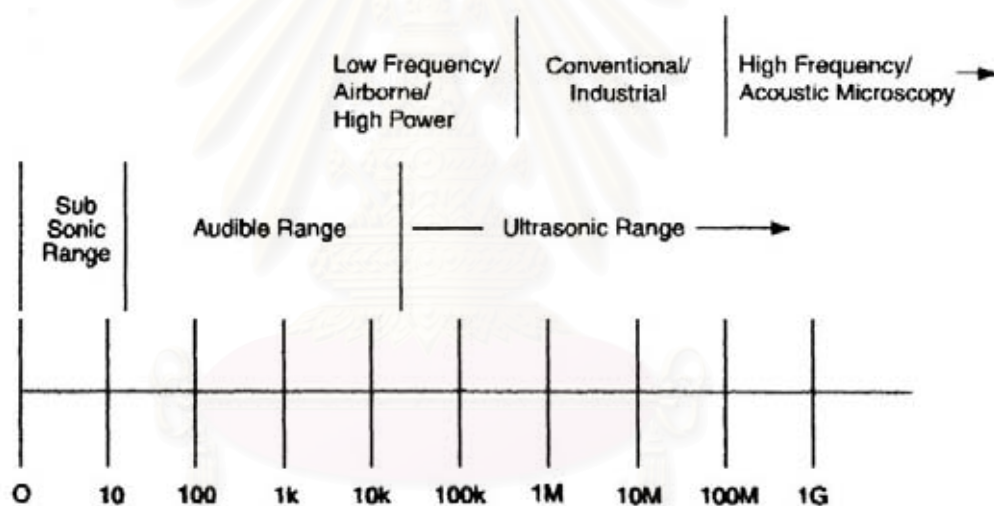
Figure 3.2.1 Range of sound in various specification of operation

(Redrawn from Panametrics, 1995)

3.2.1.1 Frequency, Period and Wavelength

Ultrasonic vibrations travel in the form of a wave, similar to the way light travels. However, unlike light waves, which can travel in a vacuum (empty space), ultrasound requires an elastic medium such as a liquid or a solid. Shown in Figure 3.6 are the basic parameters of a continuous wave (c_w). These parameters include the wavelength (λ) and the period (T) of a complete cycle.
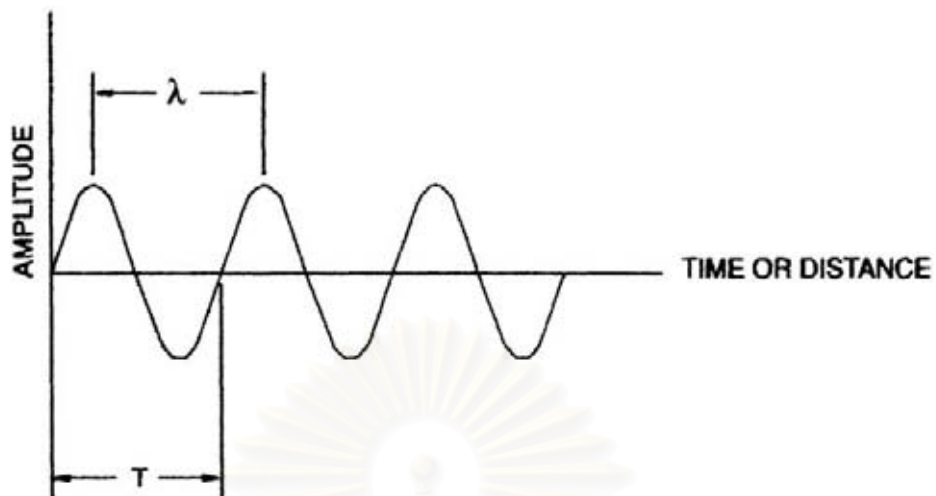
Figure 3.2.2 the basic parameters of a continuous wave

(Redrawn from Panametrics, 1995)

The number of cycles completed in one second is called frequency (f) and is measured in Hertz (Hz),

The time required to complete a full cycle is the period (T), measured in seconds. The relation between frequency and period in a continuous wave is given in Equation 3-4.

$$f = 1/T \qquad (3-4)$$

3.2.1.2 Velocity of Ultrasound and Wavelength

The velocity of ultrasound (c) in a perfectly elastic material at a given temperature and pressure is constant. The relation between c, f, l and T is given by Equation 3-5 and 3-6

$$\lambda = c/f \qquad (3\text{-}5)$$

$$\lambda = cT \qquad (3\text{-}6)$$

Table 1 lists the longitudinal and shear wave velocities of materials that are commonly tested with ultrasonics.

Table 1 Acoustic properties of Materials

Material	Longitudinal Velocity		Shear Velocity		Acoustic Impedance
	(in/μs)	(m/s)	(in/μs)	(m/s)	(kg/m^2 s x 10^6
Acrylic Resin (Prespex®)	0.107	2,730	0.056	1,430	3.22
Aluminium	0.249	6,320	0.123	3,130	17.06
Glycerine	0.076	1,920	-	-	2.42
Iron	0.232	5,900	0.127	3,230	45.93
Polystyrene	0.092	2,340	-	-	2.47
Polyvinylchloride	0.094	2,395	0.042	1,060	3.35
Silver	0.142	3,600	0.063	1,590	37.76
Steel, 302	0.223	5,660	0.123	3,120	45.45
Zinc	0.164	4,170	0.095	2,410	29.61
Water (20 ^{o}C)	0.058	1,480	-	-	1.48

Conversion Factor : 1 m/s = 3.937 x 10^{-5} in/μs

Source : Nondestructive Testing Handbook 2nd Edition Volume 7 Ultrasonic Testing ASNT 1991 ed Paul McIntire

3.2.2   Ultrasonic Transducer

An ultrasonic transducer is any device that converts one form of energy to ultrasonic wave and vice versa. In general, an ultrasonic transducer converts electrical energy to mechanical energy, in the form of sound, and vice visa. The main components are the active element, backing, and wear plate which illustrative in Figure 3.2.3.
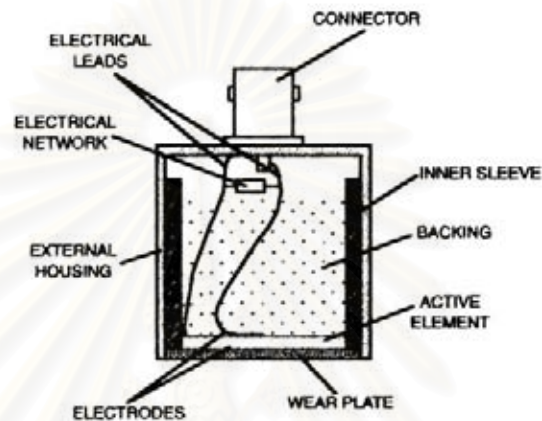
Figure 3.2.3 Main components of Ultrasonic Transducer (Panametric Inc., 1995)

(Redrawn from Panametrics, 1995)

3.2.2.1 Active Element

The Active Element, which is piezo or ferroelectric material, converts electrical energy such as an excitation pulse from a flaw detector into ultrasonic energy. The most commonly used materials are polarized ceramics which can be cut in a variety of manners to produce different wave modes. New materials such as piezo polymers and composites are also being employed for applications where they provide benefit to transducer and system performance.

3.2.2.2 Backing

The backing is usually a highly attenuative, high density material that is use to control the vibration of the transducer by absorbing the energy radiating from the back face of the active element . When the acoustic impedance of the backing matches

the acoustic impedance of the active element. The result will be heavily damped transducer that displays good range resolution but may be lower in signal amplitude. If there is mismatch in acoustic impedance between the element and the backing, more sound energy will be reflected forward into the test material. The end result is a transducer that is lower in resolution due to a longer waveform duration. But may be higher in signal amplitude or greater in sensitivity.

3.2.2.3 Wear Plate

The basic purpose of the wear plate is to protect the transducer element from the testing environment. In the case of contact transducer, the wear plate must be a durable and corrosion resistant material in order to withstand the wear caused by use on material such as steel. For immersion, angle beam, and delay line transducers the wear plate has the additional purpose of serving as an acoustic transformer between the high acoustic impedance of the active element and the water, the wedge or the delay line all of which are of lower acoustic impedance. This is accomplished by selecting a matching layer that is $\frac{1}{4}$ wavelength thick (l/4) and of the desired acoustic impedance (the active element is nominally $\frac{1}{2}$ wavelength). The choice of the wear surface thickness is based upon the idea of superposition that allows waves generated by the active element to be in phase with the wave reverberating in the matching layer. When signals are in phase, their amplitude wave enters the test piece.

Figure 3.2.4 shows the active element and the wear plate, and when they are in phase. If a transducer is not tightly controlled or designed with care and the proper materials and the sound waves are not in phase, it causes a disruption in the wavefront.
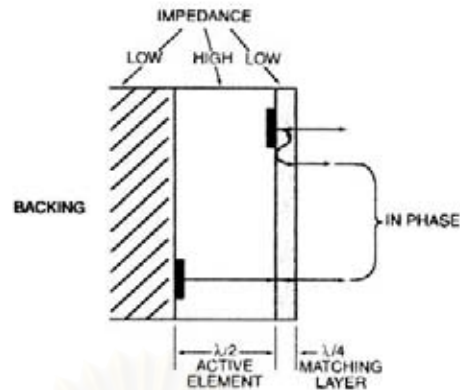
Figure 3.2.4 Shown the active element and wear plate, and when they are in phase.
(Redrawn from Panametrics, 1995)

3.3 Ultrasonic transmission technique

Measuring principle

Suppose that ultrasonic burst wave is emitted from a ultrasonic transmitter into a liquid-solid system at a particular temperature. The output wave is received at the ultrasonic receiver which is placed at certain distance away. Since the velocity of the ultrasonic wave is different in each phase shown in table 3.1, the transmission time in the liquid-solid particle system is affected by the volume concentration of solid particles on the path of the transmission of the wave. On the other hand, suppose that the ultrasonic burst wave is emitted into a gas-liquid system. The received wave in the liquid system is given by a dotted line as shown in Figure 3.2.5. when a certain amount of solid particles are added to the system, by above reason, the output wave may show a shorter transmission time.

When the wave is emitted into a gas-liquid-solid particle system, in which gas bubbles are dispersed as well as solid particles of the same concentration as in the case above at the same temperature, the output wave received at the receiver consists of the following three components:

(1) Some components of the wave are transmitted through the liquid-solid particles phase without encountering any bubbles. The output wave shows the same phase lead as that of the solid line in figure 3.2.5.

(2) Some components are affected by not only solid particles but also by bubbles and show a phase lead as shown by point t_c in figure 3.2.5(b). Although it is not known why bubbles cause the phase lead, the phase lead due to the existence of bubbles is always given by the time difference of $(t_b - t_c)$.

(3) Some components are completely blocked by bubbles and the output wave has zero-amplitude.

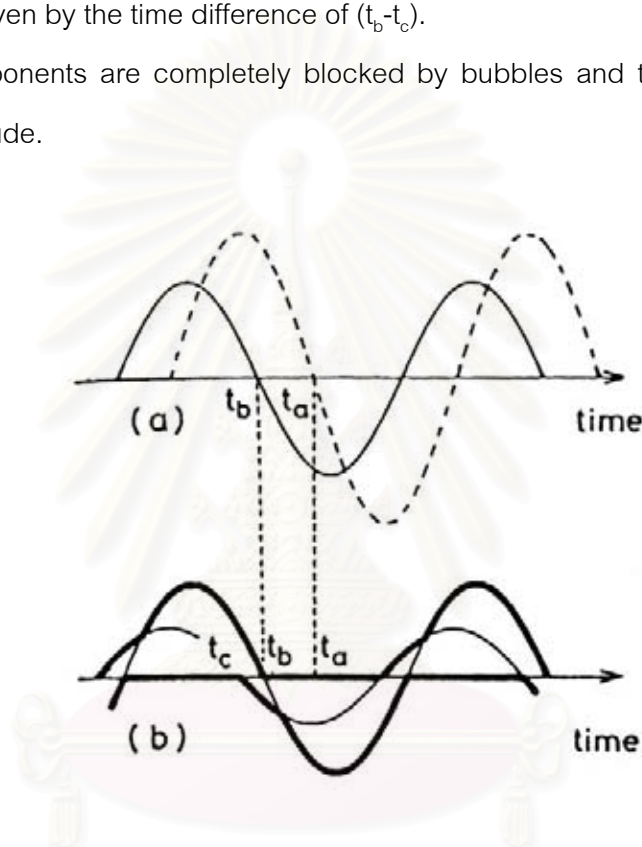Figure 3.2.5 Effect of gas, liquid and solid on phase lead and amplitude of ultrasonic wave.(Redrawn from S. Uchida et al., Proceeding of ASCON 1988)

The following general equation describes the attenuation of an acoustic wave passing through a medium:

$$dA = - \alpha A \, dZ \qquad (3\text{-}7)$$

Equation 3-7 can be integrated and arranged to give

$$A/A_0 = exp(-\alpha Z) \qquad (3\text{-}8)$$

A_0 is the signal amplitude transmitted without particles in the liquid and α is the amplitude attenuation coefficient. The attenuation of a mixture in general depends upon a number of factors which include gas holdup, bubble size, applied frequency and scattering coefficient (Chang et al., 1984; Stravs and Stockar, 1985; Bensler et al., 1987). For estimation of interfacial area by ultrasonic technique. The following relationship was found to apply by Stravs and Stockar (1985) and Bensler et al. (1987):

$$A/A_0 = exp[aZ/8\theta\ (k\ d_{sm}\ /\ 2)]$$

(3-9)

Here a is the volumetric interfacial area, Z is the travel distance in the the path. θ is the scattering coefficient, k is the wave number of the ultrasonic waves and d_{sm} is the Sauter mean diameter of particles of interest. Equation 3-9 can be modified to express amplitude ratio as a function of gas holdup when the following relationship applies between interfacial area, a , gas holdup, ε_g and Sauter mean diameter, d_{sm}:

$$a = 6\varepsilon_g/d_{sm}$$

(3-10)

Then,

$$A/A_0 = exp\ [\ Z\ /\ 8\ \theta\ (3\ k\ \varepsilon_g)]$$

(3-11)

CHAPTER IV

EXPERIMENTAL APPARATUS AND PROCEDURE

4.1 Experimental Set-up

A two-dimensional Three-Phase Fluidized Bed shown in Figure 4.1.1 will be employed to investigate the air bubbles flowing inside. (See drawing of two dimensional column in APPENDIX B)
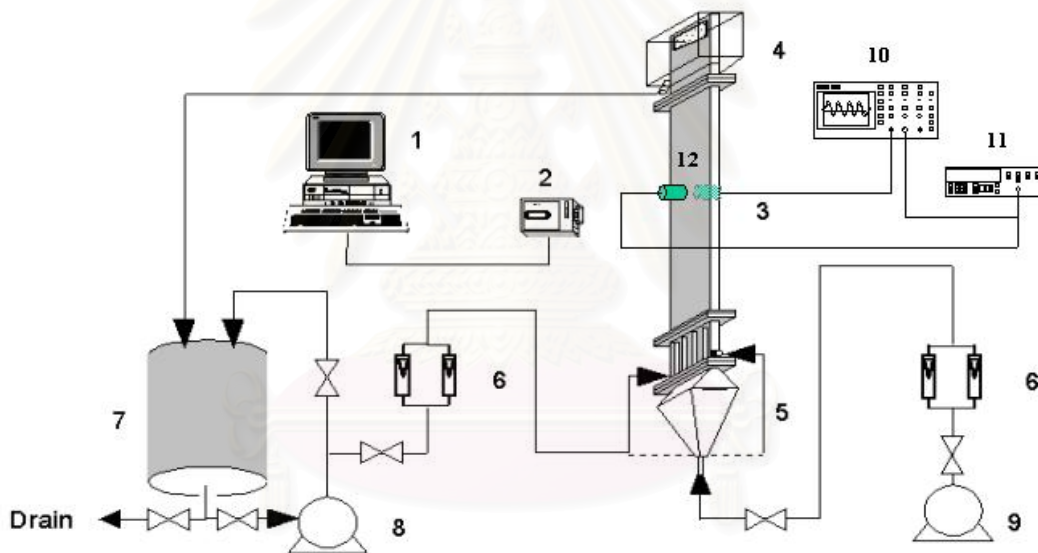
1.Computer 2. Digital Video Camera 3. Column 4. Overflow 5. Distributor
6.Flow meters 7. Water storage tank 8. Liquid pump 9. Air compressor
10. Digital Real-Time Osilloscope 11. Signal Generator 12. Ultrasonic transducer

Fig. 4.1.1 Schematic Diagram of Three-Phase Fluidized Bed Employed in the experiment.

4.1.1 Digital Video Camera (See Figure 4.1.2)

The digital video camera is used in the experiment was SONY series TRV20E. It can use snap shot mode and moving mode for recording result. For snap shot mode can be capture continuous pictures which interval of capturing picture was 2 pictures per second and resolution approximate 300,000 to 1,000,000 pixels.

Fig. 4.1.2 Digital Video Camera (SONY series TRV20E)

4.1.2 Computer and Video Graphic Acceleration Card (See Figure 4.1.3)

The computer is used in the experiment was Pentium III 550E and installed the VGA Card (ASUS AGP-V2400TNT/TV/8MB model) which can be capture the moving picture from the digital video camera in AVI file (1 to 30 frame per second) using LIVE3400 Program.

Fig. 4.1.3 Video Graphic Acceleration Card (ASUS AGP-2400TNT Model)

4.1.3 Gas and Liquid Flow Meter (See Figure 4.1.4)

Two sizes gas and liquid flow meter are used in the experiment to the control the flow rate of liquid phase (water and yeast suspension in water). The big gas flow meter was used for adjusting coarse the flow rate (ranged from 1,000 to 10,000 liters/min) and the small gas flow meter was used for adjusting fine the flow rate (ranged from 1,000 to 10,000 liters/min). Also, the big liquid flow meter was used for adjusting coarse the flow rate (ranged from 100 to 1,000 liters/hour) and the small liquid flow meter was used for adjusting fine the flow rate (ranged from 15 to 160 liters/hour)

(a)   (b)

Fig. 4.1.4 Flow Meters (a) Gas Flow Meter (b) Liquid Flow Meter

4.1.4 **Digital Real-Time Oscilloscope** (See Figure 4.1.5)

The digital real-time oscilloscope was Tektronik serie TDS 210 which has 60 MHz bandwidth. The oscilloscope display signals that carry out from the signal generator and the receiver as amplitude signal and frequency form.

4.1.5 Digital Real-Time Oscilloscope

4.1.5 **Signal Generator** (See Figure 4.1.6)

The signal generator was ARBITRARY FUNCTION GENERATOR of SONY Tectronik serie AFG 310. The generator was used for providing the simulated sine wave form at 2.25 MHz and 18.2 V for the ultrasonic transducer.

Fig. 4.1.6 Sony Signal Generator

4.1.6 **Ultrasonic Transducer** (See Figure 4.1.7)

The ultrasonic transducer was made by PANAMETRICS, INC. and transducer part number was V106-SB. The transducer was contact and VIDEOSCAN transducer type which provide heavily damped broadband performance. It was best choice in applications where good axial or distance resolution was necessary or in tests that require improved signal-to-noise in attenuating or scattering materials.

Fig. 4.1.7 Ultrasonic Transducer (Transmitter and Receiver)

4.1.7 **Particle Entrainment Prevention** (See Figure 4.1.8)

The particle entrainment prevention was made from 100 mesh screen plate and installed at the both side of column on the top of overflow section before fluid was overflow from the column.

Fig. 4.1.8 Particle Entrainment Preventing Section

4.2 Experimental Method for Visualization Technique

    4.2.1 Procedure

    1. In each experiment, air and yeast suspension in tab water (0.1 - 5 %wt) were employed as gas and liquid phase for fluidizing solid particles, which were glass beads (Diameter 250 and 500 micrometer) and yeast particles.Three section of 2D Three-phase Fluidized Bed consist of distributor section, column and overflow section. Inner column, width 300 mm, thickness 15 mm and height 900 mm (Overflow section height about 200 mm) Air and tap water were fed into the column through 14 holes of gas distributors (2.75 mm ID) and 30 holes of liquid distributors (4.76 mm ID) with the use of a compressor and a pump, respectively. Superficial velocity of both gas and liquid were varied in ranges of 0-4 centimeter/sec. Glass beads whose average size was 250 and 500 micrometer were loaded into the column before feeding air and water. Total solid concentration, which was simply calculated by the preloaded mass divided by the total volume of the column was varied in a range of 0 – 40 percent by weight.

    2. Two modes of operations with respect to liquid flow were carried out in this work. In either mode, solid particle was blocked by the particle preventing entrainment section on the top of the column for maintain solid concentration escaping out of the

column, because in the overflow screen with opening of 80 mesh was set up for blocked solid particles.

    1.1. Batch operation : The Three-Phase Fluidized Bed will be operated under $U_l = 0$, while the air was fed continuously through the compressor.

    1.2. Continuous operation : Both air and water were fed continuously with superficial velocity of 0 – 4 cm/sec.

    3. The digital images of bubbles and liquid flow as well as solid particles were captured and recorded at 3 positions along the vertical direction of the two-dimensional column using Digital Video Camera (Sony series TRV 20E).

    Remark: Both still pictures and moving picture were captured at all positions. The still pictures were transferred to a personal computer using PictureGear Program (Version 4.1 Lite) as JPG formatted files while ASUS Live 3400 program was employed for capturing the moving picture in AVI formatted files.

    4. After calibration, typical images of bubbles were analyzed by using an image processing program (Image Pro V. 3.0). The analysis provides the information on the local bubble size distribution.

4.2.2 Image Processing Procedure

4.2.2.1 Calibration Program

- Start up program by Clicking at the Icon of **Image-Pro Plus 3.0**. (See Figure 4.2.1)

- Open a file of calibration scale image. (See Figure 4.2.2)

- Click at "Measure" on the Menu Bar and click at "Calibration", then select "Spatial" Command. (See Figure 4.2.3)

- Click at "New" command and set a new name of this scale at Name Label and change Measurement Unit to centimeters. (See Figure 4.2.4)
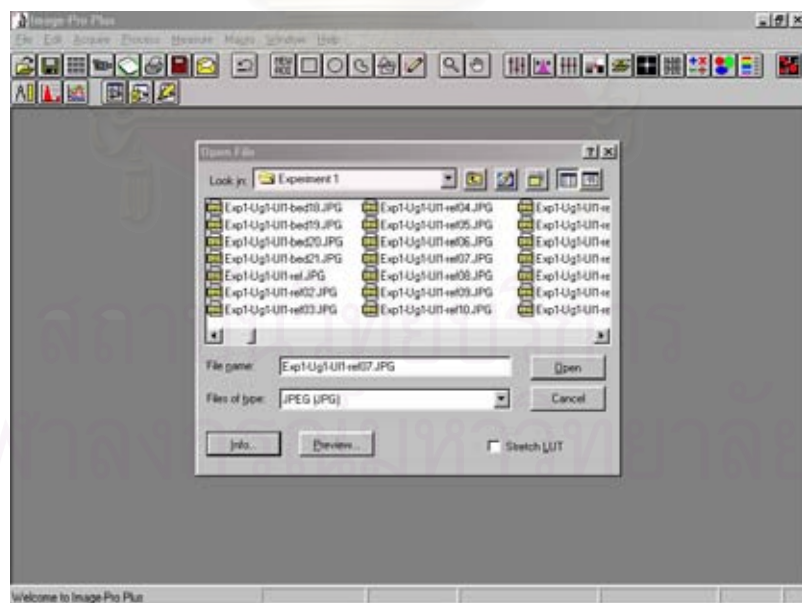
Figure 4.2.1 Calibration procedure.

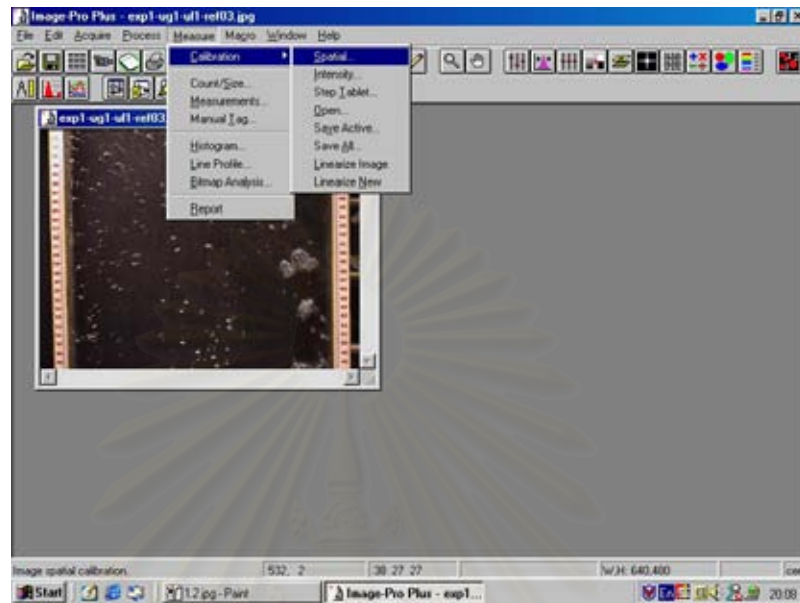Figure 4.2.2 Calibration procedure.
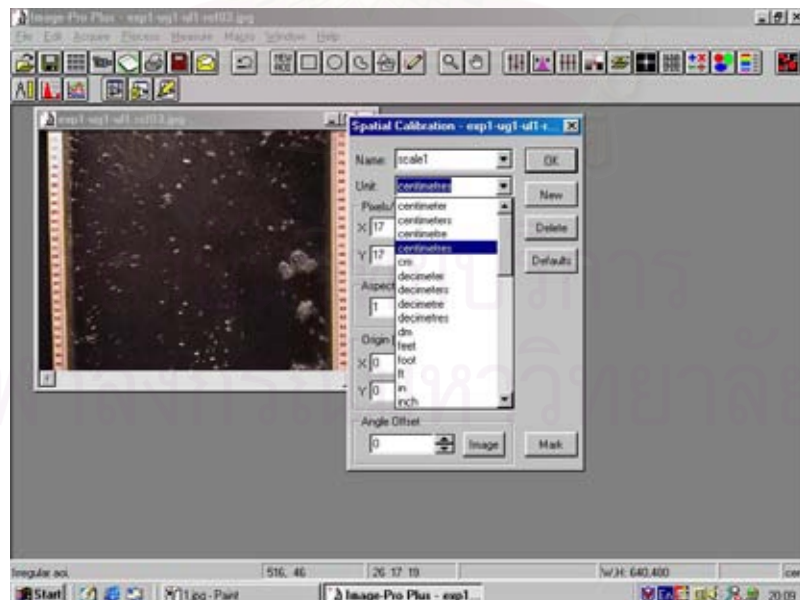
Figure 4.2.3 Calibration procedure.

Figure 4.2.4 Calibration procedure.

- Click back to the picture and then zoom picture at the position of scale. After clicking at the image of calibration scale, a white line will appear. Then using mouse to click at the edges of the line to move it overlay on the line of reference scale image. If the scale was completely equal to the reference, then define the value in "Scaling" window as 1 and then click OK. The program will be automatic save this calibrating scale. (See Figure 4.2.5)

4.2.2.2 Bubble Size Distribution Measurement

- Open the bubble image file. (See Figure 4.2.6)

- Click at "Edit" command on the Menu Bar and choose at "Convert to" command then choose "Gray Scale" command for converting the image into Black and White format. (See Figure 4.2.7)

- Click at the binarized image, "Threshold" Window will be shown. One has to adjust the value of threshold for eliminating the noise present in the images. Adjusting can be done by clicking mouse at the adjusting arrow and sliding it to right or left until the image can be seen clearly. (See Figure 4.2.8)

- Click at "Measure" command in the menu of "Count/Size" to choose "Select Measurement" command. Then select measurement type which was "Size(length)" by sliding vertical scroll bar at the left of measurement window. Size(length) command will appear at the righthand side of Filter ranges. (See Figure 4.2.9)

- Click at "Size (length)" in "Filter ranges" textbox and change the lower and upper limit size of the selected object by filling the appropriate value into at start and end box, respectively. After click "OK" button, "Count/Size Option" window was disappeared. (See Figure 4.2.10)

- After clicking at "Options" command in "Count/Size" window, select type of Outline Style which should be "Filled", Label Style as "Object#" and Label Color as "Yellow" and then click at "Fill Holes" checkbox. Then click OK. (See Figure 4.2.11)
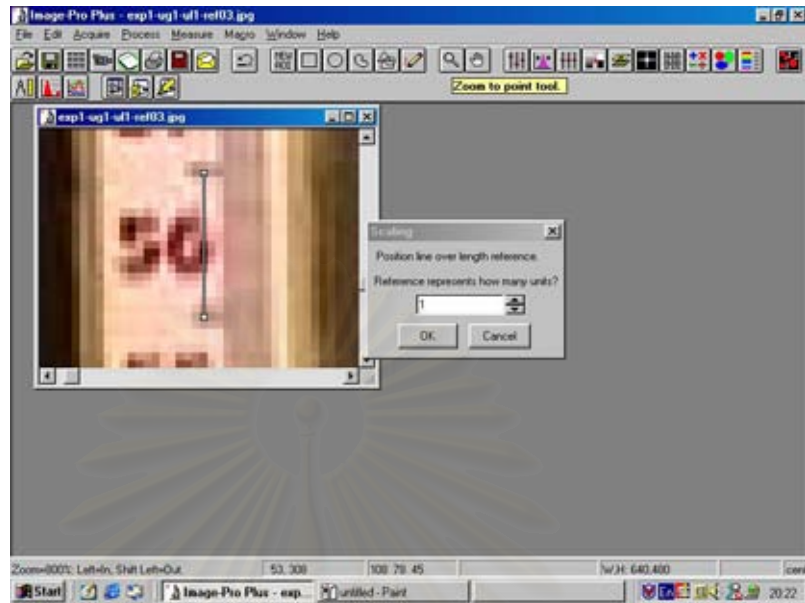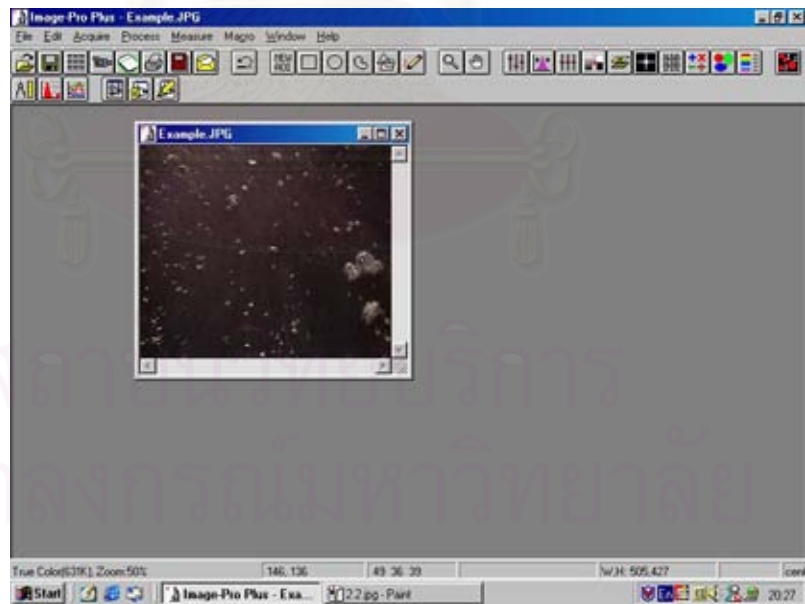
Figure 4.2.5 Calibration procedure.
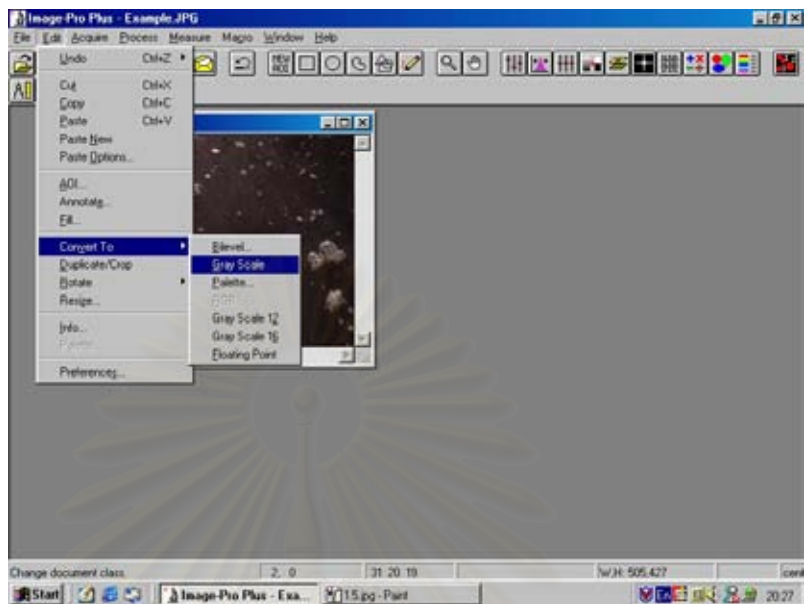

Figure 4.2.6 Bubble size measurement.
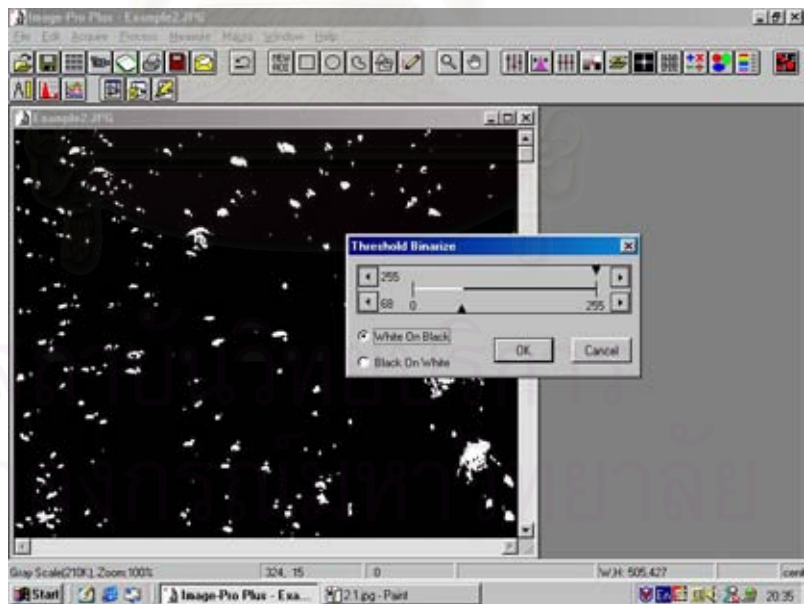
Figure 4.2.7 Bubble size measurement.

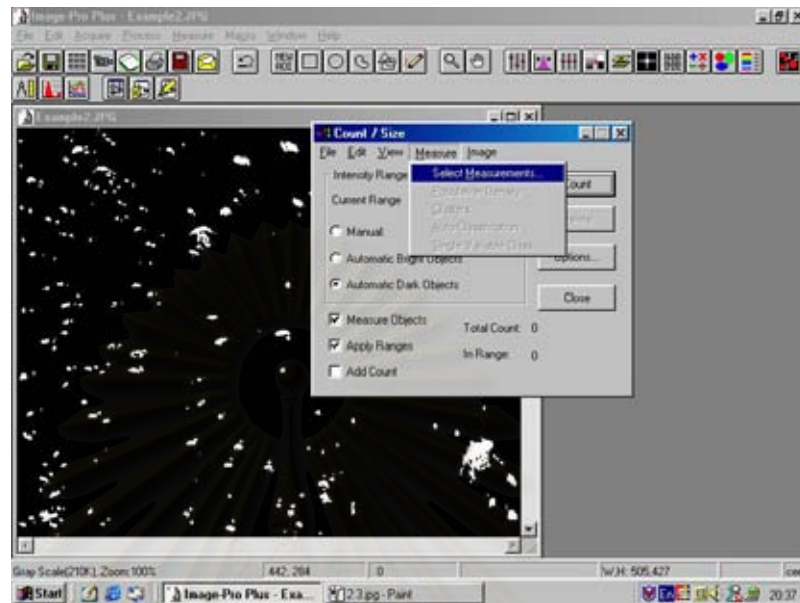Figure 4.2.8 Bubble size measurement.

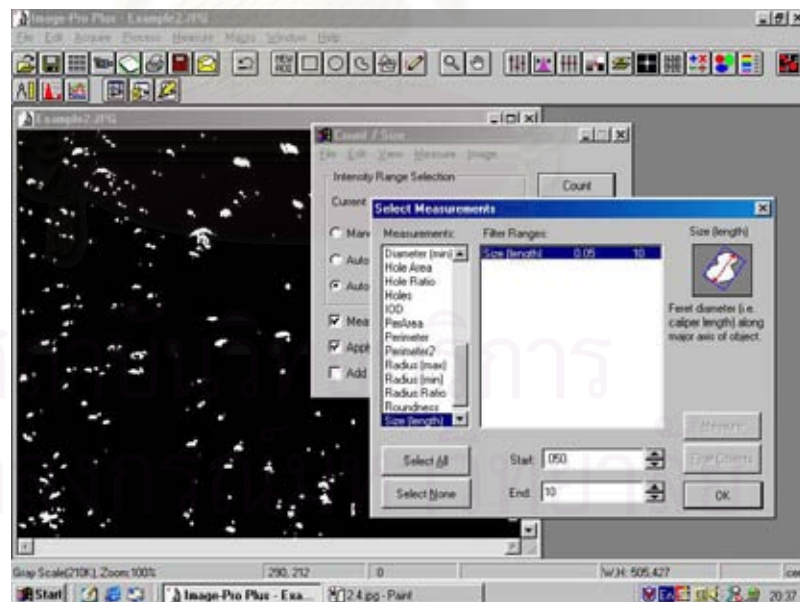Figure 4.2.9 Bubble size measurement
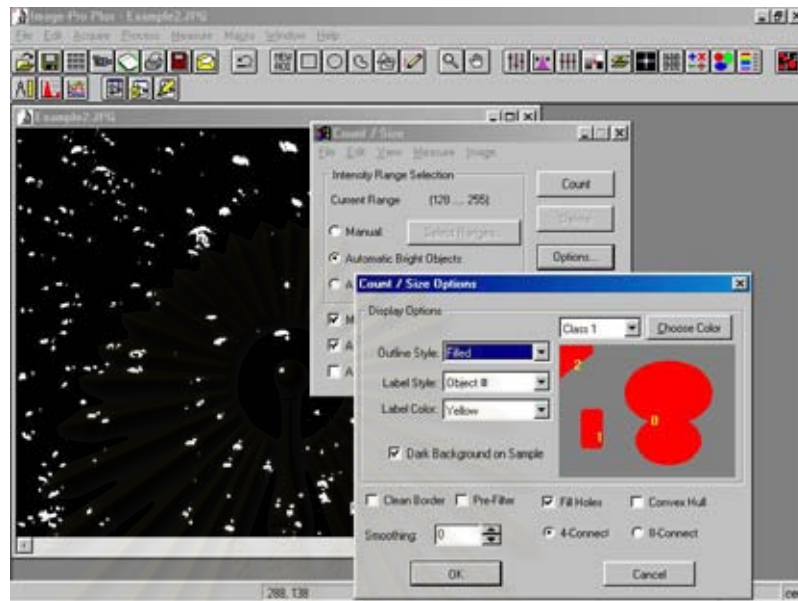

Figure 4.2.10 Bubble size measurement

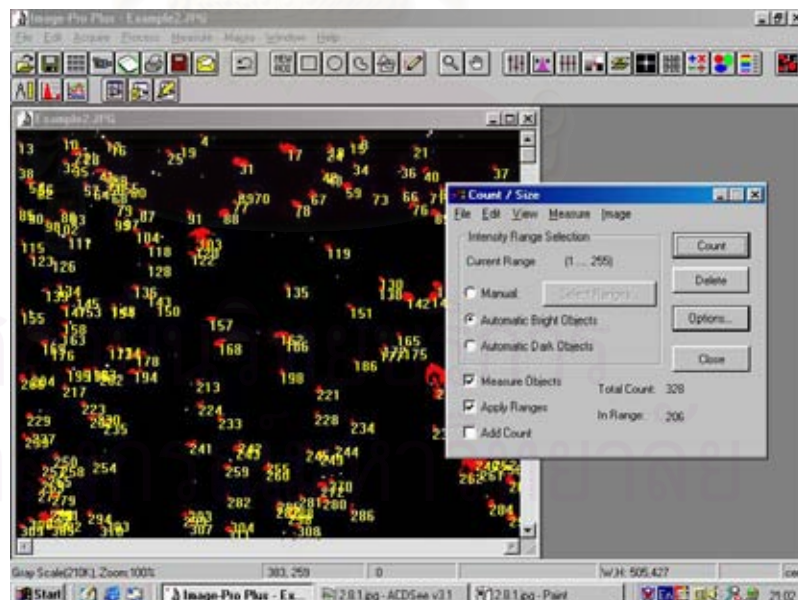Figure 4.2.11 Bubble size measurement

Figure 4.2.12 Bubble size measurement

- After clicking at "Count" command, the program will start counting and mapping the objects (bubbles) whose size was in the range determined. (Figure 4.2.12)

- Measurement data can be observed for confirmation by selecting "View" command in "Count/Size" windows.   After choosing "Select Measurement" command, another window of "Measurement Data" will be shown. One can sort the object's size from minimum to maximum by selecting "Sort up" radio button. (See Figure 4.2.13)

- Distribution curve of object (bubble) size will be drawn using Microsoft Excel, which will make use of the measurement data encrypted by the Image-Pro program. Procedure of transferring the data can be done by clicking at "File" on Menu Bar of the Measurement Data window, then click at "DDE to Excel". The data will be automatically transferred to the Excel. (See Figure 4.2.14)

- Open the transferred file using MS Excel and then use its Macros command to generate the object size distribution curve. Both "Normal" and "Log-Normal Distribution" curves can be displayed on "Graph" worksheet of MS Excel automatically. (See Figure 4.2.15)
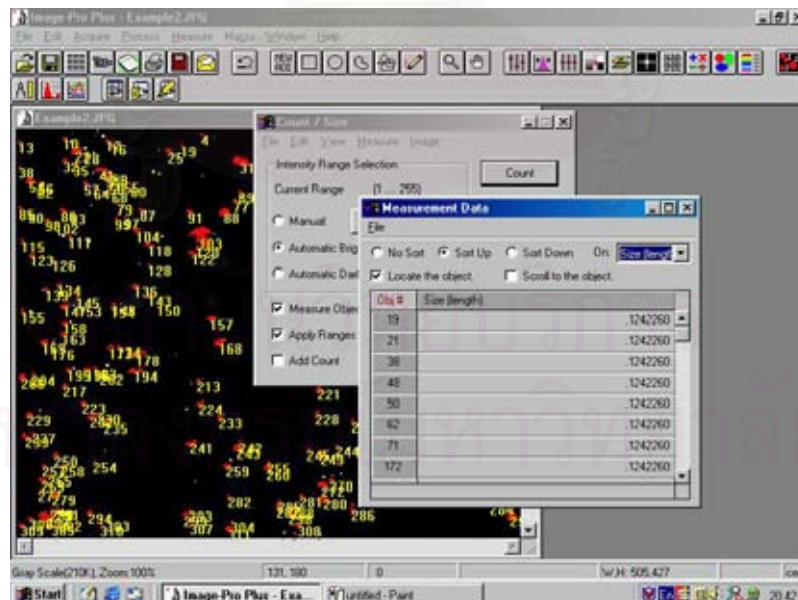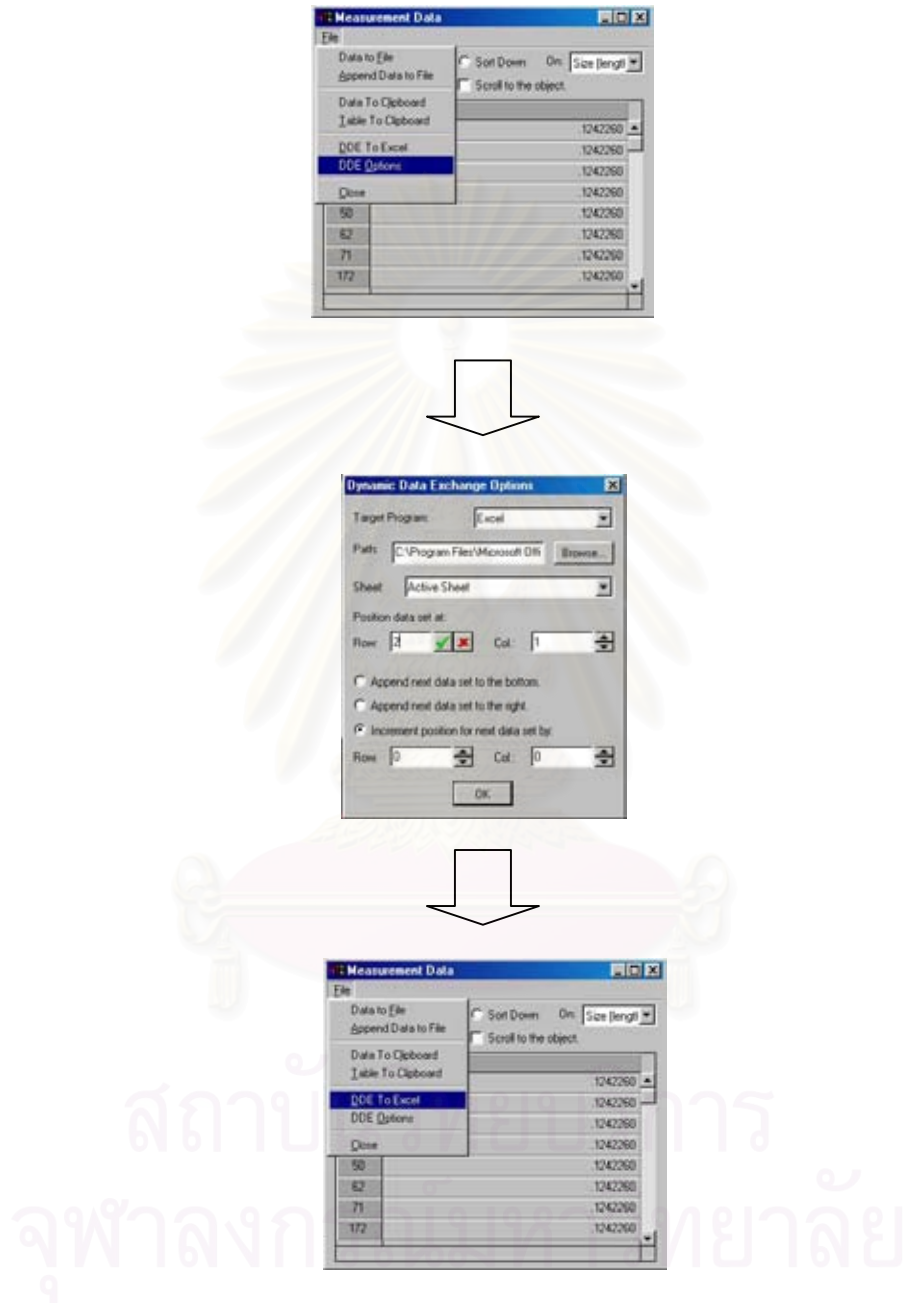

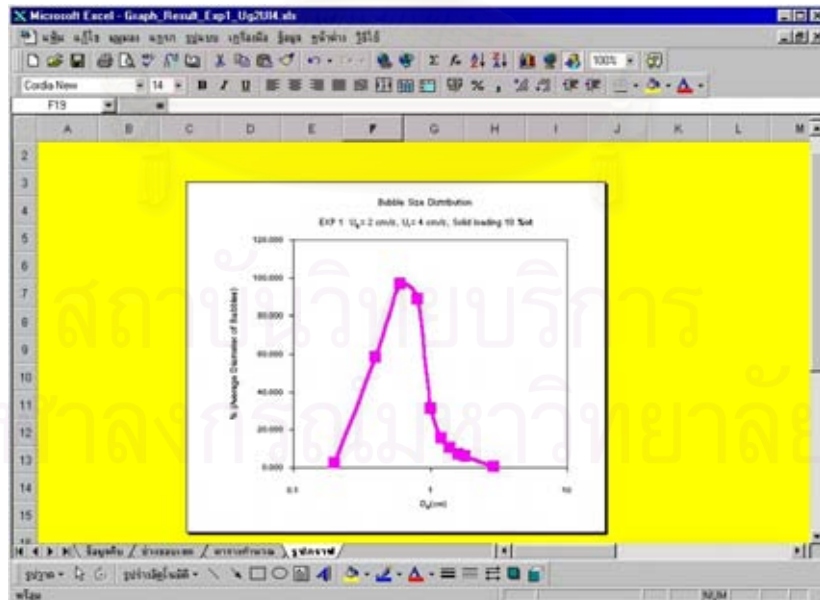Figure 4.2.13 Bubble size measurement

Figure 4.2.14 Bubble size measurement
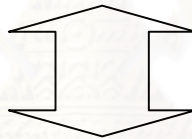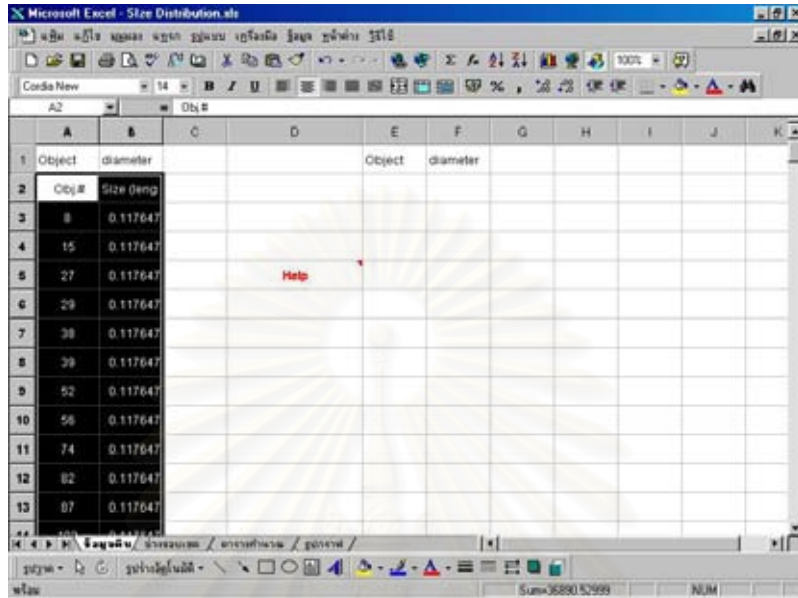
Figure 4.2.15 Bubble size measurement

4.2.3 Measurement of gas holdup and solid holdup

4.2.3.1 Static bed height method

1. Open pump and air compressor valve and adjusted flow meter at defined condition.

2. Run these condition until be steady state condition about 30 minute for first start up and each condition run about 5 minute and shut down water and air valve.

3. Measured static water surface height which decrease due to increasing superficial gas velocity with various condition.

4. Calculated Local gas holdup (ε_g) using Equation 3-3

4.2.3.2 Bubble population balance method

the solid holdup was calculated using Equation 4-1, it shown that relationship between solid concentration with solid holdup which described calculation in appendix E.

$$\varepsilon_s = \frac{1}{\left\{\left[\left(\dfrac{1}{\% S} - 1\right)\left(\dfrac{\rho_s}{\rho_l}\right)\right] + 1 + \dfrac{V_g}{V_s}\right\}} \tag{4-1}$$

The gas holdup was calculated for the following equation:

$$\varepsilon_g = \frac{V_g}{V_{Column}} \tag{4-2}$$

where

ε_s = solid holdup (-)

ε_g = gas holdup (-)

%S = solid concentration (percent by weight)

V_g = volume of gas phase in the column (cm^3)

V_s = volume of solid phase in the column (cm^3)

V_{column} = volume of the column (cm^3)

$\boldsymbol{\rho_s}$ = solid density of glass bead (g/cm^3) = 2.5 g/cm^3

$\boldsymbol{\rho_l}$ = water density at 25 $^\circ$C (g/cm^3) = 0.99708 g/cm^3

4.3 Experimental Method for Ultrasonic Technique

Procedure

- In experiment, used ultrasonic transducers (14.5 mm diameter, frequency 2.25 MHz transducers ,Panametric Inc.) for transmitter and receiver signal (amplitude signal).

- Calibrating amplitude signal using ultrasonic transmission through simulated system that established the signal independence from distance between transmitter and receiver. Then single bubble was released from bubble air pump and was controlled size by diameter of injector, through ultrasonic transmission path among both transducer and record measurement amplitude of receiver using Oscilloscope (60 MHz Digital Real-Time Oscilloscope Tectronik 200 serie).

- The bubble size was measured from the photography in each bubble size and used Image Pro 3.2's Program for measured the Ferret diameter of bubbles.

- Amplitude ratio, A/A_0 was accomplished, which A was amplitude of the transmitted signal and A_0 was amplitude of transmitted signal through liquid (water) only.

- The 50 bubble sizes were compared with the amplitude ratios for the calibrating curve. In order to solid-liquid system, 4.94 cm/sec and 6.17 cm/sec of water flow rate for glass bead 250 and 500 micrometer, respectively. These flow rate was thoroughly dispersed of solid in the column. Then the amplitude signal was recorded and calculated to the amplitude ratio.

CHAPTER V

RESULTS AND DISCUSSION

Hydrodynamics of Three-Phase Fluidized Bed , TPFB, was investigated using a combination visualization and ultrasonic transmission techniques. First, the result of gas holdups investigated using digital video image analysis was taken into account to discussion the effect of operating condition on the gas holdup. Then the solid holdup, which could not be intrusively measured using ultrasonic probe, was discussed. Flow pattern inside the TPFB was taken into consideration with respect to the change of both hydrodynamic characteristics.

5.1 Use of Image Analysis and Visualization technique

### 5.1.1 Bubble formation and its size distribution

Typical images of the bubble formation phenomena at the surface of the fluidized bed in the system were shown in figures 5.1.1 and 5.1.2. In this experiment, the gas distributor consisted of 14 holes with diameter of 0.275 cm. Therefore it was supposed that many air bubbles will be ejected simultaneously after feeding the air into the column. It could be clearly seen that the bubble formation was strongly influenced by the size of solid particles presented in the system and the superficial velocity of gas and liquid fed into the column. Under the condition of low gas superficial velocity (1.0 cm/sec), only air bubbles ejected at central of surface of the fluidized bed were observed because they could not overcome pressure due to the water and bed head.

After detachment from the fluidized bed surface, air bubbles could underwent both coalescence or disintegration. However, it could also be clearly seen that those bubbles flow consecutively like a chain or street along the height of the column. For the 250 micrometer glass beads, particle entrainment induced by the bubble wake could be

observed as shown in figure 5.1.1. The stream of particle entrainment also flew in the wavelike manner.
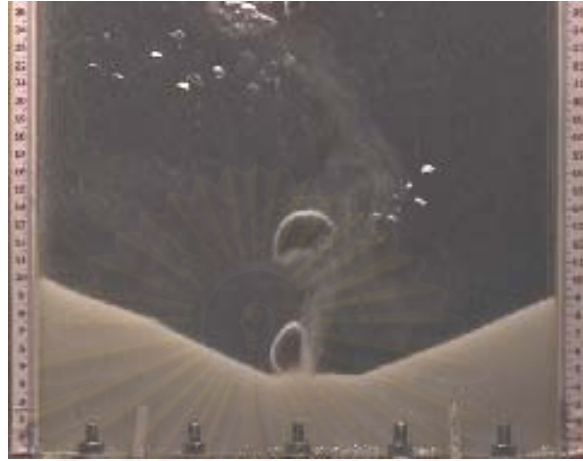
a) with 250 μm Glass Beads
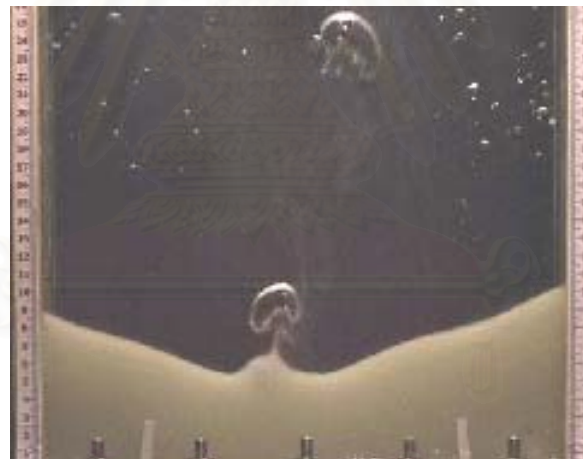
b) with 500 μm Glass Beads

Fig. 5.1.1 Bubble formation at the solid bed of Three-Phase Fluidized Bed with superficial gas velocity of 1.0 cm/sec, no liquid flow and glass bead loading of 10 % by weight

However, an increase in the gas superficial velocity could drastically change the bubble formation behavior. Air bubbles with diverse sizes could be ejected from every nozzle and then moved upward in more chaotic manners. Under the condition of the highest U_g (4 cm/s), the top surface of the fluidized bed was set in rigorous motion since air bubbles flew randomly through the solid bed. Even for the comparatively large solid particles (500 μm glass beads), the rigorous solid entrainment could also take place as evinced in Figure 5.1.2.
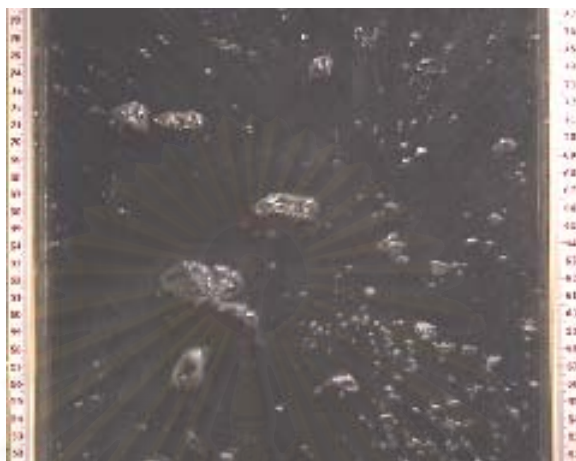

a) with 250 μm Glass Beads

b) with 500 μm Glass Beads

Figure 5.1.2 Bubble formation at the solid bed of Three-Phase Fluidized Bed with gas superficial velocity of 4.0 cm/sec, no liquid flow and glass bead loading of 10% by weight

After rising up to the middle section of the column, air bubbles underwent the processes of coalescence and disintegration, giving rise to the wider size distribution as could be seen in Figures 5.1.3 and 5.1.4. For the lower gas flow rate (U_g = 1 cm/s), air bubbles rised upward with relatively low velocity therefore no rigorous disintegration of bubbles was observed. However, in the system consisting of large particles (500 micrometer), interaction among the air bubbles and the solid particles gave rise to a number of small bubbles due to the disintegration of the bubbles flowing through the solid bed. For the glass beads with average diameter of 250 micrometer, some particles could be lifted and then dropped back into the bottom of the column. However, it should be noted that at the height of investigation, there were very few solid particles with average diameter of 500 micrometer present because the gravitational force acting on the particles became more significant than the drag force exerted by the bubble wake.

After increasing the air flow rate, the bubble disintegration became more enhanced. As shown in Figure 5.1.4, there were very few large bubbles surviving with the increasing gas superficial velocity. Small air bubbles were dispersed almost uniformly throughout the investigated area. Consequently, the gas holdup in the column became higher with the increasing of the number of air bubbles. At higher gas flow rate, small solid particles could be dragged and then suspended in the water by swarm of bubbles, leading to the increase in the apparent viscosity of the slurry of water and glass beads. This could result in the promotion of the bubble coalescence. As shown in figure 5.1.4 (a), it could be seen that solid entrainment was induced the swarm of large and small air bubbles. It should be noted further that the increasing gas velocity gave rise to the more turbulent mixing of solid particle inside the column. Some particles were dragged upward by the rising bubbles while some were dropped back especially those present near the column wall.

a) with 250 μm Glass Beads

b) with 500 μm Glass Beads

Figure 5.1.3 Distribution of air bubbles at the height of 49-72 cm above the distributor (U_g=1.0 cm/sec, U_l=0 cm/sec and glass bead loading = 10wt%)
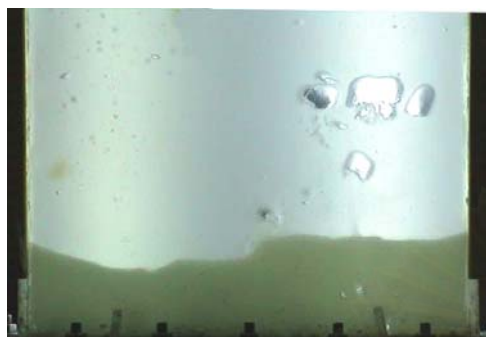
a) with 250 μm Glass Beads

b) with 500 μm Glass Beads

Figure 5.1.4 Distribution of air bubbles at the height of 49-72 cm above the distributor (U_g=1.0 cm/sec, U_l=0 cm/sec and glass bead loading = 10wt%)

When the superficial gas velocity was increased it was found that both 250 and 500 micrometer of glass beads could be fluidized and some particles would be entrained into the free board region. From experimental results, it was found that small glass beads (250 μm) were dispersed within the column more uniformly than large glass beads (500 μm) due to the fact that the small particle had less significant gravitational force than the large particle. When superficial gas velocity or superficial liquid velocity were increased, the glass bead particles became more uniformly dispersed within the column and some fraction were set in circulating motion. However in our experiment, particles could not leave away from the column because there existed the entrainment preventing section on the top of the column. Solid particles whose terminal velocities were higher than the bulk velocity could not be entrianed away from the column and returned to the column. However,an increase in the superficial liquid velocity higher than the terminal velocity of the biggest solid particles could result in the particle rise or dispersion in the column, then clogging of the small particles at the entrianment preventing section could be observed. Superficial liquid velocity had more significant influence to fluidization of the solid bed than superficial gas velocity. (It was noted that in the present experiment the terminal velocities of liquid of 250 and 500 micrometer glass bead were 4.07 and 8.15 cm/sec, respectively.)

For the system which consisted of both yeast suspension and glass bead particles it was found that visualization technique could be of use for the system of which yeast concentration was less than 0.5 wt%. When yeast concentration became higher than 1 wt% bubbles motion could not be clearly observed by visualization technique. However, for bubbles smaller than 0.2 mm it was found that the bubbles could still survive and be observed in the system as illustrated in Figures 5.1.5 - 5.1.6. By comparison to the system without yeast suspension , in the system with yeast suspension, air bubbles still exhibited almost the same motion. However, an increase in the concentration of yeast suspension could result in more enhanced bubble coalescence, leading to the larger bubble size as could be seen in Figures 5.1.5 and 5.1.6.

a) yeast concentration 0.1 wt%

b) yeast concentration 0.5 wt%
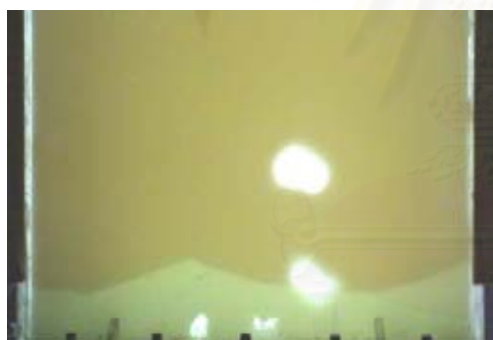
c) yeast concentration 1.0 wt%

d) yeast concentration 2.0 wt%

Fig. 5.1.5 Bubbles formation in various yeast concentration at solid bed (U_g=1.0 cm/sec, U_l=0 cm/sec and glass bead loading = 10wt%)
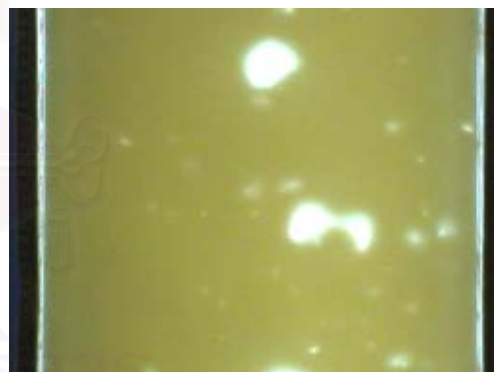
a) yeast concentration 0.1 wt%

b) yeast concentration 0.5 wt%

c) yeast concentration 1.0 wt%

d) yeast concentration 2.0 wt%

Fig. 5.1.6 Distribution of air bubbles in various yeast concentration at height of 49-72 cm above the distributor (U_g=1.0 cm/sec, U_l=0 cm/sec and glass bead loading = 10wt%)

5.1.2 Macroscopic flow pattern in Three-Phase Fluidized Bed

Figures 5.1.7 and 5.1.8 illustrate the flow pattern in Three-Phase Fluidized Bed operated without liquid flow. At low gas flow rate (U_g = 1.0 cm/s), there were only a small number of bubbles present in the system. Bubbles could undergo both disintegration and coalescence during its motion along the column. Comparison between Figure 5.1.7 (a) and (b) reveals that there was only insignificant influence of solid particles on the flow of liquid and bubbles in the system.

a) with 250 μm Glass Beads   b) with 500 μm Glass Beads

Figure 5.1.7 Flow pattern inside Three-Phase Fluidized Bed loaded with different size of glass beads (U_g = 1.0 cm/sec, U_l = 0 cm/sec and glass bead loading = 10 wt%)

However, an increase in the air flow rate from 1.0 to 4.0 cm/sec gave rise to a remarkable change in the flow pattern in the system (Figure 5.1.8). With the presence of small solid particles (250 μm), the macroscopic flow induced by the swarm of bubbles with diverse sizes could suspend the solid particles by making them move upward,

resulting in uniform solid dispersion in the system. However, for the larger particles (500 μm), the induction due to the bubble swarms was still too small compared with the gravitational force. In addition, the fluidized bed of the large particles could also play a role as another extra bubble distributor, which could break large bubbles into smaller ones. After leaving the fluidized bed, those small bubbles could again undergo the coalescence process to form larger bubbles present in the fast bubble flow region.

When consider flow pattern in the system consisting of yeast suspension it was found that the bubble flow pattern was still similar to that of the system without yeast suspension as could be seen in Figure 5.1.9.

a) with 250 μm Glass Beads   b) with 500 μm Glass Beads

Fig. 5.1.8 Flow pattern inside Three-Phase Fluidized Bed loaded with different size of glass beads (U_g = 4.0 cm/sec, U_l = 0 cm/sec and glass bead loading = 10 wt%)
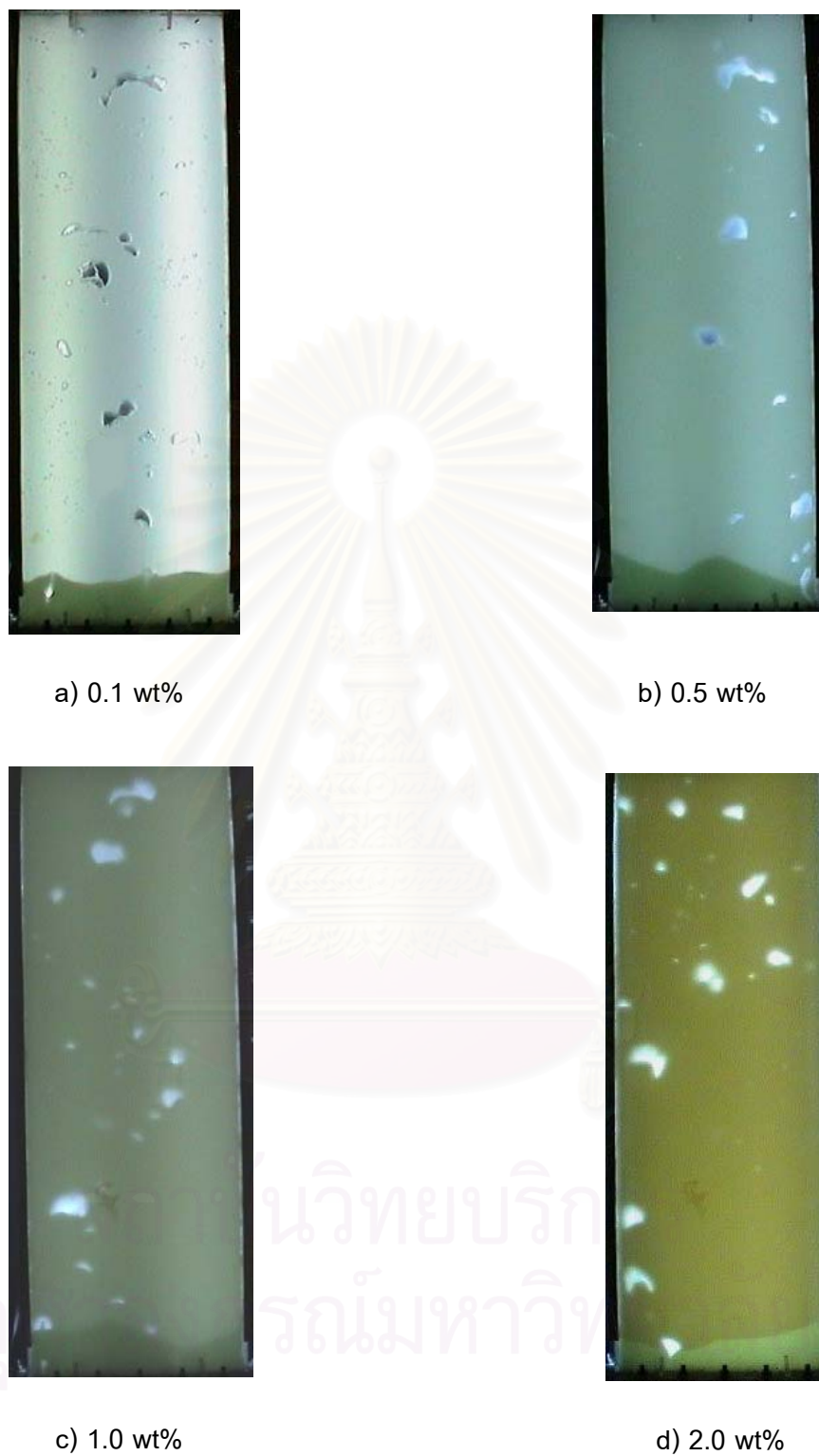
a) 0.1 wt%

b) 0.5 wt%

c) 1.0 wt%

d) 2.0 wt%

Figure 5.1.9 Flow pattern inside Three-Phase Fluidized Bed loaded with various yeast concentration (U_g = 1.0 cm/sec, U_l = 0 cm/sec and glass bead loading = 10 wt%)

The flow pattern of bubbles and solid particles could be investigated. From the experiment, it was found that the motion of bubbles and solid particles would occur in the inside of column. Bubbles were injected from the nozzle of the distributor. At high U_g, bubbles were injected from all nozzles and in steady state the flow pattern of bubbles was as follows:

1. When U_g was very low, bubbles only occurred at one side of column because 2-3 nozzles from 14 nozzles in the total entirely injected bubbles. As a result, at the lower region of the column, the descending bubble motion was close to the either wall of the column. In addition, at the center of column height the upward bubble motion occurred in the middle of column width and the bubble flow pattern was the descending flow and the vortical flow of the small bubble occurred at near the wall region. Under this condition the vortex size was large and the descending flow did not occurred in the entirety of column height especially at high U_g. due to the effect of the upward liquid flow and the buoyancy of the bubble.

2. At high U_g and steady state, the swarm of bubbles were injected from all nozzles and coalescence became to larger and flow upward to the top of the column. The flow pattern of the bubble was zigzag. At the condition which the balance of upward flow and downward flow, the bubble directly flowed upward to the top of the column, but not usually, although the bubble size was large. According to all through the end of height of the column, bubbles flowed downward close to the wall of the column and in the region between the wall and near the centerline of column the vortex was continuously formed from the top to the bottom of the column. The vortex was formed due to the contact of the downward flow and the zigzag upward flow. The solid particles motion occurred due to the effect of liquid and bubble motions. Consequently, the upward motion of solid particle near the centerline of the column and the downward motion at the both regions near the wall were observed.

According to the gravity force, it was clearly observed for the large solid particle. The solid particle sometimes settling through the channel between the vortical flow region and the fast bubble flow region.

5.1.3 Effect of superficial gas velocity on the average bubble size and its distribution

The experiment results revealed that as superficial gas velocity was increased, bubble size slightly decreased. As illustrated in Figure 5.1.10 an increase in superficial gas velocity led to a decrease in population of large bubbles. Also, at higher superficial gas velocity, air bubbles induced the bulk flow, which exhibited four distinct regions, namely vortical flow region, descending flow region, fast bubble flow region and central plume region. It was in good agreement with the results reports by Tzeng, J.-W. et al. (1993)

In the vortical flow region, most of bubbles moved upward with the spiral motion. There was only insignificant collision among bubbles in this region. In contrary, bubbles moved upward rectilinearly with more rigorous collision in the fast bubble flow region. The collision resulted in the far less instability of bubbles. It could also be seen that an increase in superficial gas velocity led to the increasing width of the fast bubble flow region. On the other hand, the central plume region, which consisted of very small bubbles, became less clear to be observed when the superficial gas velocity was increased. From the bubble size analysis, it was clearly seen that the bubbles present in this system exhibited the log-normal distribution as shown in figure 5.1.10. An increase in superficial gas velocity from 1 to 4 cm/sec, while the superficial liquid velocity was fixed at 1 cm/sec, led to a decrease in the average sized of bubbles from 0.483 to 0.4475 cm and variance decreased from 2.348 to 1.874.

As described above, this could be implied as an increase in the bubble disintegration. Akita and Yoshida (1974) also found that bubble size decreased with increasing superficial gas velocity. A decrease in large bubble (d_B > 1 cm) population around descending flow region resulted in the decreasing average bubble size.

Table 5.1.1 Geometric mean diameter and deviation of bubbles with superficial liquid velocity constant (1 cm/sec) and GB500 40% by weight

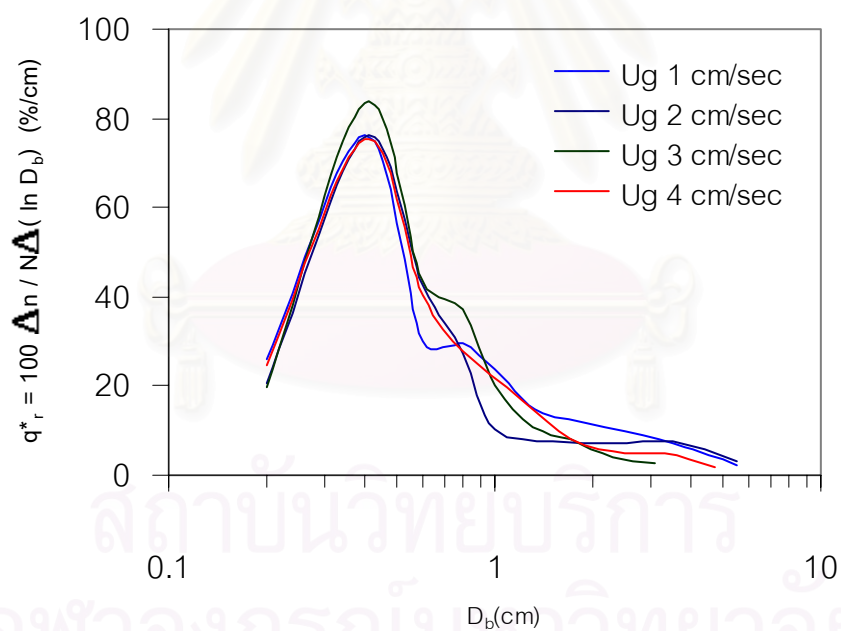| U_g (cm/sec)	Bubbles diameter (cm)	σ (-)
1	0.483	2.348
2	0.481	2.277
3	0.450	2.128
4	0.448	1.874

Fig. 5.1.10 Bubble size distribution in various superficial gas velocity at constant superficial liquid velocity with 500 micrometer glass beads and solid loading 40 wt%

From Figures 5.1.11 and 5.1.12, it could be seen that an increase in superficial gas velocity gave rise to an increase in gas holdup. This could be implied that an increase in volume of air fed into the system could also lead to formation of small bubbles. Small bubbles around descending flow region and vortex flow region were produced and circulated in the system while large bubbles rapidly moved to the top of column. Figure 5.1.11 illustrates that solid particle size affect to the gas holdup. It was found that the gas holdup decreased with an increase in solid particle size and solid concentration. This could be implied that small glass bead could induce more small bubbles in the system. From the experiment observation it was found that bubbles could come to contact with small glass bead particles which were well dispersed through the column. The disintegration rate could be implied to increase as the interaction among bubbles and solid particle became more rigorous.
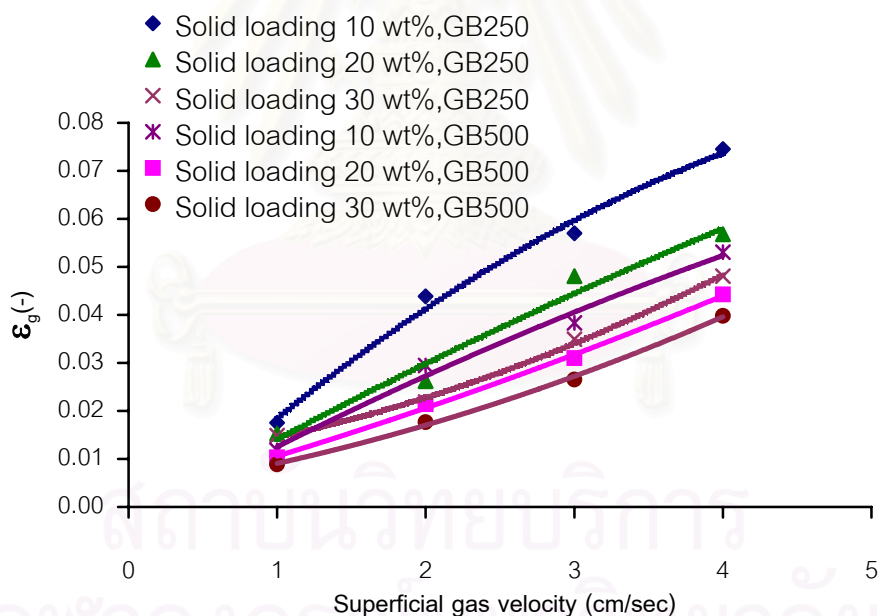
5.1.11 Comparison of relation between superficial gas velocities to gas holdup of 250 and 500 glass bead particle at superficial liquid 6.17 cm/sec using static surface water height method.

In addition, for the system consisted of various solid concentration, it was found that the increasing solid concentration could reduce the gas holdup. This could be considered that an increase in the solid concentration led to an increase in apparent viscosity of the solid-liquid mixture, resulting in the bubble disintegration. Either for the case of 250 or 500 micrometer glass bead particles, an increase in the solid concentration gave rise to a decrease in the gas holdup. However, for the small glass bead particle, the effect of the increasing solid concentration became more significant due to the fact that the small glass beads could be dispersed uniformly throughout the bed. Figures 5.1.12 and 5.1.13 shew that the gas holdups which were measured by observation of static liquid height and by visualization method were slightly different. The gas holdup obtained from the visualization method, which made use of integration of volume of bubble emerged in the whole column, was relatively lower than that of the static liquid height method. As shown in Figure 5.1.13, comparison of the gas holdups obtained from both methods exhibited correlation coefficient (R^2) of 0.9947, 0.9895 and 0.9756 for the systems of which the solid loading were 10, 20, and 30 wt%, respectively. The difference of the gas holdups obtained from two alternatives were implied to be caused by the assumption employed in the measurement. The assumption are described as follows;

1)   For calculating volume of all bubble, all bubbles in the system were assumed to have oblate ellipsoidal shape. Bubble breadth had been measured by visualization and then the equivalent bubble diameter was calculated. It was found that the estimation using this method generally provided an error of 20 %.(Appendix E3)

2)   It was found that bubbles population became increased with the increasing superficial gas velocity. Although the increasing superficial gas velocity affected to an increase in bubble flux but it was found that small bubbles were induced by the bulk descending flow nearly the column wall from top to bottom of the column. This phenomena could be comparatively clearly seen at high superficial gas velocity.

3)   For visualization method, fine bubbles was neglected from measurement bubble due to the difficulty of detection.
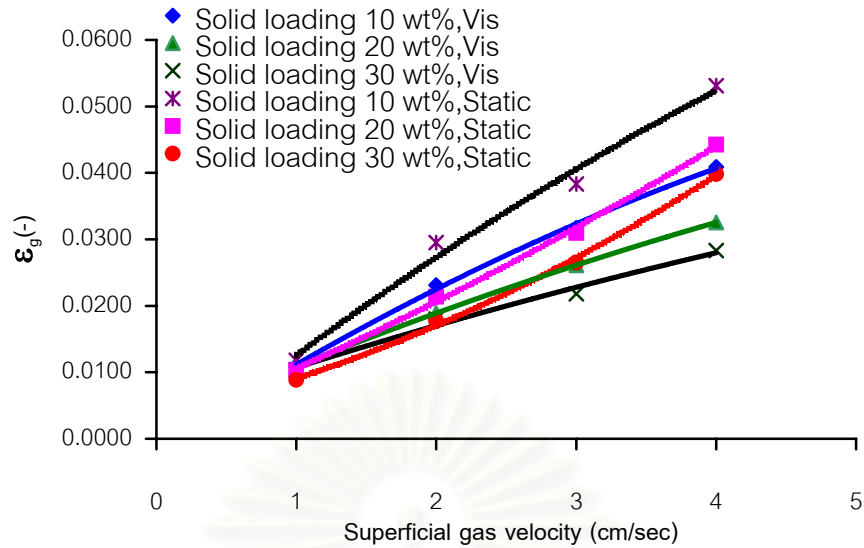
Figure 5.1.12 Relation between superficial gas velocities to gas holdup of measured by static surface water height (Static) method and image analysis method (Vis) at superficial liquid velocity 6.17 cm/sec.
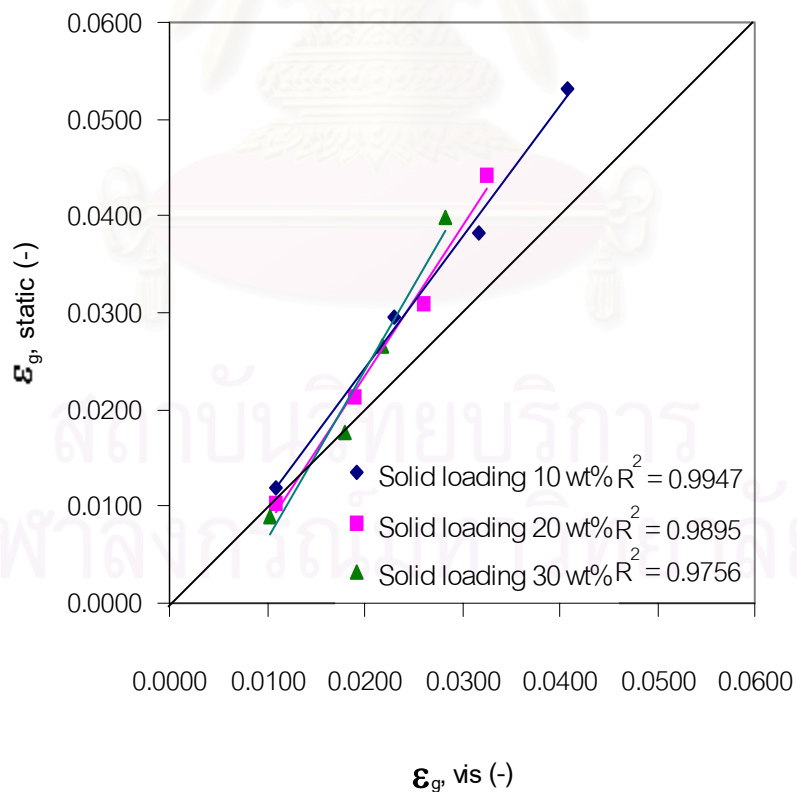

Figure 5.1.13 Relation between superficial gas velocities to gas holdup of measured by static surface water height method and visualization method.

Finally, when superficial gas velocity increased, solid holdup slightly decreased in three conditions of solid loading due to an increase in gas phase in the system. In addition, the solid holdup acquired using the visualization method and the determined by the mass balance from Equation 4-1. It is found that volumetric of gas had the less effect on solid holdup as shown in Figure 5.1.14.
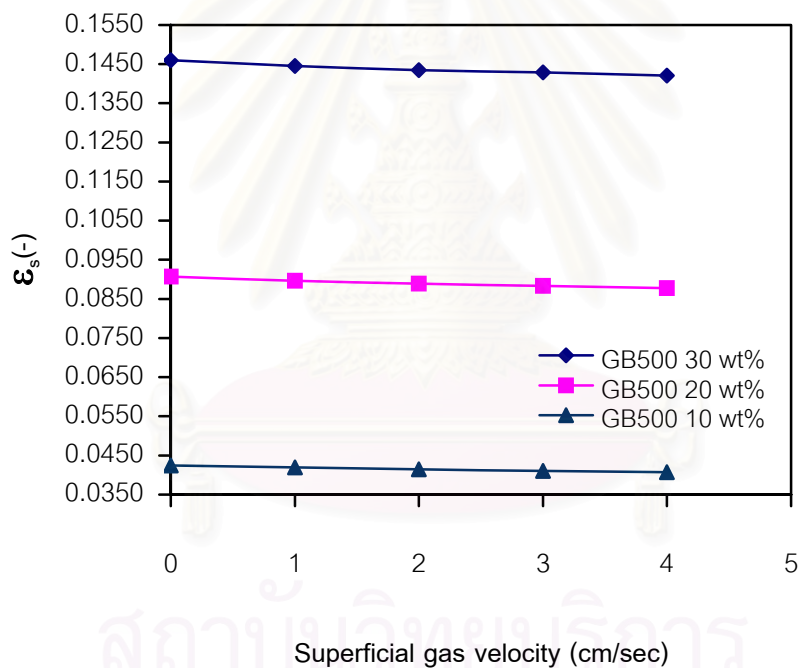

Figure 5.1.14 Relation between superficial gas velocities and solid holdup determined by image analysis method (Vis) at superficial liquid velocity 6.17 cm/sec.

5.1.4 Effect of superficial liquid velocity on the average bubble size and its distribution

From Figure 5.1.15, the experiment results shew that as superficial liquid velocity was increased, the average bubble size became smaller. From the bubble size analysis as shown in Figure 5.1.15 and Table 5.1.2, it was found that the average bubble size was slightly decreased similar to the case of the increasing gas velocity. When the superficial liquid velocity was increased from 1, 2, 3 to 4 cm/sec the average bubbles size became slightly decreased from 0.483, 0.481, 0.476, and 0.470 cm while the standard deviation was decreased from 2.348, 2.118, 1.949, to 1.932, respectively. According to Ostergarrd (1964), Rigby et al (1970), and Lee et al. (1974) the similar results for low liquid velocities were also reported. Bubble became smaller with the increasing superficial liquid velocity because the high liquid flux affected to the more uniform dispersion of glass beads which in turn increased the probability of collision among bubbles and solid particles. At low superficial gas velocity and high superficial liquid velocity, coalescence of bubble slightly occurred and then the bubble disintegration became more enhanced.

Table 5.1.2 Geometric mean diameter and deviation of bubbles with superficial gas velocity constant (1 cm/sec) and GB500 40% by weight

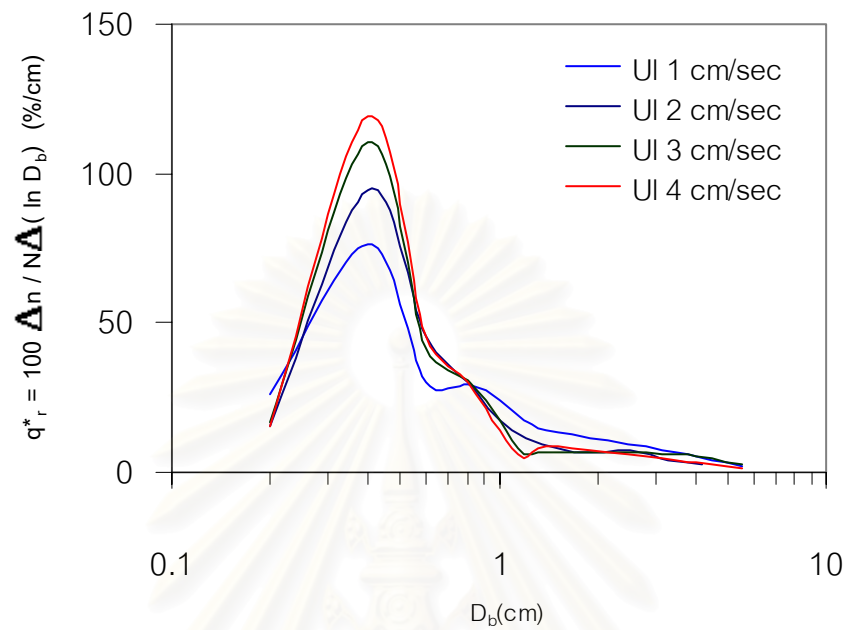| U_l (cm/sec)	Bubbles diameter (cm)	σ(-)
1	0.483	2.348
2	0.481	2.118
3	0.476	1.949
4	0.470	1.932

Fig. 5.1.15 Bubble size distribution in various superficial liquid velocity at constant superficial gas velocity with 500 micrometer glass beads and solid loading 40 wt%

5.1.5 Effect of solid particle on the average bubble size and its distribution

The experiment results shew that the average bubble size for the system of 500 micrometer glass bead was larger than that of the system of 250 micrometer glass bead under the condition of the same percentage of loading. The small the particle, the larger the surface area and the more the particle number. The smaller particles could be fairly well dispersed in the column. So there was more collision among the small particles and the bubbles. From the bubble size distribution as shown in Figure 5.1.16 and Table 5.1.3, it could be seen that an increase in the glass bead size from 250 to 500 micrometer under the same condition (U_g 4 cm/sec, U_l 1 cm/sec and glass bead loading 40 % by weight) led to an increased in the average bubble size from 0.442 cm to 0.448 cm and its deviation were 1.827 and 1.874, respectively.

Interestingly in the system with yeast suspension (concentration 1 % by weight), it was found that there existed many small bubbles near the column wall. For the experiment result obtained from the visualization method, bubble size distribution within the system of the yeast suspension system was smaller than that of the system without yeast suspension as illustrated in Table 5.1.3. The effect of the glass bead size in the system of yeast suspension was also similar to that of the system without yeast suspension. The average bubble size increased from 0.369 cm to 0.376 cm but its standard deviation decreased from 1.952 and 1.859. This interesting phenomena would be investigated in more detail later on.

Table 5.1.3 Geometric mean diameter and deviation of bubbles with both glass beads size and similarity to condition.

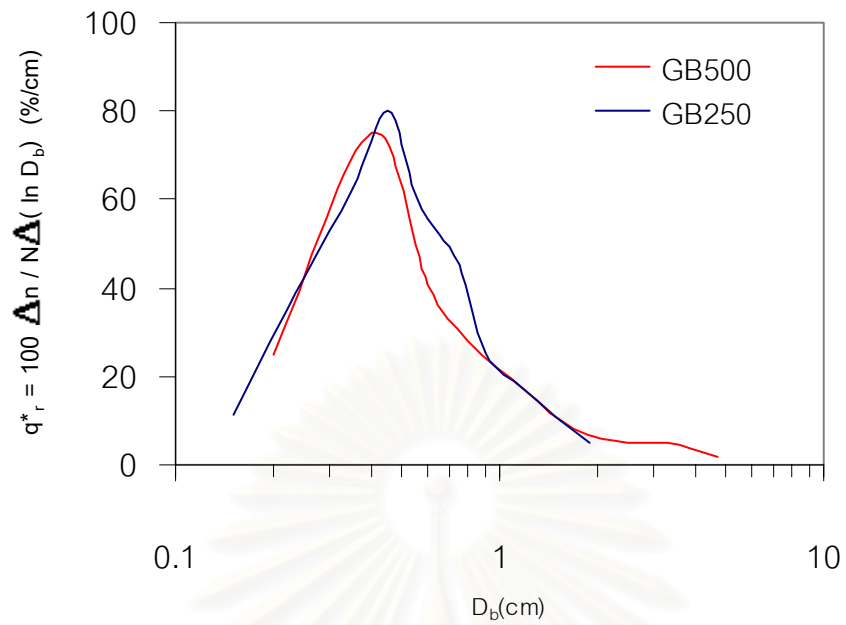| Condition	Bubble diameter (cm)	σ(-)
GB250	0.442	1.827
GB500	0.448	1.874
GB250 with yeast conc. 1 wt%	0.369	1.952
BG500 with yeast conc. 1 wt%	0.376	1.859

Fig. 5.1.16 Bubble size distribution of 250 and 500 micrometer glass bead (U_g 4 cm/sec, U_l 1 cm/sec and solid loading 40 wt%)
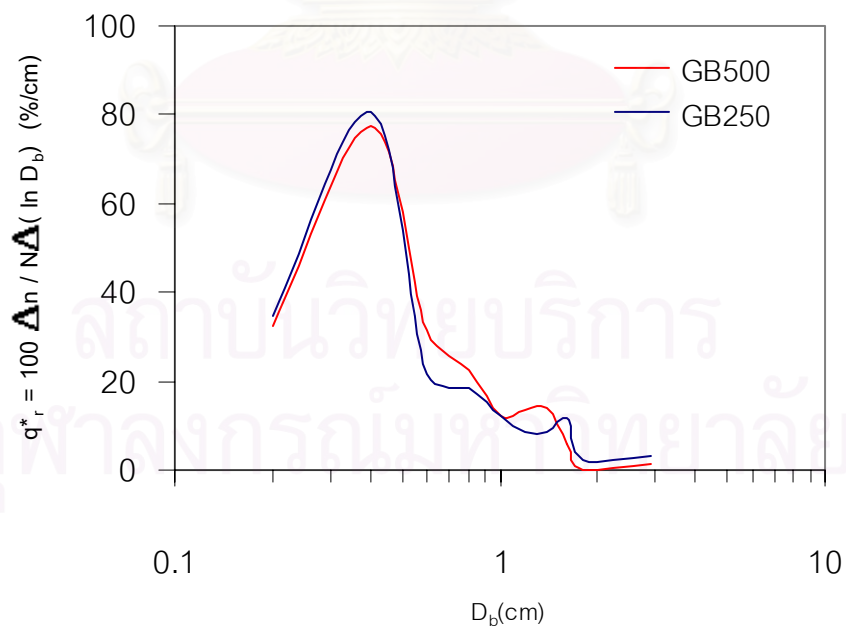

Fig. 5.1.17 Bubble size distribution of 250 and 500 micrometer glass bead at yeast concentration 0.1 wt% (U_g = 4 cm/sec, U_l = 1 cm/sec, solid loading = 10 wt%)

5.2 Measurement of the solid holdup using Ultrasonic transmission technique

5.2.1 Effect of solid particle to amplitude ratio

Figure 5.2.1 and 5.2.2 illustrated that effect of solid concentration of 250 and 500 micrometer glass bead and yeast concentration on the amplitude ratio of transmitted ultrasonic signal (A/A_0). The experiment result shows that the amplitude ratio decreases with the increasing solid concentration. An increase in the nominal particle size resulted in a slightly decrease in the amplitude ratio. Stolojanu, V. and Prakash A. (1997) also reported that the amplitude ratio decreased exponentially with increasing solid concentration. The reason for the phenomenon was implied as the ultrasonic signal randomly scattered the signal struck solid particles present in the column. Scattering was often the predominant form of attenuation in the heterogeneous material.

For the system with yeast suspension in the water, the less effect of yeast on the amplitude ratio as compared with glass bead particles was found. Figure 5.2.2 shows that when yeast concentration was increased affect to amplitude ratio was slightly decreased.

Figure 5.2.3 shows that relation between solid holdup with amplitude ratio of 500 micrometer glass bead which were dispersed in the column with the superficial liquid velocity of 6.17 cm/sec. It was found that the amplitude ratio at various superficial gas velocities was declined with the increased solid holdup. This is resulted from the fact that when the more solid particles presented in the column the signal lead to the more scattered and absorbed of the ultrasonic. We made use of Figure 5.2.3 for measurement of the solid holdup in the three phase fluidized bed column.
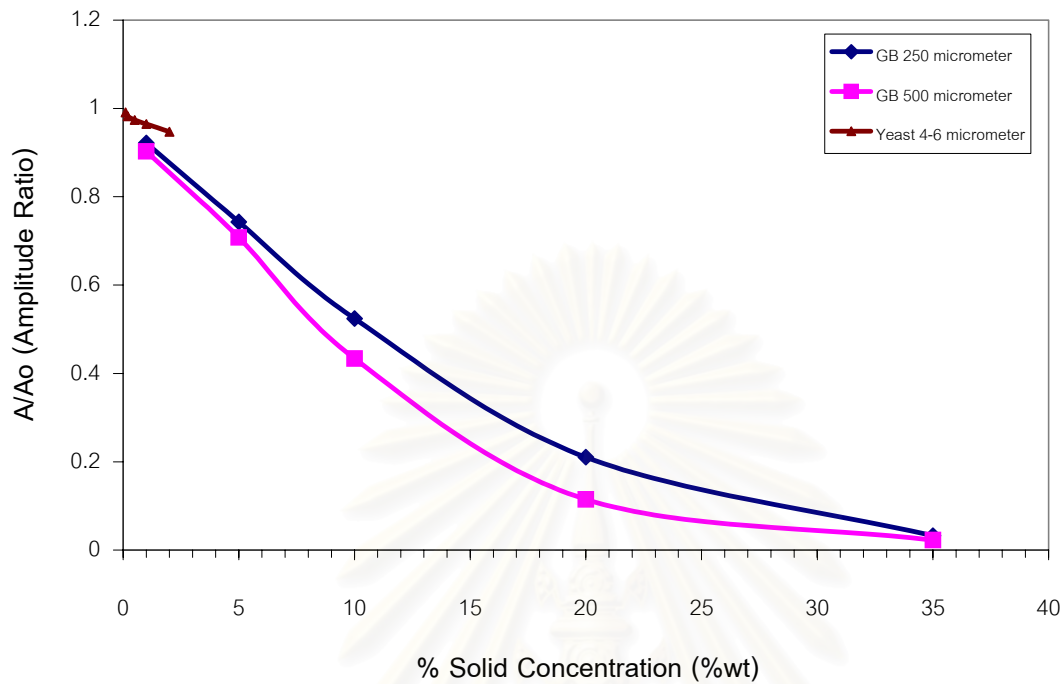
Fig. 5.2.1 Relation between solid concentration of 250 and 500 micrometer of glass bead and yeast suspension to the amplitude ratio.
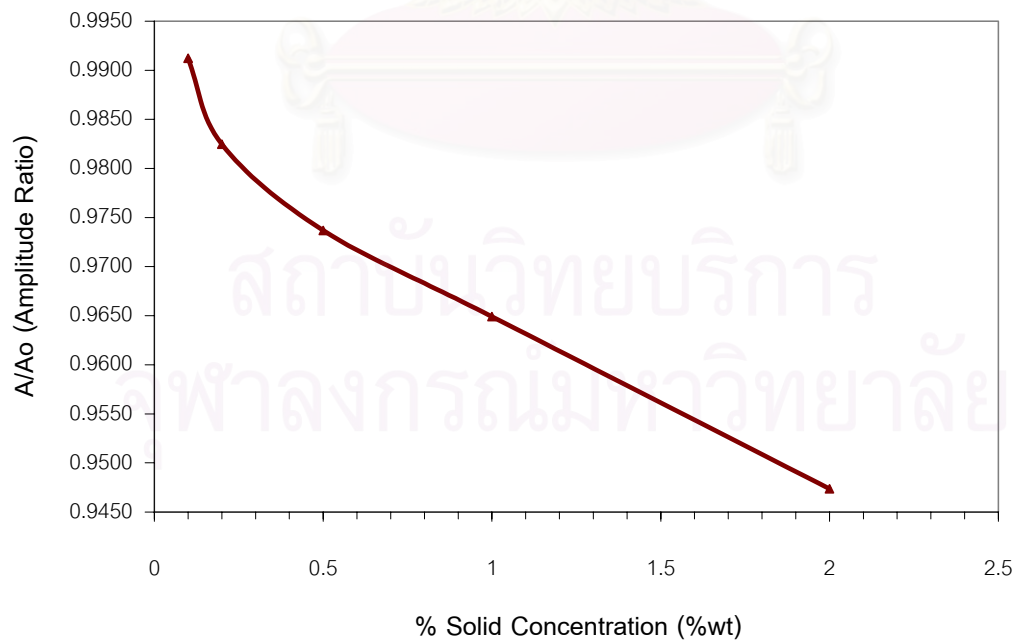

Fig. 5.2.2 Relation between yeast concentration in the water to the amplitude ratio.

5.2.2 Measurement of the solid holdup affected by the superficial gas velocity

Figure 5.2.3 shows the representative result of the superficial gas velocity exhibiting influence on the solid holdup of the system, which consisted of 500 micrometer glass beads with the superficial liquid velocity of 6.97 cm/sec. Emerging of gas bubble made the solid holdup become lower compared with that of the system without gas bubbles. However, an increase in U_g from 1 to 4 cm/sec slightly led to a decrease in the solid holdup. Especially, the increasing of U_g higher than 3 cm/sec had an insignificant effect on the solid holdup. This could be implied that the injection of gas bubbles into the column led to the existence of the gas holdup. The higher the superficial gas velocity, the higher the gas holdup, in turn, the lower the solid holdup. However, the effect of U_g on ε_s was very limited due to the restriction of solid leading, which was employed in our system. As mentioned above, under the high solid loading conditions, not only the visualization technique but also the ultrasonic transmission technique faced with difficulties due to the hindering effect of solid particles. The higher solid concentration could give rise to the more opaque suspension which became hardly to be observed. Simultaneously, the transmitted signal became more scattered in the system of higher solid loading.
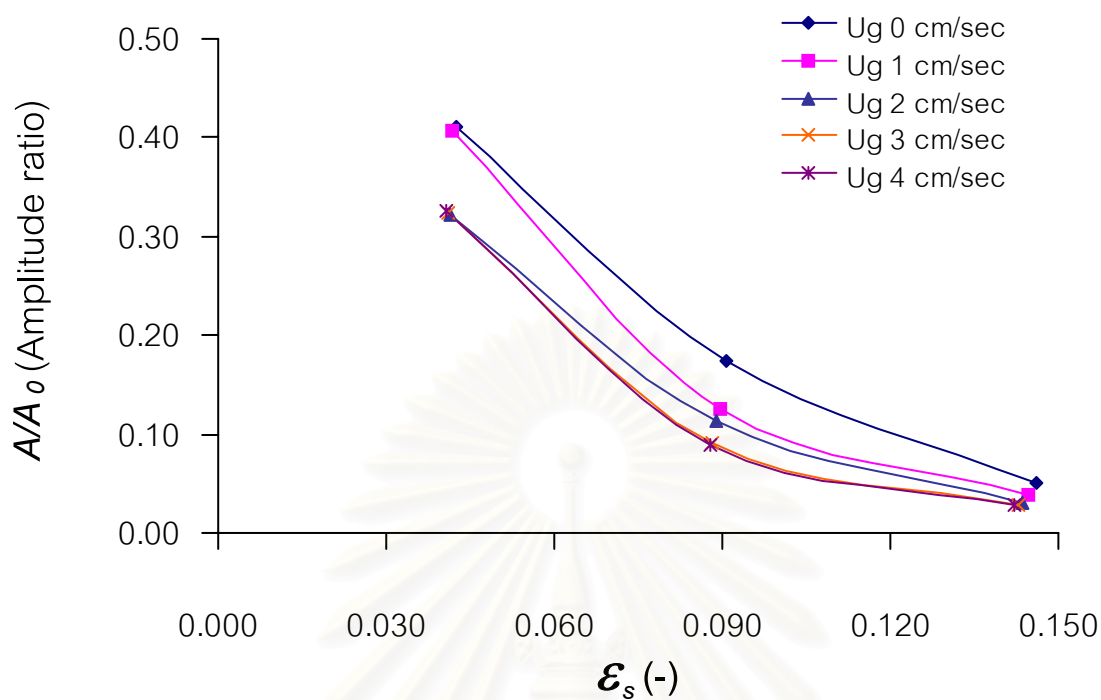
Fig. 5.2.3 Relation between solid holdup with amplitude ratio at various superficial gas velocity, superficial liquid velocity constant (6.97 cm/sec) and GB500

However, with regarding to information of both ε_g and ε_s as well as the flow regimes with the Three Phase Fluidized Bed investigated in this work, it could be concluded that the ultrasonic technique would provide the full picture of the hydrodynamics of Three Phase Fluidized Bed, leading to the insight into the complicated phenomena which could affect the design and operation of such reactor.

CHAPTER VI

CONCLUSION

6.1 Conclusion

The result presented in this experiment led to the conclusion as follows;

1.   The flow pattern in gas-liquid-solid system can be represented by four distinct flow regions based on the local liquid flow characteristics and bubble dynamics. These regions, namely descending flow, vortical flow, fast bubble flow, and central plume regions. Bubble was injected from nozzles upon superficial gas velocity and small bubble coalesced to become large bubble and moved from bottom to top at the centerline of the column. Small bubbles were downward either side of the column and vortex or spiral motion could be seen between descending flow region and fast bubble flow. Solid particle was moved from the bottom due to dragforce and bubble wake, it was found that in all regions of bubble, solid particle was dispersed and moved around the region. It is pronounced that solid particle motion was spiral or vortex in the vortical flow region and downward in descending flow region. These patterns could be occurred in the system with yeast suspension.

2.   Superficial gas velocity and superficial liquid velocity affected the bubble size, solid and gas holdups. When both superficial liquid and gas velocity were increased, bubble size distribution decreased and its deviation were decreased. The average of bubble size were 0.47-0.48 cm. In addition, the solid holdup was slightly decreased with increasing gas velocity and increased with increasing liquid velocity. In contrary, the gas holdup was increased with increasing gas velocity and decreased with increasing liquid velocity.

3.   The solid particle motion could be collision with bubbles and disintegration. For small particles (250 μm glass bead) could be collided and bubbles were disintegrated better than large particles (500 μm glass bead). So the average bubble

size for the system consist of 250 μm glass bead slightly smaller than the system consist of 500 μm glass bead.

    4.   For yeast suspension water exceed 1 %wt, the ultrasonic transmission technique was more suitable than visualization technique. However, the ultrasonic transmission could be employed when the glass bead loading was more than 30 wt%.

    5.   For ultrasonic transmission technique, solid concentration, superficial gas velocity bubble size and solid particle size have effect to ultrasonic signal. Increasing of these factors could decreased the signal.

6.2 Recommendation for Future Work

    1.   Investigation of the condition higher than the condition which employed in this experiment.

    2.   Investigation of the effect of foam which occurred at the overflow section.

    3.   For Ultrasonic transmission technique, ultrasonic transducer (receiver and transmitter) should be attached on the surface column using the clamp due to the signal depend on the force which press on the column.

    4.   For the system was consisted of 250 micrometer glass bead particles and operated at high gas and liquid velocity. When the overflow section was clogged, the column started to leak. Thus, the experiment at this condition should be designed to develop a device for preventing the clogging of small particles at the screen.

REFERENCES

Chen, Z., Zheng, C., Feng Y., and H. Hofmann. Local bubble Behavior in Three-Phase Fluidized Beds, <u>Can. J. Chem. Eng.</u>, 76, 315, 1998.

Comte, M. P., Bastoul, D., Hebrard, G., Roustan, M., and Lazarova, V. Hydrodynamics of a Three-Phase Fluidized Beds-the inverse turbulent bed, <u>Chem. Eng. Sci.</u>, 52(22), 3971, 1997.

Fan, L. S., Satija, S. and Wisecarver, K. Pressure fluctuation measurements and flow regime transitions in gas-liquid-solid Fluidized Beds, <u>AIChE.</u>, 32, 338, 1986.

Heinrich Kuttruff. <u>Ultrasonics fundamentals and applications</u>. U.S.A.: ELSEVIER APPIED SCIENCE,1991.

Hideki Miura and Yoshinori Kawase. Hydrodynamic characteristics of gas-liquid-solid three-phase fluidized beds, <u>Region sysm. on Chem. Eng.</u>, 1996.

Kikuchi, R., Tsutsumi, A. and Yoshida, K. Fractal aspect of hydrodynamics in a Three-Phase Fluidized Bed, <u>Chem. Eng. Sci.</u>, 51(11), 2865, 1996.

Krishna, R., de Swart, J. W., Ellenberger, J., Martina, G. B. and Maretto, C. Gas holdup in slurry bubble columns : Effect of column diameter and slurry concentration, <u>AIChE.</u> 43(2), 311, 1997.

Lawrence C. Lynnworth. <u>Ultrasonic measurement for process control</u>. U.S.A.: Academic Press Inc., 1989.

Lee, S., Sopia L., and De Lasa, H. I. Evaluation of bubble length distributions in Three-Phase Fluidized Bed, <u>AIChE.</u>, 36, 1763, 1990.

Liang-Shih Fan and Katsumi Tsuchiya. Bubble wake dynamics in liquds and liquid-solid suspensions. U.S.A.: Butterworth-Heinemann, 1990.

Liang-Shih Fan. Gas-liquid-solid fluidization engineering. U.S.A.: Butterworths Publishers, 1989.

Okamura, S. , Uchida, S., Katsumata, T., and IIDa., K. Measurement of solid holdup in a three-phase fluidized bed by an ultrasonic technique, Chem. Eng. Sci., 44(1), 196-198, 1989.

Rajamani Krishna, Jeroen W. A. de Swart, Jurg Ellenberger, Gilbert B. Martina, and Cristina Maretto. Gas holdup in slurry bubble columns: Effect of column diameter and slurry concentrations, AIChE., 43(2), 311-315, 1997.

Soong, Y., Gamwo, I. K., Blackwell, A. G., Harke, F. W. and Schehl, R. R. Ultrasonic characterizations of slurry concentration in the slurry reactor, AIChE Symp. Ser., 313(92), 20, 1996.

Soong, Y., Gamwo, I.K., Blackwell, A.G., Harke, F.W., Schehl, R.R., and Zarochak, M.F. Ultrasonic characterizations of slurry concentration in the slurry reactor, AIChE Symposium series, 92 , 20-24, 1996.

Stolojanu, V., and Prakash. Hydrodynamic measurements in a slurry bubble column using ultrasonic techniques, Chem. Eng. Sci., 52 (21/22), 4225-4230, 1997.

Tzeng, J.-W. , Chen, R.C. and Fan., L.-S Visualization of flow characteristics in a 2-D bubble column and three-phase fluidized bed, AIChE., 39(5), 1993.

Uchida, S. , Okamura, S., and Katsumata, T. Measurement of longitudinal distribution of solids holdup in a three-phase fluidized bed by ultrasonic technique. Can. J. Chem. Eng., 67,166-169,1989.

Warsito, Maezawa, A., Uchida, S. and Okamura S. A model for simultaneous measurement of gas and solid holdups in a bubble column using ultrasonic method, Can. J. Chem. Eng., 73, 734-743, 1995.

Warsito, Maezawa, A., Uchida, S., and Okamura, S. Method for simultaneous measurement of gas, liquid, and solid holdups in slurry bubble column using ultrasonic technique, Proceeding of ASCON, 271-276, 1995.

Wasito, M. Ohkawa and Uchida, S. Hydrodynamic of Three-phase fluidized bed measured by ultrasonic penetration technique, Region Symposium on Chem. Eng., 1996.

Wasito, Ohkawa, M., Maezawa, A., and Uchida, S.. Flow structure and phase distributions in a slurry bubble column, Chem. Eng. Sci., 52(21/22), 3941-3947, 1997.

Yasunishi, A., Fukuma, M., and K. Muroyama. Measurement of behavior of gas bubbles and gas holdup in a slurry bubble column by a dual electroresistivity probe method, J. of Chem. Eng. of Japan., 19(5), 1986.

Yee Soong, Isaac K. Gamwo, Fred W. Harke, Arthur G. Blackwell, Richard R. Schehl, and Michael F. Zarochak. Measurement of solids concentration by an ultrasonic transmission technique, Chem. Eng. Technol. 20, 47-52, 1997.

APPENDICES

APPENDIX A

A1. Specification of experimental equipment

A1.1 Digital Video Camera Sony series TRV 20E

- Recording System using Mini DV cassette about 1 hour for SP recording mode and 1.5 hour for LP mode.
- Image device is $\frac{1}{4}$ type Charge Coupled Device (CCD) approximate 1,070,000 pixels ; For effective still picture is 1,000,000 pixels and effective moving picture is 690,000 pixels.
- Lens Carl Zeiss and combined power zoom lens, Filter diameter is 37 mm, 10x for Optical zoom and 120x for Digital zoom.
- Approximate Mass including the battery pack is 780 grams.
- Approximate Dimension is 71x93x170 millimeters.
- Dimension LCD screen is 72.4x50.4 millimeters and about 1120x220 of total dot number.

- Memory Stick 32 MB
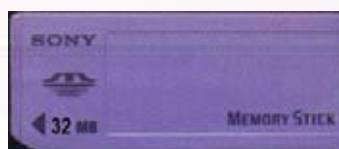
Table A1 Amount of the picture which used these mode.

Image Size	640x480	1152x864
SUPER FINE (SFN)	164 images	52 images
FINE (FINE)	329 images	104 images
STANDARD (STD)	494 images	ages

A1.2 Accessories

Tripod

Wide and Tele Conversion Lens

- Wide lens, enables the shooting of even wider angle pictures and convenient when shooting in cramped locations. This external attachment telephoto lens provides an approximate magnification power of 0.6.
- Tele lens, convenient for shooting objects at a distance and this external attachment telephoto lens provides an approximate magnification power of 2.0.

Wide and Tele Conversion Lens

A1.3 Video Graphic Acceleration Card

- AUSUS AGP-V2400TNT/TV/8MB model

- Built-in NVIDIA RIVA TNT^{TM} 128-bit 3D Graphics and Video Accelerator

- Built-in quality video capture and crystal clear TV-Out

- Bus mastering DMA 2X 66MHz AGP V1.0 Interface with full sideband and "Execute" model support

- High performance 128-bit 2D/GUI/DirectDraw acceleration

A1.4 Flow Meter of Gas and Liquid

- Gas flow meter : 1-10 liters/min for big gas flow meter and 200-2500 cc/min for small gas flow meter

- Liquid flow meter : 100-1,000 liters/hr. for big liquid flow meter and 15-160 liters/hr. for small gas flow meter

A1.5 Rotary Pump

Q_{max} : 100 liters/minute

H_{max} : 36 meters

Pump Power : 1 Hp

Current Electrical used : 220 Volts 50 HZ

Rotary Pump

A1.6 Air Compressor

- Regulator adjusted constant pressure is 1 kg/cm^3

Air Compressor

A1.7 Digital Real-Time Oscilloscope

- **Tektronik** Series TDS 210

- Bandwidth : 60 MHz

- Sample Rate : 1 GS/s eash channel

- Diamension : 304 mm x 151 mm x 120 mm

- Weight (oscilloscope only) : 1.5 kg

A1.8 Ultrasonic Transducer

- PANAMETRIC INC.

- Series V106

- 303 stainless steel case

- Standard connector style is a Straight BNC (SB)

- Dimension AxBxC : 16.0 mm x 29.5 mm x 31.7 mm
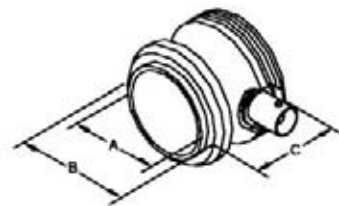
APPENDIX B

B1. Drawing of the two-dimension column

B1.1 Schematic of Three-phase fluidized bed aparatus
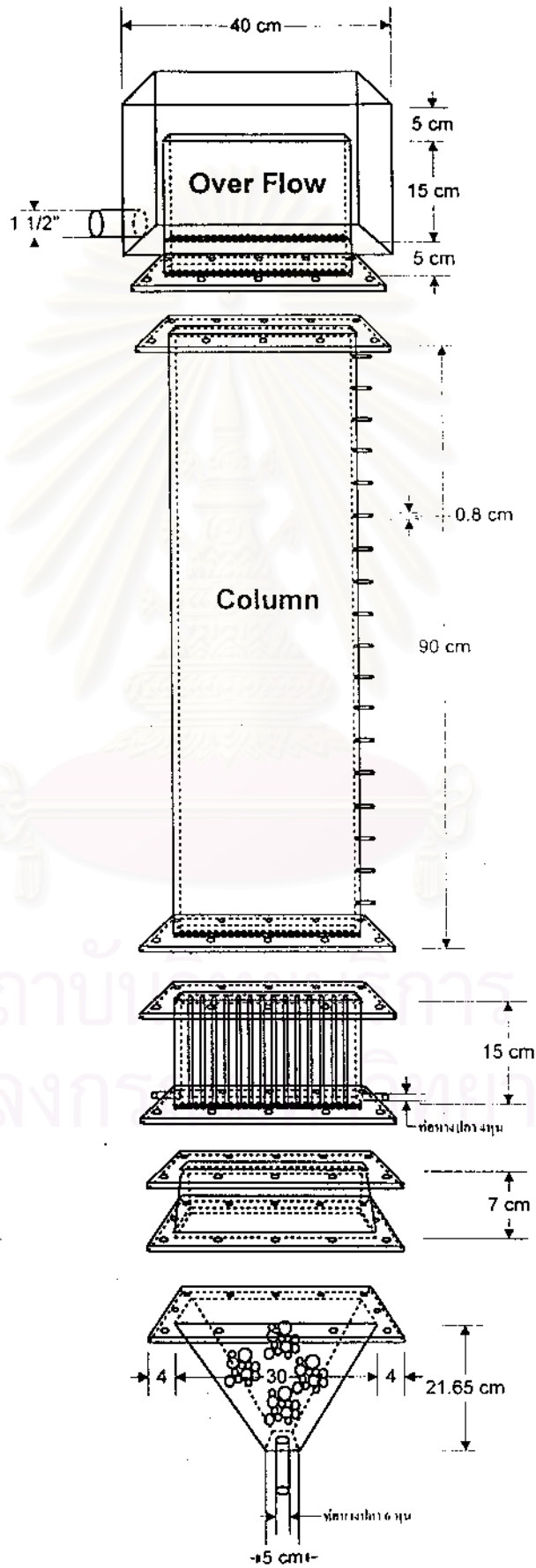
B1.2 Fluidizing Bed column

Top View

2 cm

2 cm

2.7 cm

39.2 cm   30 cm

5.87 cm

1.5 cm

4 cm

10.7 cm

Fluidized Bed

0.8 cm

90 cm

Back View

90 cm

9 cm

9 cm

9 cm

9 cm

9 cm
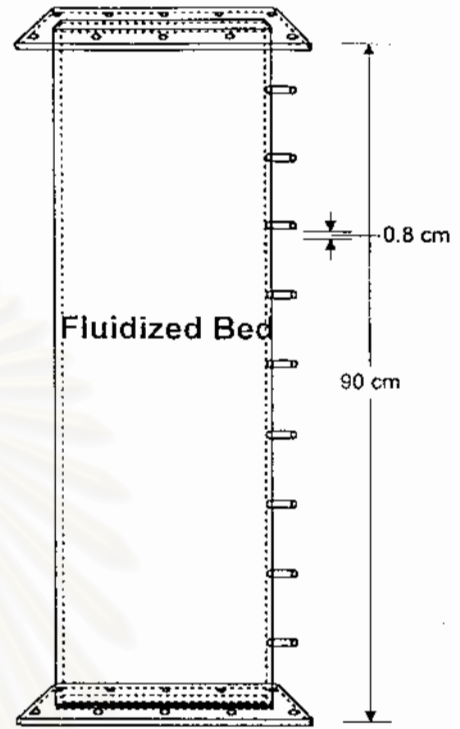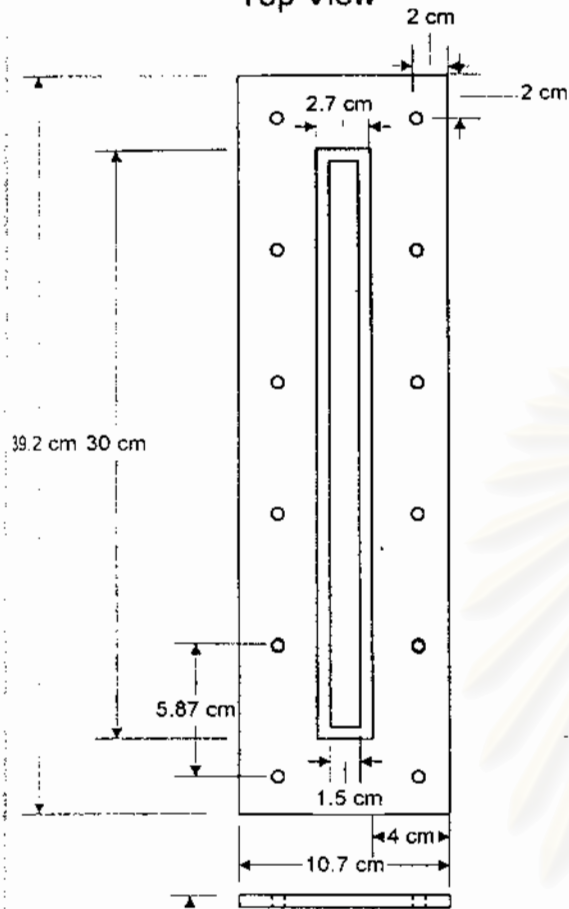
B1.3 Overflow section

Top View
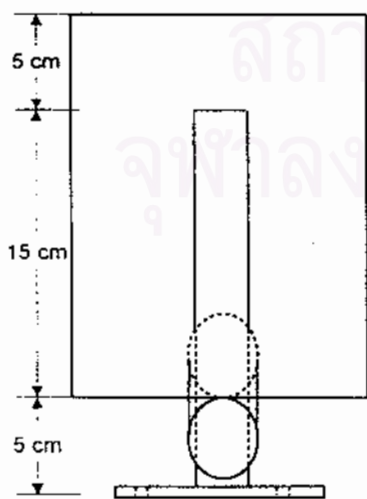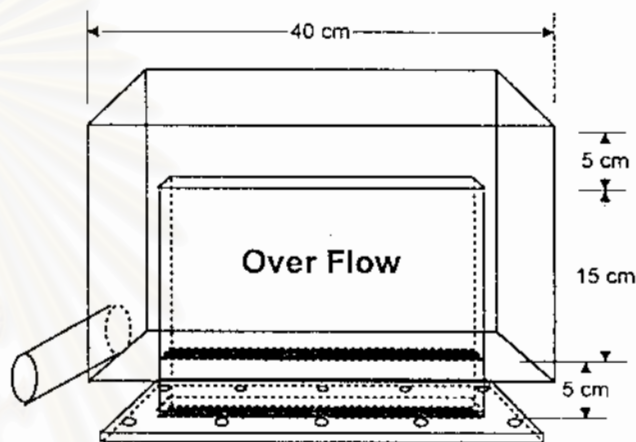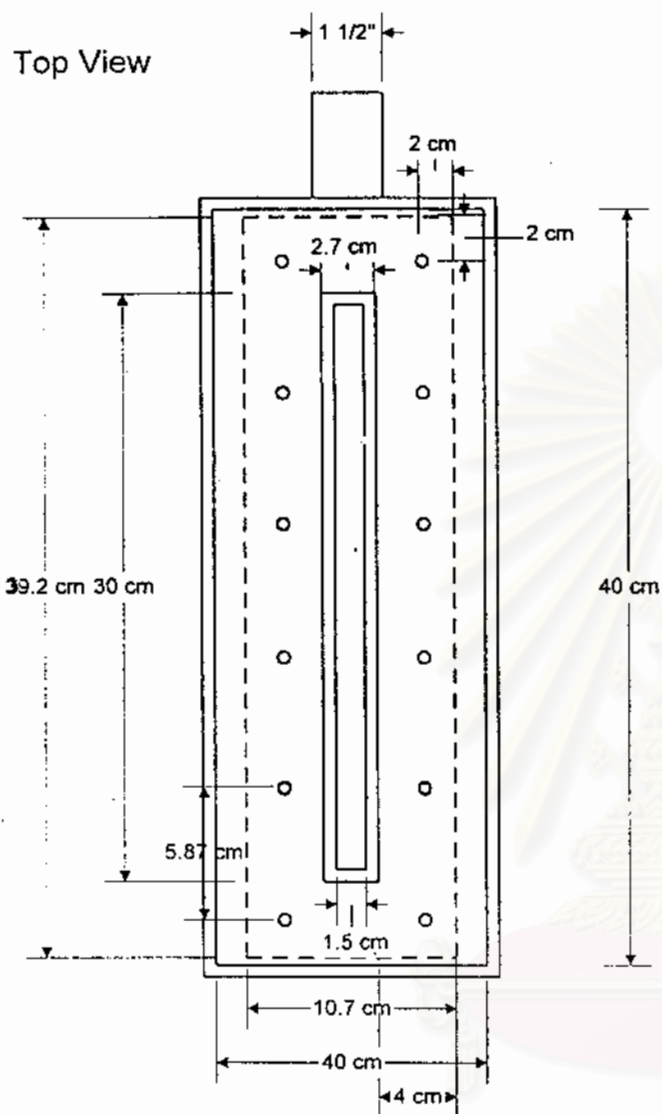
side view
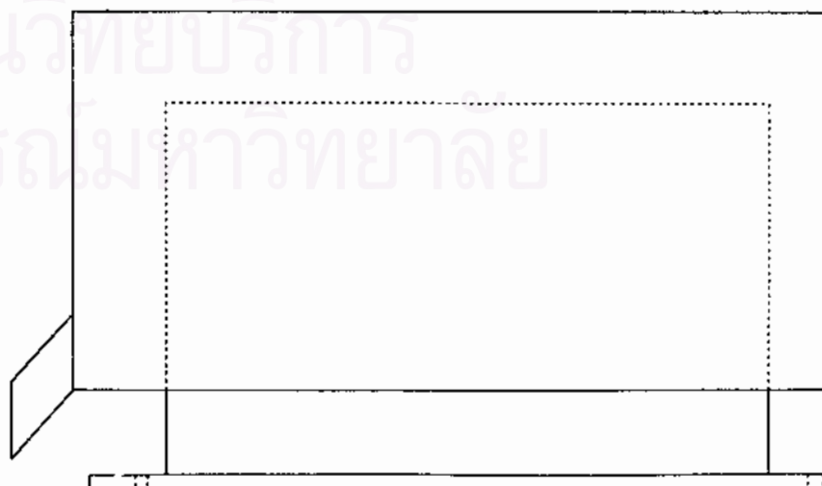
B1.4 Distributor section

Disdribution section I

Top View
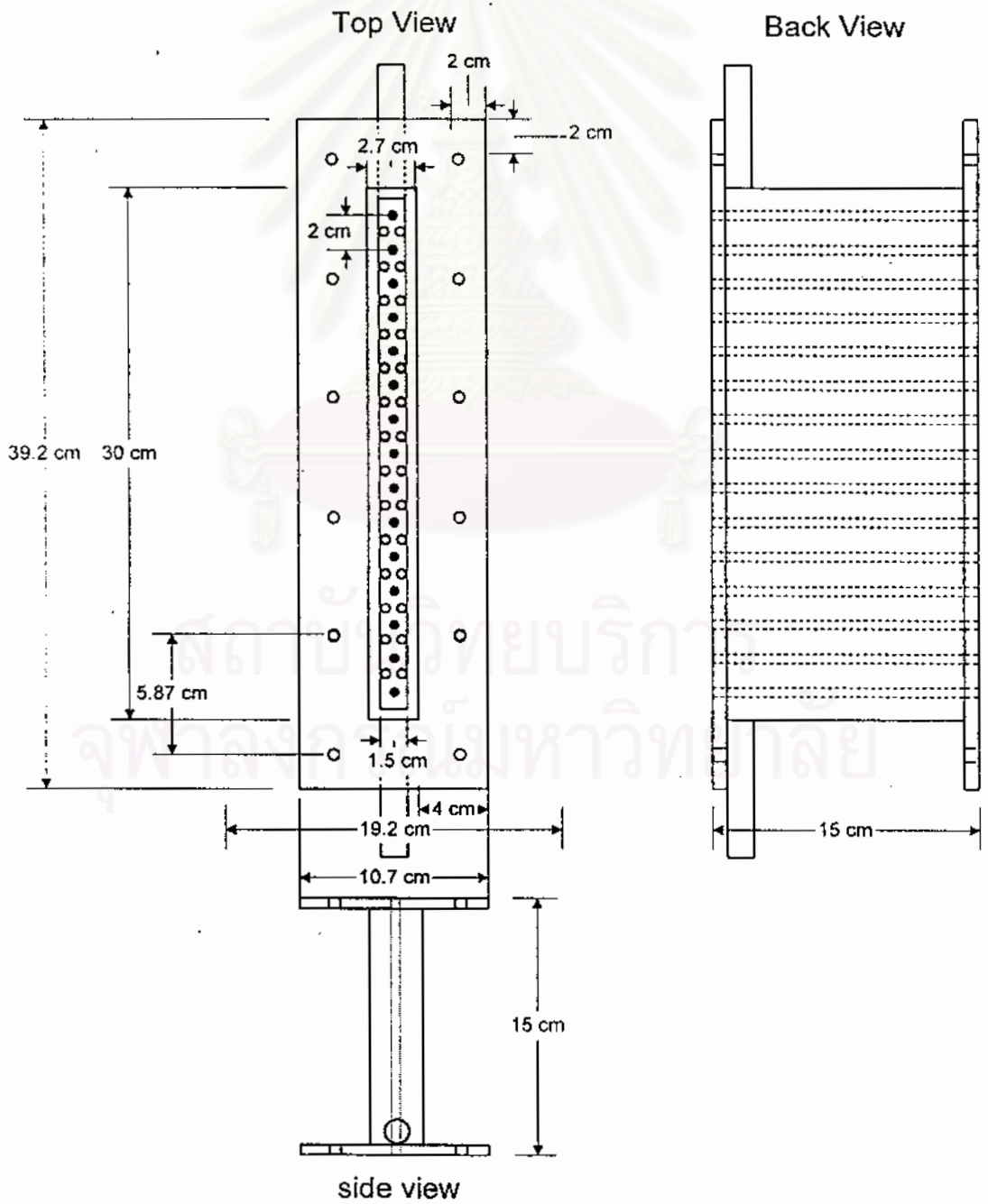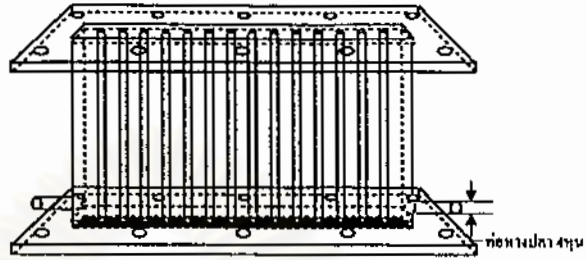
Back View

side view

Disdribution section II

Top View

2 cm

2 cm

2.7 cm

12.5 mm.

4.8 mm.

39.2 cm   30 cm

5.87 cm

10 cm

4 cm

19.2 cm

10.7 cm

Back View
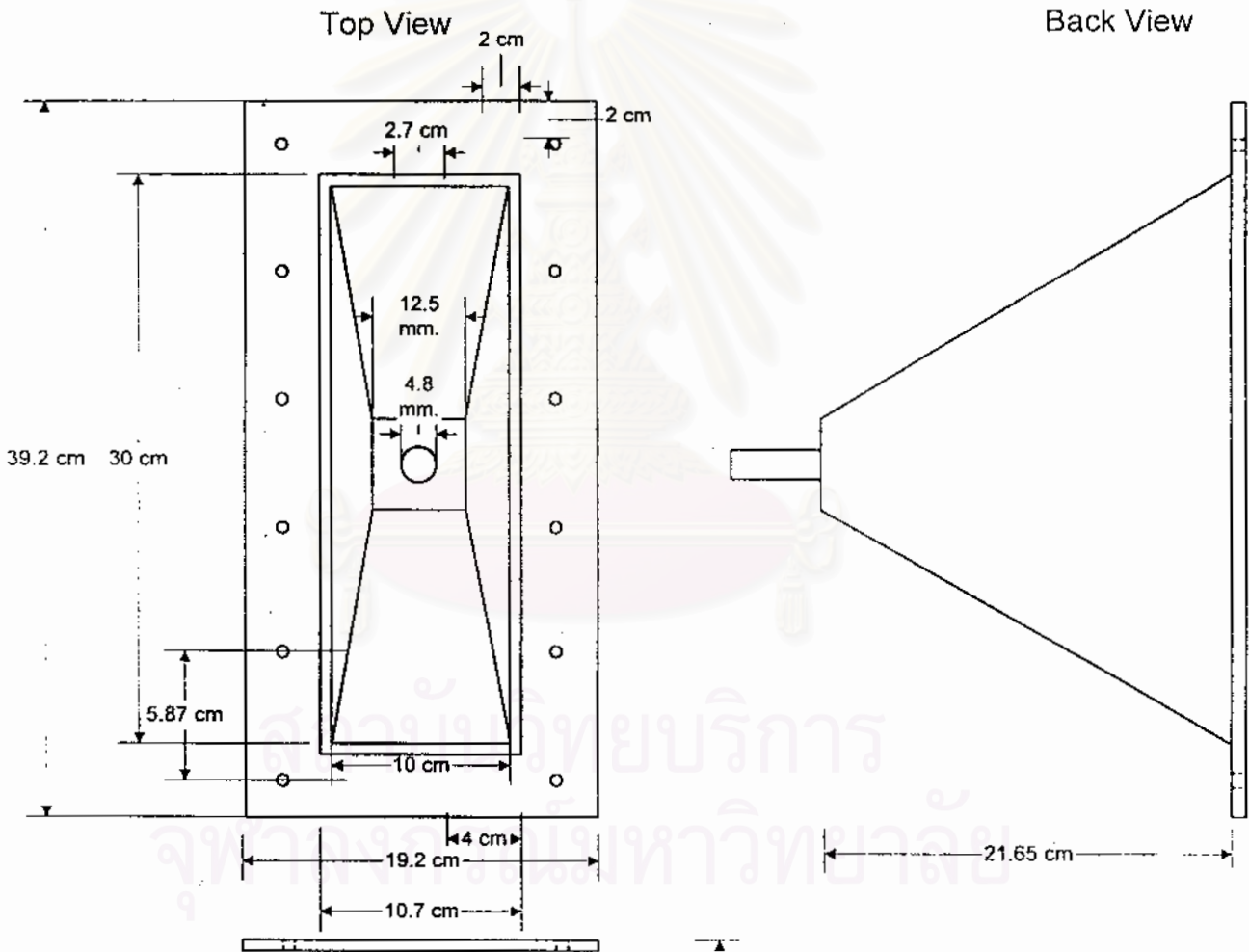
21.65 cm

side view

21.65 cm

Disdribution section III

Top View

2 cm

2 cm

2.7 cm

Back View

39.2 cm   30 cm

5.87 cm

1.5 cm

4 cm

19.2 cm

10.7 cm

17.6 mm.

17.6 mm.

side view
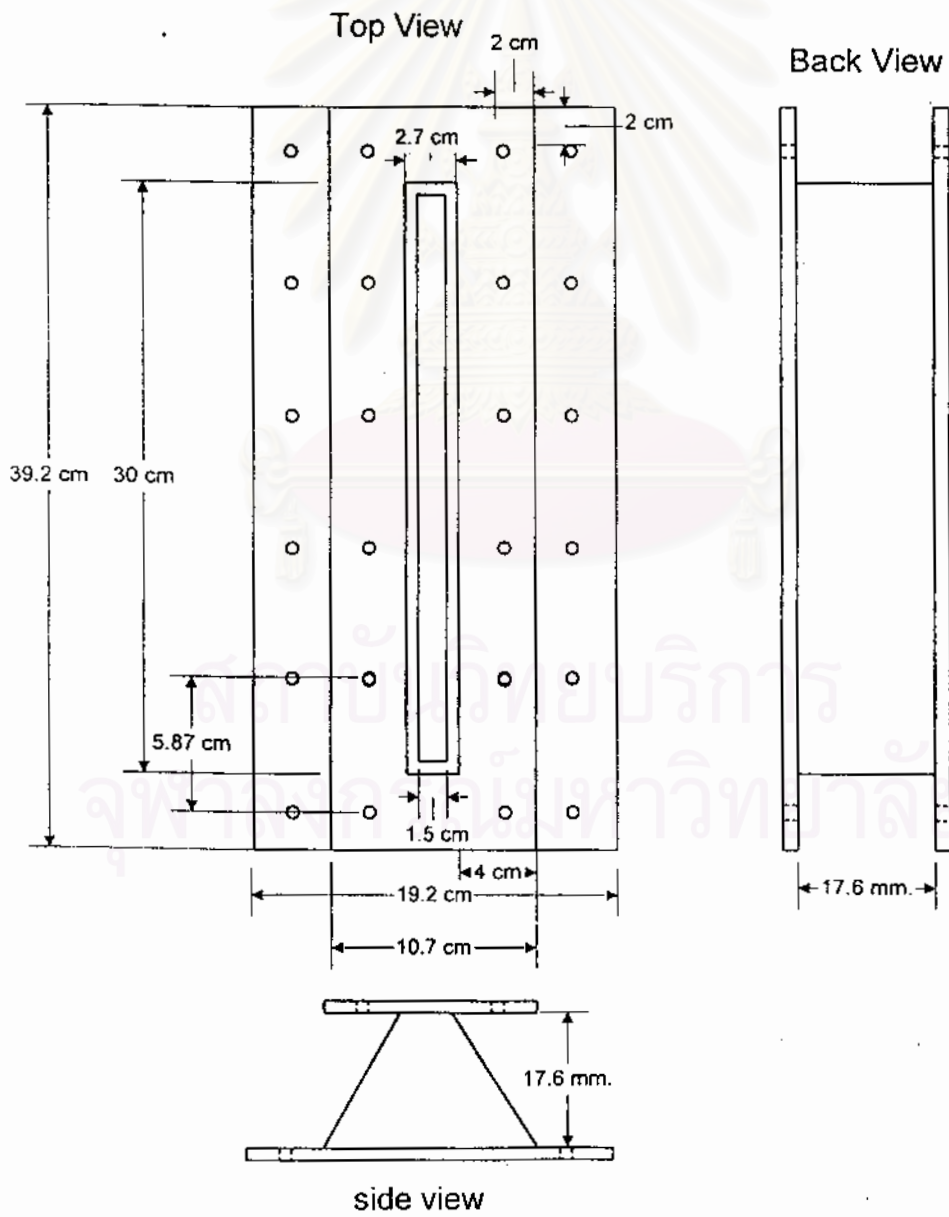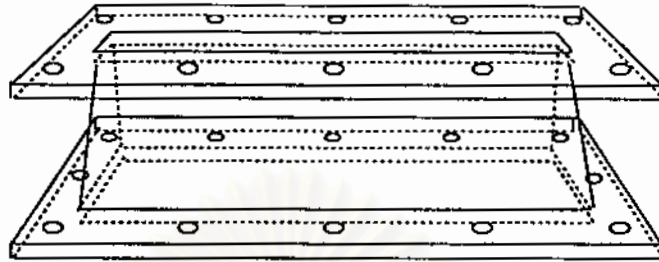
APPENDIX C

C1. Glass bead 500 micrometer, solid loading 10 %wt at Ug 1 cm/sec and Ul constant (6.17 cm/sec)
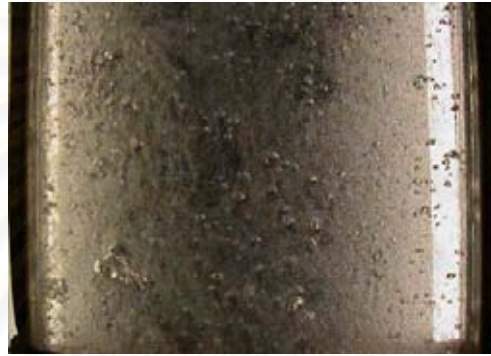
Sample 1-1

Sample 1-2

Sample 1-3

C2. Glass bead 500 micrometer, solid loading 10 %wt at Ug 2 cm/sec and Ul constant (6.17 cm/sec)
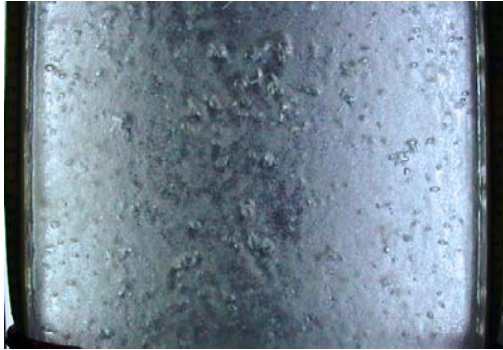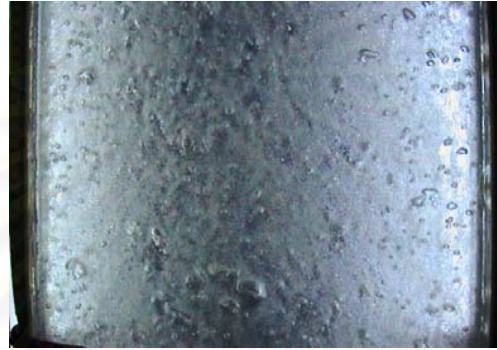

Sample 2-1

Sample 2-2

Sample 2-3

C3. Glass bead 500 micrometer, solid loading 10 %wt at Ug 3 cm/sec and Ul constant (6.17 cm/sec)

Sample 3-1

Sample 3-2

Sample 3-3

C4. Glass bead 500 micrometer, solid loading 10 %wt at Ug 4 cm/sec and Ul constant (6.17 cm/sec)

Sample 4-1

Sample 4-2

Sample 4-3

C5. Glass bead 500 micrometer, solid loading 20 %wt at Ug 1 cm/sec and Ul constant (6.17 cm/sec)

Sample 5-1

Sample 5-2

Sample 5-3

C6. Glass bead 500 micrometer, solid loading 20 %wt at Ug 2 cm/sec and Ul constant (6.17 cm/sec)
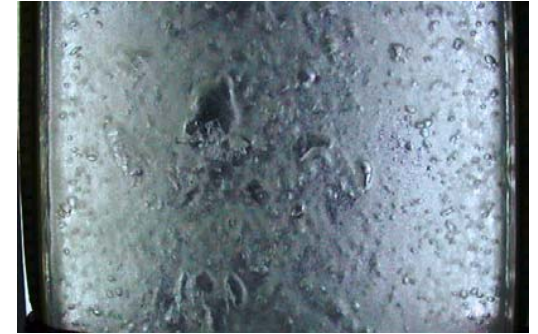

Sample 6-1

Sample 6-2

Sample 6-3

C7. Glass bead 500 micrometer, solid loading 20 %wt at Ug 3 cm/sec and Ul constant (6.17 cm/sec)

Sample 7-1   Sample 7-2   Sample 7-3

C8. Glass bead 500 micrometer, solid loading 20 %wt at Ug 4 cm/sec and Ul constant (6.17 cm/sec)

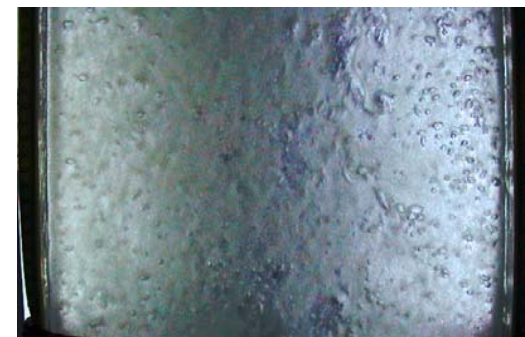Sample 8-1   Sample 8-2   Sample 8-3

C9. Glass bead 500 micrometer, solid loading 30 %wt at Ug 1 cm/sec and Ul constant (6.17 cm/sec)

Sample 9-1

Sample 9-2

Sample 9-3

C10. Glass bead 500 micrometer, solid loading 30 %wt at Ug 2 cm/sec and Ul constant (6.17 cm/sec)

Sample 10-1

Sample 10-2

Sample 10-3

C11. Glass bead 500 micrometer, solid loading 30 %wt at Ug 3 cm/sec and Ul constant (6.17 cm/sec)

Sample 11-1

Sample 11-2

Sample 11-3

C12. Glass bead 500 micrometer, solid loading 30 %wt at Ug 4 cm/sec and Ul constant (6.17 cm/sec)

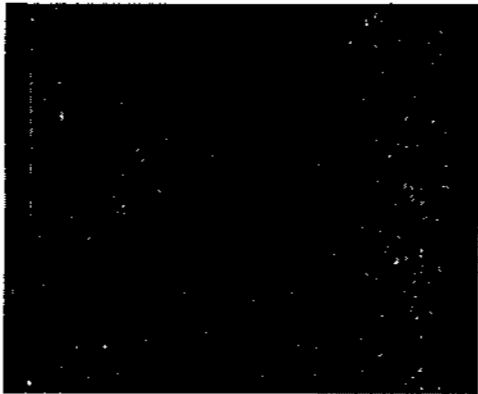Sample 12-1

Sample 12-2

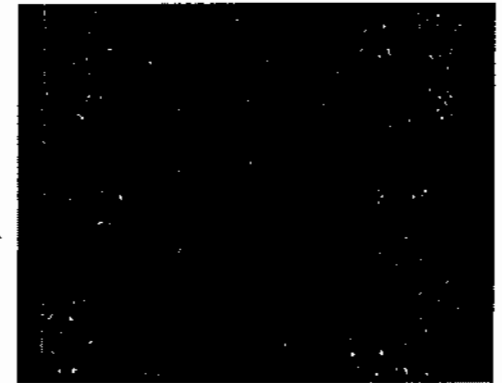Sample 12-3

C13. Glass bead 250 micrometer, solid loading 10 %wt at Ug 1 cm/sec and Ul constant (6.17 cm/sec)

Sample 13-1

Sample 13-2

Sample 13-3

C14. Glass bead 2 50 micrometer, solid loading 10 %wt at Ug 2 cm/sec and Ul constant (6.17 cm/sec)

Sample 14-1

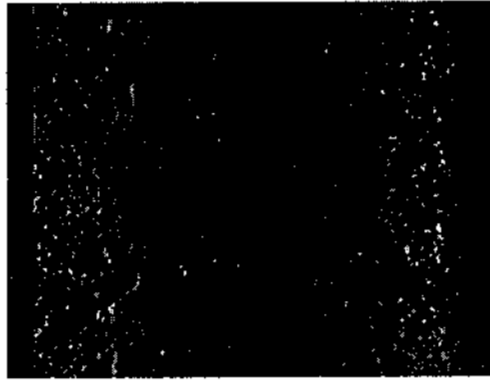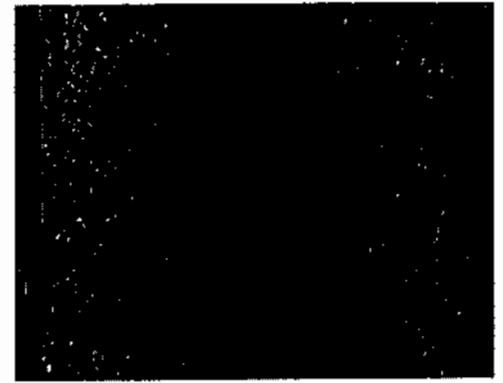Sample 14-2

Sample 14-3

C15. Glass bead 250 micrometer, solid loading 10 %wt at Ug 3 cm/sec and Ul constant (6.17 cm/sec)
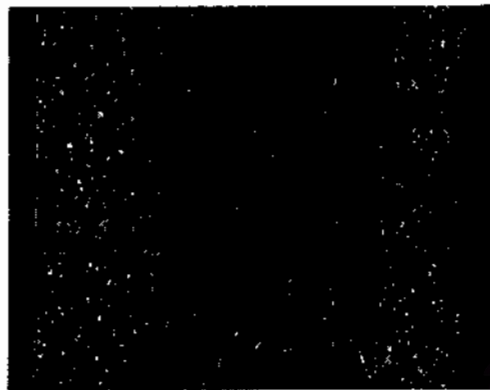

Sample 15-1

Sample 15-2

Sample 15-3

C16. Glass bead 250 micrometer, solid loading 10 %wt at Ug 4 cm/sec and Ul constant (6.17 cm/sec)
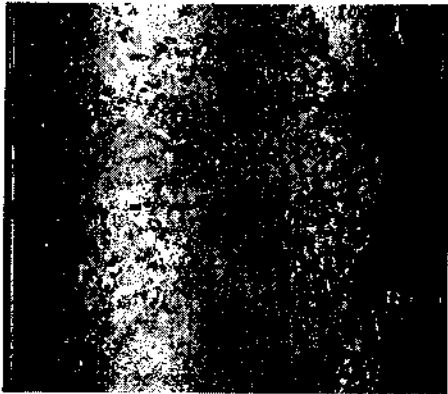

Sample 16-1

Sample 16-2

Sample 16-3

C17. Glass bead 250 micrometer, solid loading 20 %wt at Ug 1 cm/sec and Ul constant (6.17 cm/sec)

Sample 17-1

Sample 17-2

Sample 17-3

C18. Glass bead 250 micrometer, solid loading 20 %wt at Ug 2 cm/sec and Ul constant (6.17 cm/sec)

Sample 18-1

Sample 18-2

Sample 18-3

C19. Glass bead 250 micrometer, solid loading 20 %wt at Ug 3 cm/sec and Ul constant (6.17 cm/sec)

Sample 19-1

Sample 19-2

Sample 19-3

C20. Glass bead 250 micrometer, solid loading 20 %wt at Ug 4 cm/sec and Ul constant (6.17 cm/sec)

Sample 20-1

Sample 20-2

Sample 20-3
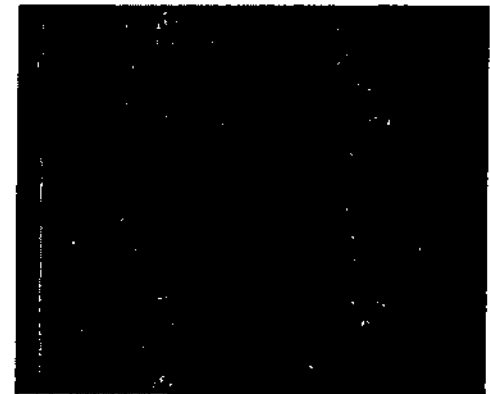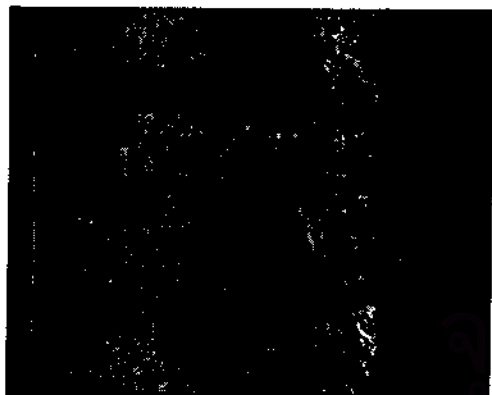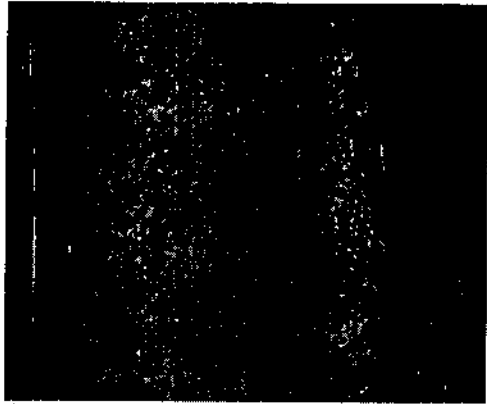
C21. Glass bead 250 micrometer, solid loading 30 %wt at Ug 1 cm/sec and UI constant (6.17 cm/sec)

Sample 21-1

Sample 21-2

Sample 21-3

C22. Glass bead 250 micrometer, solid loading 30 %wt at Ug 2 cm/sec and UI constant (6.17 cm/sec)
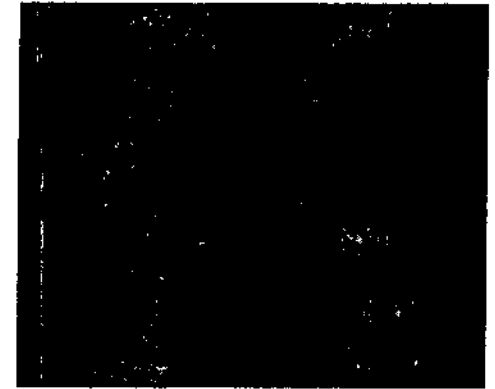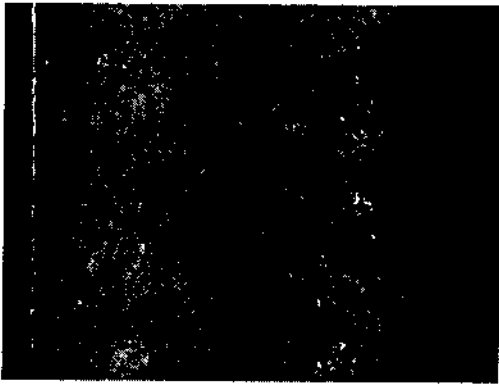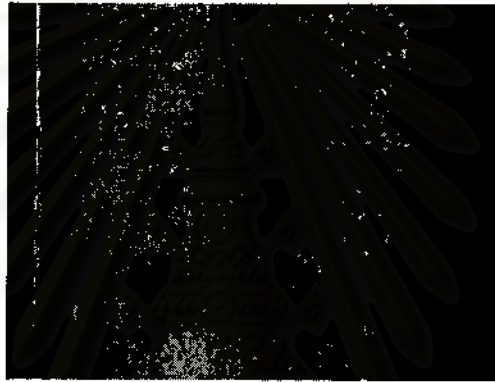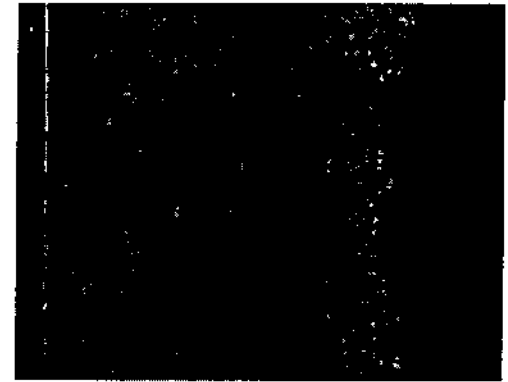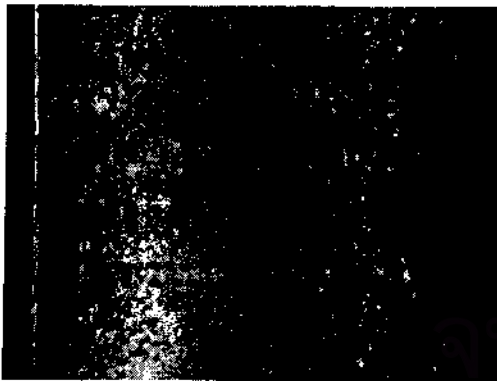

Sample 22-1

Sample 22-2

Sample 22-3

C23. Glass bead 250 micrometer, solid loading 30 %wt at Ug 3 cm/sec and Ul constant (6.17 cm/sec)
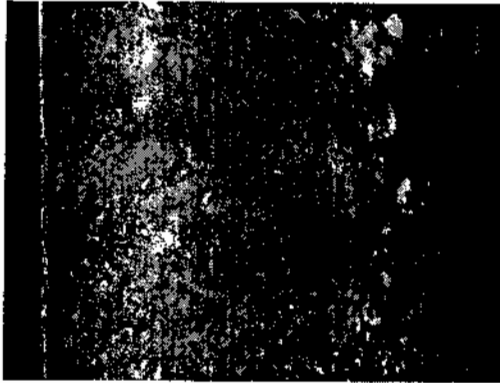
Sample 23-1
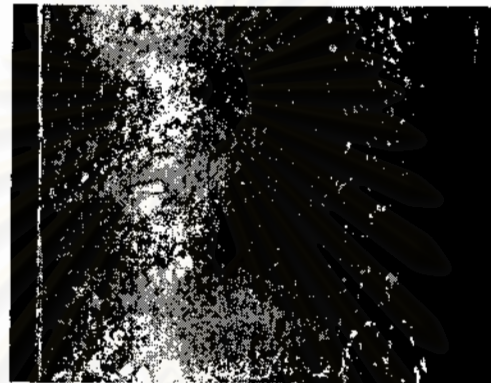
Sample 23-2
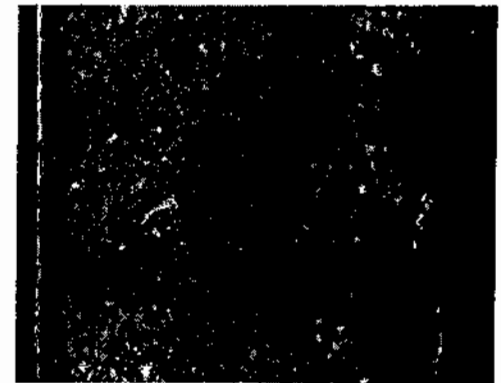
Sample 23-3

C24. Glass bead 250 micrometer, solid loading 30 %wt at Ug 4 cm/sec and Ul constant (6.17 cm/sec)

Sample 24-1
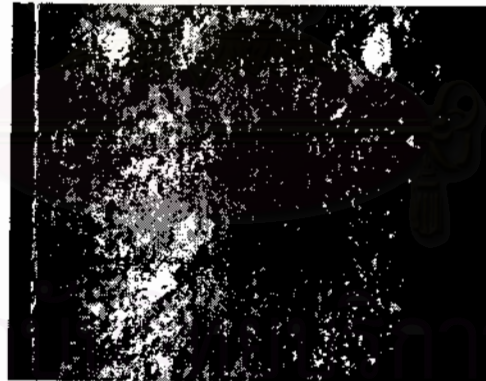
Sample 24-2
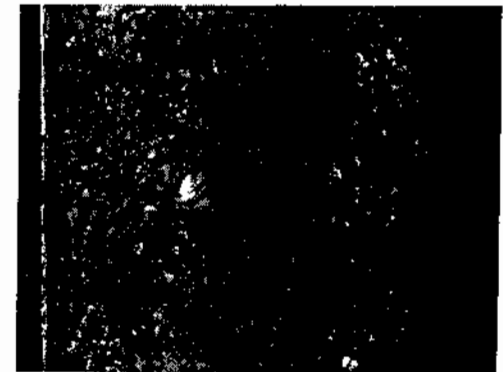
Sample 24-3

APPENDIX D

APPENDIX D

Ultrasonic transmission technique

D1. Relationship between bubble size with amplitude ratio

Figure D.1 shows that size of bubble emerging in the column has effect on amplitude of ultrasonic signal passing the column. When bubble size becomes larger, it affects to a decrease amplitude ratio. Bubble size is measured as ferret bubble diameter having range of 0.7 cm to 1.2 cm. Since the ultrasonic transducers are employed in the experiment have contact surface diameter about 1.4 centimeter thus bubbles with the size larger than about 1.4 centimeter could hardly be detected by these transducers.
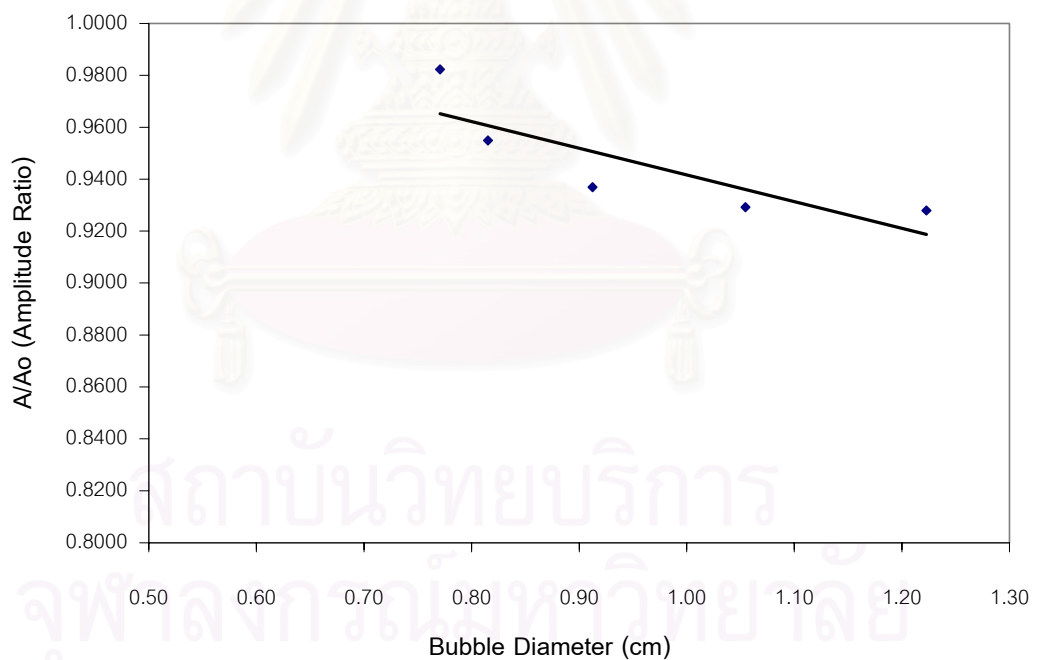
Fig. D.1 Relation between bubbles diameter to amplitude ratio (A/A_0) in bubble column system.

D2. Effect of Superficial Gas Velocity to Amplitude ratio

Figures D.2 and D.3 illustrate the change in the amplitude ratio of the transmitted ultrasonic signal in the column as a function of superficial gas velocity with the system consisting of glass bead with average size of 250 and 500 micrometer, respectively. It could be clearly seen the amplitude ratio decreases with the increasing superficial gas velocity. Yee Soong et al. (1997) and V. Stolojanu and A. Prakash (1997), they found similar results and described that the signal is reduced due to the ultrasound wave strikes the boundary between the two media (air and water) which the impedances of two media are widely separated, the most of the wave is reflected back in the first medium (water) with little transmission into the second medium (air). Thus, it colud be assumed that the ultrasound wave cannot penetrate through much of the air-water interface due to the acoustic impedence mismatch of this combination.

For the system of 250 micrometer glass beads, the amplitude ratios decreases more significantly, while the small glass beads are dispersed more uniformly in the column. Similarly for the system of 500 micrometer glass beads, it shown in Figure F.3 that when superficial gas velocity is increased the amplitude ratio also becomes decreased. This experimental results is similar indicated to the system of 250 micrometer of glass bead expect for the system with lowest solid concentration (10 %wt) due to slightly solid particles in the system and as increasing superficial gas velocity affect to dispersion of glass bead are no uniformed.
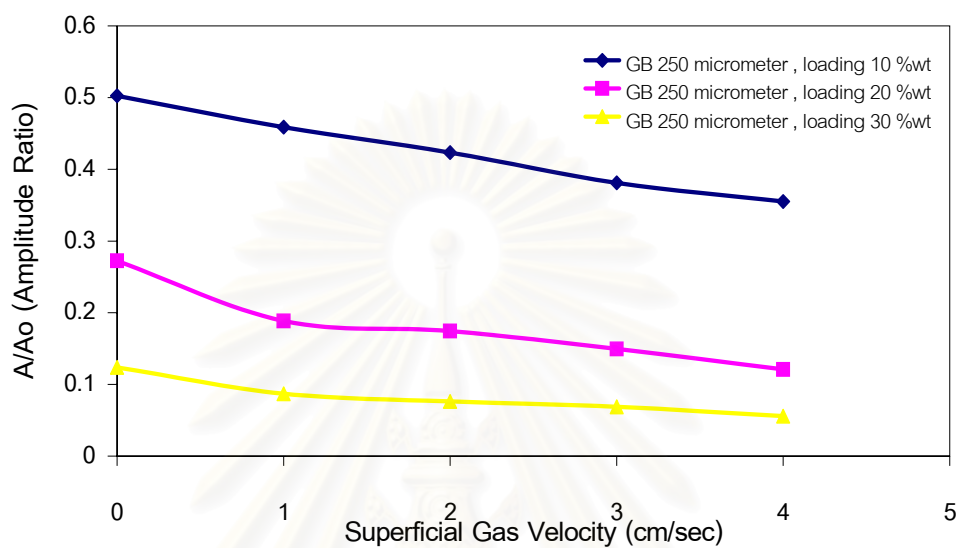
Fig. D.2 Relation between superficial gas velocity to amplitude ratio (A/A_0) at various superficial gas velocity (Glass bead 250 micrometer and superficial liquid velocity is constant at 4.94 cm/sec)
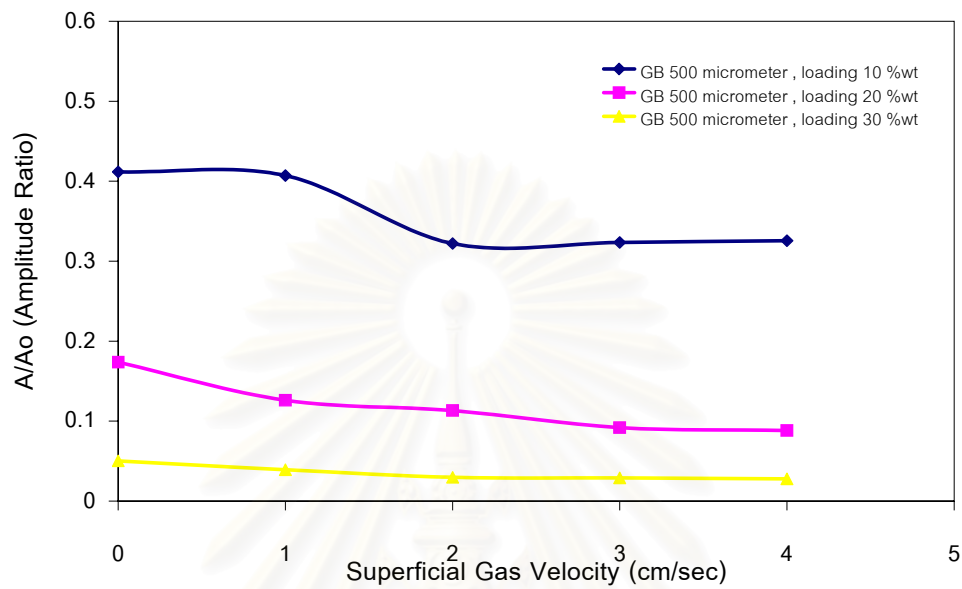
Fig. D.3 Relation between superficial gas velocity to amplitude ratio (A/A_0) at various superficial gas velocity (Glass bead 500 micrometer and superficial liquid velocity is constant at 6.17 cm/sec)

D3. Effect of Superficial Liquid Velocity to Amplitude ratio

From the experiment found that superficial liquid velocity no effect to amplitude ratio due to ultrasonic wave is generated by the signal generator as sine wave form and continuous signal mode. But we found that when static surface water height is changed affect to difference time are changed. Thus, we defined that the amplitude singal which measured from the receiver due to the ultrasonic wave transmission through only water to be the reference amplitude ratio (A_o)

APPENDIX E

E1. Calculation of terminal velocity of glass bead 250 and 500 micrometer

Assume that the system is transition flow ; $2 < Re < 500$

$$U_T = d_w [\,(4/225)\,(\rho_w - \rho_a)^2\, g^2 \,/\,(\mu_a \rho_a)]^{1/3} \qquad \ldots\ldots\ldots(E1.1)$$

where

ρ_w	= Particle density	= 2,500 kg/m^3
ρ_a	= fluid (water) density at 25 $^\circ$C	= 997.08 kg/m^3
μ_a	= viscosity of water at 25 $^\circ$C	= 0.8937 x 10^{-3} kg/m.s
g	= gravitational acceleration	= 9.81 m/s^2
d_w	= particle diameter	= 250 and 500 micrometer

Substituting into Equation (E1.1).

For GB 250 micrometer;

U_T = 250x10^{-6}[(4/225)(2,500-997.08)^2(9.81)^2/(0.8937x10^{-3})(997.08)]$^{1/3}$

= 0.0407 m/s = 4.07 cm/s

For GB 500 micrometer;

U_T = 500x10^{-6}[(4/225)(2,500-997.08)^2(9.81)^2/(0.8937x10^{-3})(997.08)]$^{1/3}$

= 0.0815 m/s = 8.15 cm/s

Check; For GB 250 mm ; U_T = 4.07 cm/s , and GB 500 mm ; U_T = 8.15 cm/s

$$Re = \rho VD/\mu \qquad \ldots\ldots\ldots (E1.2)$$

Substituting into Eq. (D1.2)

Re_{250} = (997.08 x 0.0407 x 250x10^{-6}) / 0.8937x10^{-3}

= 11.35

Re_{500} = (997.08 x 0.0815 x 250x10^{-6}) / 0.8937x10^{-3}

= 45.46

E2. Calculation bubble height (h) using empirical correlation of Wellek et al. (1966)

Applicable range: $Eo < 40$ and $Mo \leq 10^{-6}$

$$E = 1 + 0.163 Eo^{0.757} \qquad \ldots\ldots\ldots(E2.1)$$

E = bubble eccentricity = b/h

Check; Eötvös number and Morton number

      Eötvös number and Morton number could be calculated by equation (E2.2) and (E2.3), respectively.

$$Eo = g\rho_w d_e^2 / \sigma \qquad \ldots\ldots(E2.2)$$

$$Mo = g\mu_w^4 / \rho_w \sigma^3 \qquad \ldots\ldots(D2.3)$$

ρ_w = water density at 25 $^\circ$C = 997.08 kg/m^3

g = gravitational acceleration = 9.81 m/s^2

σ = interfacial tension of water at 25 $^\circ$C = 72.18 mN/m = 72.18 x 10^{-3} kg/s^2

μ_w = water viscosity at 25 $^\circ$C = 0.8937 x 10^{-3} kg/m.s

d_e = equivalent bubble diameter (m)

Sustituting in Equation (E2.2) and (E2.3)

$$Eo = [9.810 \times 997.08 \times (1.7180 \times 10^{-2})^2]/72.18 \times 10^{-3}$$
$$= 39.99$$

$$Mo = [9.810 \times (0.8937 \times 10^{-3})^4] / [997.08 \times (72.18 \times 10^{-3})^3]$$
$$= 1.67 \times 10^{-11}$$

Summary, both Eötvös number and Morton number was in applicable range, thus we could be used this correlation for estimate the bubble height.

E3. Relationship between solid concentration with solid holdup and gas holdup.

% solid concentration, $\%S = \dfrac{W_s}{W_s + W_l}$

$$= \dfrac{\rho_s V_s}{\rho_s V_s + \rho_l V_l}$$

$$\%S = \dfrac{1}{1 + \left(\dfrac{\rho_l}{\rho_s}\right)\dfrac{V_l}{V_s}} \qquad \dots\dots(E3.1)$$

Solid holdup, $\varepsilon_s = \dfrac{V_s}{V_s + V_l + V_g}$

$$\dfrac{1}{\varepsilon_s} = 1 + \dfrac{V_l}{V_s} + \dfrac{V_g}{V_s}$$

$$\therefore \qquad \dfrac{V_l}{V_s} = \dfrac{1}{\varepsilon_s} - 1 - \dfrac{V_g}{V_s} \qquad \dots\dots(E3.2)$$

Whithin the obsevation space, thus exist the total bubble volume of ΔV_g which could be calculated using d_B appeared around each intervals.

$$V_{g1} = f(Z)$$

$$V_g = \int_0^z V_{g1}\,dz$$

and $V_s = \dfrac{W_s}{\rho_s}$
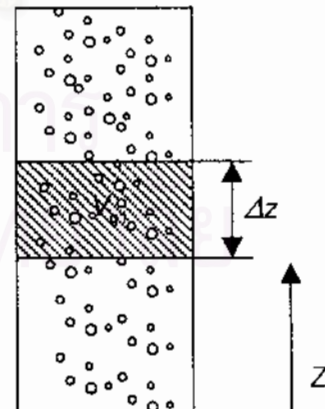
Substituting in Equation (E3.1)

$$\%S = \dfrac{1}{1 + \left(\dfrac{\rho_l}{\rho_s}\right)\left(\dfrac{1}{\varepsilon_s} - 1 - \dfrac{V_g}{V_s}\right)}$$

$$\varepsilon_s \quad = \frac{1}{\left\{\left[\left(\dfrac{1}{\%S}-1\right)\left(\dfrac{\rho_s}{\rho_l}\right)\right]+1+\dfrac{V_g}{V_s}\right\}} \qquad \ldots\ldots\ldots(E3.3)$$

Gas Holdup

$$\varepsilon_g \quad = \frac{V_g}{V_g + V_s + V_l}$$

by

$$V_l \quad = V_{Column} - V_s - V_g$$

$$\varepsilon_g \quad = \frac{V_g}{V_{Column}} \qquad \ldots\ldots\ldots(E3.4)$$

APPENDIX F

Table F1. Calculation solid and gas holdups by measurement volumetric bubble with visualization method of GB500 and U_l constants

%S	U_g	Experimental No.			V_{g1} avg. (cm³)	V_g	V_s	V_g/V_s	ρ_s/ρ_l	ε_s	V_l	ε_g
		1	2	3								
10	1	11.65	10.26	12.16	11.36	55.80	210	0.2657	2.51	0.0420	4,819.20	0.0110
10	2	24.80	23.05	23.86	23.90	117.44	210	0.5592	2.51	0.0415	4,757.56	0.0231
10	3	30.65	33.57	34.36	32.86	161.44	210	0.7688	2.51	0.0411	4,713.56	0.0317
10	4	46.55	41.91	38.47	42.31	207.87	210	0.9899	2.51	0.0407	4,667.13	0.0409
20	1	11.51	12.68	9.65	11.28	55.42	448.8	0.1235	2.51	0.0897	4,580.78	0.0109
20	2	20.04	20.24	18.51	19.60	96.28	448.8	0.2145	2.51	0.0889	4,539.92	0.0189
20	3	27.05	25.29	28.66	27.00	132.65	448.8	0.2956	2.51	0.0883	4,503.55	0.0261
20	4	32.93	33.87	34.30	33.70	165.57	448.8	0.3689	2.51	0.0877	4,470.63	0.0326
30	1	11.82	11.07	9.40	10.76	52.88	758.8	0.0697	2.51	0.1445	4,273.32	0.0104
30	2	19.35	18.05	18.56	18.65	91.64	758.8	0.1208	2.51	0.1434	4,234.56	0.0180
30	3	22.78	24.81	20.12	22.57	110.89	758.8	0.1461	2.51	0.1429	4,215.31	0.0218
30	4	28.98	27.27	31.64	29.30	143.94	758.8	0.1897	2.51	0.1420	4,182.26	0.0283

Table F2. Calculation solid and gas holdups by measurement volumetric bubble with visualization method with GB500 and glass bead 40 % by weight

U_g	U_l	Experimental No.			V_{g1} avg (cm^3)	V_g	V_s	V_g/V_s	ρ_s/ρ_l	ε_s	V_l	ε_g
		1	2	3								
1	1	35.50	38.20	35.23	36.29	178.27	210	0.8489	2.51	0.1783	4,696.73	0.0351
1	2	34.23	32.13	33.75	34.32	168.63	210	0.8030	2.51	0.1797	4,706.37	0.0332
1	3	31.65	32.57	32.36	32.15	157.97	210	0.7523	2.51	0.1814	4,717.03	0.0311
1	4	28.55	29.91	28.47	28.95	142.24	210	0.6774	2.51	0.1839	4,732.76	0.0280
2	1	48.51	47.68	49.65	48.79	239.72	448.8	0.5341	2.51	0.1889	4,396.48	0.0471
2	2	45.04	46.24	44.21	45.06	221.40	448.8	0.4933	2.51	0.1903	4,414.80	0.0435
2	3	38.05	40.29	39.23	39.19	192.54	448.8	0.4290	2.51	0.1927	4,443.66	0.0379
2	4	35.93	36.87	36.40	36.39	178.80	448.8	0.3984	2.51	0.1938	4,457.40	0.0352

F3. Calculation the volumetric of bubbles with the assumption in the shape of bubbles , ellipsoid and sphere shape , and its error.

Exp. No.	Bubble breadth, exp (cm)	Bubble height, exp (cm)	Volume of elipsoid*, exp (cm^3)	Volume of sphere**, exp (cm^3)	% error	Volume of ellipsoid***, Wellek et al. (cm^3)	% error	Volume of ellipsoid****, Wellek et al. (cm^3)	% error
1	0.78	0.56	0.18	0.25	39.29	0.21	18.3	0.17	2.2
2	0.72	0.44	0.12	0.20	63.64	0.17	42.2	0.14	16.7
3	0.56	0.39	0.06	0.09	43.59	0.08	31.6	0.06	5.5
4	0.56	0.44	0.07	0.09	27.27	0.08	16.6	0.06	18.5
5	0.89	0.56	0.23	0.37	58.93	0.30	29.1	0.27	17.2
6	0.50	0.44	0.06	0.07	13.64	0.06	5.9	0.04	31.3
7	0.83	0.67	0.24	0.30	23.88	0.25	3.2	0.21	14.0
8	0.83	0.44	0.16	0.30	88.64	0.25	57.1	0.22	41.5
9	0.44	0.33	0.03	0.04	33.33	0.04	26.2	0.03	18.7
10	0.89	0.44	0.18	0.37	102.27	0.30	64.3	0.28	55.2

* Volume ofEllipsoid, $4/3 \pi a^2 b$ ** Volumetric of Sphere $4/3 \pi a^3$ *** Volume ofEllipsoid, $4/3 \pi a^2 b_{estimate\,de}$ **** Volume ofEllipsoid, $4/3 \pi a^2 b_{cal\,de}$

BIOGRAPHY

Mr. Pornthep Sittisak was born on May 7, 1974, in Phitsanuloke, Thailand. He was graduated from Srinakharinwirot University with a Bachelor Degree of Engineering (Chemical Engineering) in 1996 and worked as a chemical engineer at Kanchanaburi Sugar Industry Co.,Ltd., U-Thai Tani province. Then he had pessued his study for Master Degree of Engineering at Department of Chemical Engineering, Faculty of Engineering , Chulalongkorn University since 1998. He finally achieved his goal of getting his Master of Engineering (Chemical Engineering) in 2001 by conducting a research on investigating the hydrodynamic of Three-Phase Fluidized Bed.